

Spatiotemporal Analysis of Indian Summer Monsoon Rainfall Variability: Identifying Multi-decadal Trends, Trend Reversals, and the Underlying Factors

A thesis submitted in partial fulfilment of the requirements
for the degree of

Doctor of Philosophy

by

Swagatika Chakra

(Roll No. 19330003)

Under the supervision of

Prof. R. D. Deshpande

Geosciences Division

Physical Research Laboratory, Ahmedabad, India



Discipline of Earth Sciences

Indian Institute of Technology Gandhinagar, India

2024

Dedicated

to

“My family for their constant love and support”

*“Prof. R. D. Deshpande who taught me the value of persistence, hard work,
and hope in life”*

“Those who are fascinated by the wonders of Earth, Water, and Atmosphere”

and

“Everyone who helped make this journey possible”

Declaration

I declare here that this thesis report represents my ideas in my own words, and I have included others' ideas with appropriate citations from sources. I also declare that I have followed all principles of academic honesty and integrity and have not misrepresented, fabricated, or falsified any idea/fact/source/data in my submission. I understand that any violation of the above can cause disciplinary action by the institute and can also evoke penal action from the sources that have thus not been properly cited or from whom proper permission has not been taken when needed.

Date: 25th November, 2024

(signature)
Swagatika Chakra
(Roll No. 19330003)



Discipline of Earth Sciences
Indian Institute of Technology, Gandhinagar
Gandhinagar, Gujarat - 382355

CERTIFICATE

It is to certify that the research work contained in the thesis titled "**Spatiotemporal analysis of Indian summer monsoon rainfall variability: Identifying multi-decadal trends, trend reversals and the underlying factors**" by Ms. Swagatika Chakra (Roll no: 19330003) has been carried out under my supervision and this work has not been submitted elsewhere for a degree. I have read this dissertation, and in my opinion, it is fully adequate, in scope and quality, for the degree of Doctor of Philosophy.

Date: 25th November, 2024

(signature)
Prof. R. D. Deshpande
(Thesis Supervisor)
Geosciences Division
Physical Research Laboratory,
Ahmedabad, India

Acknowledgments

As I conclude my Ph.D. thesis, I wish to express my heartfelt gratitude to those who have provided unwavering support with a dedicated spirit. These individuals, who have been an integral part of my life as teachers, friends, and colleagues, deserve my deepest appreciation.

First and foremost, I offer praises and thanks to God, the Almighty, for showering His blessings upon me throughout my research, enabling me to complete it successfully.

I cannot adequately convey my deep gratitude and respect for my supervisor, Prof. R. D. Deshpande. He has inspired me to become an independent researcher and helped me realize the power of critical reasoning and hard work. It was a great privilege to work and study under his guidance, and I am deeply thankful for his affection and empathy. I also extend my heartfelt thanks to his wife and family for their acceptance and patience during our discussions about my research and thesis preparation.

I express sincere thanks to the members of my doctoral studies committee (DSC), Dr. Arvind Singh, Dr. Amzad Hussain Laskar, and Prof. Som Kumar Sharma, for their critical evaluation and valuable suggestions. I am indebted to my collaborator, Dr. Vishnu S. Nair (Assistant Professor at the Indian Institute of Science Education and Research Thiruvananthapuram), for lending his expertise and intuition to my scientific problems. My deepest gratitude extends to the geosciences faculty members at the Physical Research Laboratory (PRL): Prof. Sanjeev Kumar, Prof. M.G. Yadava, Prof. J.S. Ray, Prof. Ravi Bhushan, Prof. A.D. Shukla, Dr. A.K. Sudheer, and Dr. V. Goswami for their valuable inputs during seminars and coursework. I am also thankful to Dr. A. Guharay and Dr. Narendra Ojha for clarifying my doubts related to the thesis work.

I am grateful to the Department of Space, Government of India, for the research grant that enabled me to pursue my Ph.D. at PRL. I extend my sincere gratitude to Dr. Anil Bhardwaj, Director of PRL, and Prof. Rajat Moona, Director of IIT Gandhinagar, for providing the necessary facilities to carry out my research. My thanks also go to the Dean and academic committee of PRL and IIT Gandhinagar.

This thesis would not have been possible without the support of the staff members of the PRL library, computer center, administration, and accounts section. I am grateful to the staff of the canteen, housekeeping, dispensary, and security personnel for providing me with a healthy and safe stay at PRL.

I am forever thankful to my seniors cum lab mates, Dr. Harsh Oza and Dr. Amit Pandey, for sharing their experience related to both thesis and off-thesis work. I consider myself fortunate to have Dr. Harsh Oza as an elder brother and Dr. Amit Pandey as a good friend during my thesis period. I am also grateful to Mr. Akash Ganguly, one of my lab mates, for his assistance with computational and programming work. My sincere thanks go to my other lab mates, Mr. Virendra Kumar Padhya, Dr. Naveen Kumar Pandey, and Dr. Saranya P. for their help with the thesis work.

I am extremely grateful to my parents for their love, care, and sacrifices in educating me and preparing me for my future. My deepest thanks go to my husband, Mr. Ratikanta Khuntia, for his love, understanding, and unwavering support in completing this research. I also appreciate the support from my in-laws and the cheers from my younger brothers and sisters.

I am profoundly grateful to my dear friends, Sonali, Priya, Kimi, Mansi, Srikanta, and Swayamprajna, for always being there for me and showing empathy.

I acknowledge Deepika, Abdur, Himanshu, Partha, Deepak, Aishwarya, Siddhartha, Sanjit, Deva, Ajayeta, Chandrima, Nazir, Abul, Shreya, Ranjan, and Rahul, who have been wonderful seniors and friends. I am fortunate to have enjoyed friendships with a diverse group of people during my five years at PRL. I am particularly thankful to Himanshu for his critical feedback on the writing and figures, which helped improve the overall quality of the thesis. I also appreciate the support of my batchmates — Birendra, Santunu, Vineet, Bijoy, Gaurav, Neha, Saumya, Kshitiz, Bharathi, Saurabh, and Rithvik.

Finally, my thanks go to all those who have supported me in completing this research, directly or indirectly.

(Swagatika Chakra)

Abstract

The shifting pattern of Indian summer monsoon rainfall is a significant concern, as it constitutes 80% of the annual precipitation of India. Hence, the changing rainfall pattern impacts freshwater availability, food production, and the economy of our country which is home to 18% of the world's population. Unlike temperature, rainfall changes over a region are dynamic and depend on several factors. Key components of the Indian summer monsoon circulation system, such as the Low-level Jet stream, Monsoon trough, Mascarene high, Tibetan low, Tibetan high, and the Tropical easterly jet stream, etc. play a crucial role in affecting monsoon rainfall. Additionally, distant factors like the El Niño Southern Oscillation, Pacific Decadal Oscillation, Atlantic Multidecadal Oscillation, etc. also influence monsoon rainfall by modulating the summer monsoon circulation system. Alongside these large-scale processes, regional factors such as low-pressure systems over the Bay of Bengal and mesoscale processes like changes in land use and land cover also significantly impact rainfall patterns.

Given the importance of summer monsoon rainfall to the nation and its high spatiotemporal variability, it is crucial to identify region-specific rainfall patterns over extended periods and understand the processes governing this rainfall. Extensive research has been conducted on Indian summer monsoon rainfall to identify temporal patterns and investigate the underlying factors. The current understanding of long-term rainfall variability in India primarily relies on linear and monotonic trend analysis over large geographical areas. However, this approach often overlooks multi-decadal non-monotonic trends, trend reversals, and anomalies embedded within long-term rainfall patterns. Proper identification of these long-term monsoon rainfall patterns and their regional characteristics is essential for a comprehensive understanding of the processes that govern rainfall.

In the above backdrop, the primary scientific objective of this doctoral research is to develop a robust method for identifying significant multi-decadal rainfall trends and the specific time windows during which these trends occur in the long-term rainfall dataset. This was achieved by developing an innovative methodology capable of pinpointing trend reversals in long-term rainfall datasets, enabling the identification of region-specific rainfall patterns and a deeper understanding of the processes that govern these patterns. For the analysis of long-term rainfall patterns, this study has utilized 120 years of daily 0.25° rainfall gridded data from 1901 to 2020, obtained from the India Meteorological Department. The summer monsoon rainfall patterns are examined in conjunction with other meteorological parameters such as wind speed and direction, humidity, sea surface temperature, and 2m air temperature to understand the rainfall governing processes.

The major scientific outcome of this doctoral research is the identification of significant multidecadal rainfall trends and trend reversal points in the Indian summer monsoon rainfall from 1901 to 2020 across India's four rainfall homogeneous regions at the district level. This was achieved using an innovative methodology involving mathematical and statistical tools, including a 31-year moving average of percentage departure of summer monsoon rainfall, 15-year sliding trend analysis, K-Means clustering, Z-score normality tests of clusters, and an area-based criterion for determining prominent timeframes of trend reversal.

Three significant time frames were identified—1930s, 1960s, and 1980s—during which notable rainfall trend reversal events coincided across different regions of India. These time frames reveal north-south and east-west asymmetries in rainfall patterns, indicating that the coherent regions of rainfall are not fixed but change over time. The 1980s event is particularly notable for affecting approximately 50% of the geographical area, while the 1930s event exhibited the most significant rainfall variation, with over 30% of the area experiencing substantial deviations from the long-term average.

The 1930s trend reversal event, marked by a shift from increasing to decreasing rainfall trends with anomalously higher rainfall in central and northeast India, and from decreasing to increasing trends with anomalously lower rainfall in the south peninsular region, reveals a north-south asymmetry. This event is studied to understand rainfall-governing processes. Changes in land-sea thermal contrast from early twentieth-century warming to mid-twentieth-century cooling played a key role in lower-level monsoon circulation while, the Atlantic Multidecadal Oscillation and Pacific Decadal Oscillation influenced upper-level circulation, leading to increased monsoon depressions and storms over the Bay of Bengal in the 1930s, followed by weakened monsoon circulation, causing rainfall anomalies and north-south pattern asymmetry.

The long-term Indian summer monsoon rainfall pattern is extensively studied in this work. The major outcomes of this work are (1) formation of a robust and innovative methodology for identifying rainfall patterns, (2) identification of the three prominent region-specific rainfall trend reversals across India, and (3) identification of the governing processes responsible for one of the identified patterns (1930s). The research limitations and future research opportunities emerging from this thesis are also presented at the end of this thesis.

Keywords: Indian summer monsoon; Multidecadal trends; Trend reversals; Rainfall extreme; Land-sea thermal gradient; Early twentieth century warming; Mid-twentieth century cooling; Monsoon depression

Contents

Abstract	i
List of Tables	vii
List of Figures	ix
List of Abbreviations	xiii
Chapter 1	1
Introduction	1
1.1. Monsoon climate:	1
1.2. Formation of monsoon climate:	2
1.3. Indian monsoon system:	3
1.4. Motivation:.....	10
1.5. Objectives:	14
1.6. Study Area:	14
Chapter 2	19
Proposed method	19
2.1. Data retrieval:	19
2.2. Conversion of gridded rainfall time series to district rainfall time series:.....	19
2.3. Multidecadal patterns in summer monsoon rainfall:	20
2.4. Rainfall pattern recognition:	22
2.5. K-means clustering of inflection points:.....	26
2.6. Identification of optimal number of clusters:	27
2.7. Identification of prominent clusters:.....	28
2.7. Cramer's <i>t</i> -test:	29
Chapter 3	33
Prominent summer monsoon rainfall trends and trend reversal events observed in four rainfall homogeneous regions of India	33
3.1. Distribution of inflection points:.....	34
3.2. Identification of optimal number of clusters:	36
3.3. Identification of prominent clusters:.....	41
3.4. Superimposed normalized frequency of inflection points:.....	49

3.5. Spatiotemporal distribution of prominent rainfall trend reversals:	51
3.6. Meridional and zonal asymmetry in rainfall:	52
3.7. Summary:	54
Chapter 4.....	57
Insights into Indian summer monsoon rainfall variability: Early twentieth century warming vs. Mid-twentieth century cooling.....	57
4.1. Introduction:	57
4.2. Data & Methods:	59
4.3 Results & Discussion:	61
4.4 Summary:	75
Chapter 5.....	79
Summary and scope for future works.....	79
5.1. Summary:	79
5.2. Limitations:	83
5.3. Scope for the future works:	84
References	85
Lists of Publications	101
Thesis work.....	101
Published	101
Under Preparation	101
Contributing author.....	101

List of Tables

Table 1. 1 Temporal variability of Indian summer monsoon rainfall and their driving factors.6

Table 3. 1 The total number of districts of each region along with the districts having monotonic trends lacking inflection points, exhibiting non-systematic trends, and where inflection points were identified in the moving average rainfall departure patterns and studied further.....33

Table 3. 2 Cluster range, cluster center, skewness, excess kurtosis, their standard errors, and Z-scores of all H-type and L-type clusters for four rainfall homogeneous regions of India.37-40

Table 3. 3 Number of districts and its percentage to the total number of districts of the region, area of districts and its percentage to the total area of the region, having inflection points and rainfall at the inflection years significantly different from the long-term average, within the prominent clusters. 47-48

List of Figures

Fig. 1. 1 a) Topographic Map of India. Spatial distribution of (b) climatological (1961-1990 average) summer monsoon rainfall, (c) climatological contribution of summer monsoon rainfall to the annual rainfall in terms of percentage, and (d) interannual variability (1961-1990) of summer monsoon rainfall in term of one standard deviation rainfall amount across India...4

Fig. 1. 2 (a) 1901-2003 summer monsoon rainfall time series (pink dotted line) and the associated trend (pink solid line) of India (b) 31-year moving average rainfall time series (green solid line), 31-year Cramer’s t-test values (blue squares), and two multidecadal trends (Purple solid line) are added in (a) (Modified after Guhathakurta and Rajeevan (2008)). 11

Fig. 1. 3 (a) Meteorological subdivisions, and (b) Rainfall homogeneous regions of India as defined by the IMD. Andaman and Nicobar, and Lakshadweep are not considered.15

Fig. 2. 1 Time series in summer monsoon rainfall of Bijapur district (Karnataka) from 1901 to 2020 (represented by bars). Purple (pink) bars indicate higher (lower) rainfall than the climatological standard normal of 441 mm. The black curve shows the 31-year moving average pattern of % departure from the climatological standard normal. The overall pattern displays three distinct trends, with two decreasing trends alternating with an increasing trend. Rainfall trend reversals occurred in the 1930s and 1960s, evident from the inflection points (around valley and peak) in the moving average % departure pattern.22

Fig. 2. 2 15-year sliding trend value (green squares) for the 31-year moving average of % departure in summer monsoon rainfall. Consistent positive values indicate increasing trend and negative values indicate decreasing trend. Inflection points, where the trend changes from positive to negative (H-type: 1967) or negative to positive (L-type: 1931), signify rainfall trend reversals.....24

Fig. 2. 3 (a) 5-year, (b) 11-year, (c) 15-year, (d) 21-year, (e) 25-year, and (f) 31-year sliding trend analysis in the moving average monsoonal rainfall % departure time series of Bijapur district, Karnataka.25

Fig. 2. 4 31-year moving Cramer’s t-value (maroon dots). Years with t-values beyond ± 1.96 (significant at 0.05) indicate extreme rainfall significantly higher or lower than the long-term (1901–2020) average. 1931 and 1967 are not only point of rainfall trend reversal but also year of extreme rainfall for Bijapur district, as the climatological rainfall is significantly lower and higher respectively, than the long-term average. 31

Fig. 2. 5 Methodology flow chart for identification of trend reversal and anomalous years in the long-term summer monsoon rainfall pattern. 32

Fig. 3. 1 Histogram plot of H-type (blue bar) and L-type (red bar) inflection points identified from the districts’ moving average % departure patterns of summer monsoonal rainfall coming under (a) northwest, (b) central, (c) northeast, (d) south peninsular India. Each bar corresponding to a specific year indicates the number of districts experiencing an inflection point in that particular year. 35

Fig. 3. 2 Cluster range, cluster center, district and area covered by each cluster in terms of percentage of six L-type and H-type clusters identified from K-means clustering technique for (a) northwest, (b) central, (c) northeast, (d) south peninsular India. The green-colored numbers denote the percentage of area covered, while maroon-colored numbers represent the percentage of districts of the region. Clusters highlighted with a rectangle, indicating prominent clusters. 42

Fig. 3. 3 The prominent summer monsoon rainfall trend reversals and rainfall trends observed in (a) northwest, (b) central, (c) northeast, and (d) south peninsular India. The identified trend reversals are categorized into three periods: the 1930s, 1960s, and 1980s. 43

Fig. 3. 4 Amplified superimposed frequency of inflection points of similar types (a) H-type and (b) L-type of all regions, pairwise, signifying coherence in rainfall trend reversals among regions. Amplified superimposed frequency of opposite types of inflection points (c) L-type of one region with H-type of other regions signifying asymmetry in rainfall trend reversal. 50

Fig. 3. 5 Districts within the homogeneous rainfall regions underwent the three prominent summer monsoon rainfall trend reversal events around (a) the 1930s, (b) the 1960s, and (c) the 1980s. 53

Fig. 3. 6 Graphical summary of region-wise summer monsoon rainfall pattern.	56
Fig. 4. 1 Spatial distribution of districts experiencing 1930s summer monsoon rainfall trend reversal.	61
Fig. 4. 2 (a) Track of depressions and storms forming over the Bay of Bengal, (b) Annual time series of low-pressure systems forming over the Bay of Bengal during the summer monsoon season.	63
Fig. 4. 3 The epochal difference (ETCW - Mid-20C Cooling) in (a) the GPI and relative contribution of (b) the absolute vorticity term, (c) vertical wind shear term, (d) the potential intensity term and (e) the relative humidity term to the changes in the GPI over the head Bay of Bengal between these two epochs.	65
Fig. 4. 4 (a) 1925-1986 climatology of 850hPa wind speed (shaded) and wind direction (vector), (b) epochal difference (ETCW avg.- mid-20C cooling avg.) of 850hPa wind speed (shaded) and direction (vector) over Indian Summer monsoon region, (c) 1925-1986 climatology of vertical integrated moisture transport VMIT (shaded) and direction (vector), (d) epochal difference of VMIT (shaded) and direction (vector). Red dots represent statistically significant difference in the wind speed and VIMT between ETCW and mid-20C cooling period at 0.05 level of significance.	67
Fig. 4. 5 (a) 1925-1986 climatology (b) Epochal difference (ETCW avg.- mid-20C cooling avg.) of sea surface temperature and 2m air temperature over the land mass. Red dots represent statistically significant difference in the temperature between ETCW and mid-20C cooling period at 0.05 level of significance.	70
Fig. 4. 6 Epochal difference (ETCW avg.- mid-20C cooling avg.) (a) 200hPa wind speed and direction, (b) vertical wind shear and direction, and (c) average upper tropospheric temperature (shaded) and wind direction (vector) between 200hPa and 500hPa. Red dots in a and b represent statistically significant differences in the 200hPa wind speed and vertical wind shear between the ETCW and mid-20C cooling period at 0.05 level of significance.	72
Fig. 4. 7 Summary of processes governing 1930s summer monsoon rainfall pattern.	77

List of Abbreviations

AMO	Atlantic Multidecadal Oscillation
AMSL	Above Mean Sea Level
BoB	Bay of Bengal
ENSO	El Nino Southern Oscillation
IDW	Inverse Distance Weighted
IGP	Indo-Genetic Plains
IMD	India Meteorological Department
IMDLIB	India Meteorological Department Library
IOD	Indian Ocean Dipole
ISM	Indian Summer Monsoon
ISMR	Indian Summer Monsoon Rainfall
ITCZ	Intertropical Convergence Zone
LLJ	Low-Level Jet
LPS	Low-Pressure Systems
MJO	Madden-Julian Oscillation
NAO	North Atlantic Oscillation
NE	Northeast
NetCDF	Network Common Data Form
PDO	Pacific Decadal Oscillation
SST	Sea Surface Temperature
STA	Southern Tropical Atlantic
SW	Southwest
TEJ	Tropical Easterly Jet
AIR	All-India Rainfall
ETCW	Early Twentieth Century Warming
ECMWF	European Centre for Medium-Range Weather Forecasts
ERA-20C	ECMWF Reanalysis of Twentieth Century

CRU TS	Climate Research Unit gridded Time Series
HadISST	Hadley Centre Global Sea Ice and Sea Surface Temperature
GPI	Genesis Potential Index
VIMT	Vertical Integrated Moisture Transport

Chapter 1

Introduction

1.1. Monsoon climate:

Since the early twentieth century, monsoon regimes have been classically defined by the seasonal reversal of winds [*Ramage*, 1971; *Li and Zeng*, 2000]. In contrast, the modern definition of a monsoon climate incorporates both the seasonal reversal of surface winds and the rainfall contrast between the rainy summer and dry winter seasons, as proposed by *Webster* [1987]. The summer (winter) season includes months from May to September (November to March) for the northern hemisphere and November to March (May to September) for the southern hemisphere. According to the classical definition, the monsoon domain is limited to the eastern hemisphere, encompassing the Asian, Indian Ocean, Australian, and tropical African monsoon systems. However, based on the modern definition, the monsoon domain extends to both the eastern and western hemispheres and includes eight regional monsoon systems: (i) Indian (South Asian); (ii) western North Pacific; (iii) East Asian; (iv) Australian; (v) North American; (vi) South American; (vii) North African; and (viii) South African [*Yim et al.*, 2014]. The modern definition uses two criteria of rainfall to delineate these monsoon systems: (i) the precipitation difference between the summer and winter seasons exceeds 300 mm, and (ii) the summer precipitation contributes more than 50% to the annual total. Because of the socio-economic and scientific importance of rainfall, it is necessary and important to delineate monsoon systems by the modern definition.

These regional monsoon systems have unique characteristics such as topography, land-ocean configuration, and land-ocean-atmosphere interaction. The East Asian monsoon is

controlled by the zonal contrast of the Asian continent (Asian low) and the Pacific Ocean (western Pacific subtropical high) [Wang *et al.*, 2017]. The North African monsoon is driven by the strong land-ocean thermal contrast between the extremely hot Sahara desert and the cold tongue of the equatorial Atlantic Ocean. The American monsoon is characterized by the seasonal reversal of rainfall as the inter-tropical convergence zone (ITCZ) stays over the northern hemisphere throughout the year because of the vast equatorial Pacific and Atlantic cold tongue of sea surface temperature (SST) which makes it difficult for the seasonal reversal of winds. The Indian monsoon system is the strongest one among the other regional monsoon systems. The northerly presence of the Tibetan Plateau, which acts as a heat source during the summer enhances the north-south temperature contrast, the existence of the east African highlands helps to strengthen the cross-equatorial winds and Somalia jet streams that further facilitate upwelling in the west Arabian Sea and create zonal SST gradient, accelerate the Indian summer monsoon winds.

1.2. Formation of monsoon climate:

In the pioneering theory of Halley [1753], under the assumption of the annual variation of solar radiation as an imposed forcing, the monsoon circulation was recognized as a land-sea breeze circulation driven by the land-sea thermal contrast. As such, the land-ocean configuration and the related thermal contrast determine the fundamental patterns and structure of the monsoon circulation, which are important for understanding the regional monsoon characteristics [Webster, 1987].

According to Wang *et al.*, [2012], land-sea thermal contrast alone is neither a necessary nor a sufficient condition for the formation of monsoon climate. Without annual variation of solar radiation, it is impossible to create a seasonal reversal of wind and rainfall contrast between dry and wet seasons by the land-sea thermal contrast, which suggests that the

land-sea thermal contrast is not a sufficient condition. The annual cycle of insolation can lead to ITCZ migration and seasonal reversal of winds in an aqua planet (without land), which suggests that the land-sea contrast is not a necessary condition [*Chao and Chen, 2001*]. However, the heat capacity of the land surface is responsible for the exceptional meridional displacement of the ITCZ (beyond 20° of the equator) which would have been limited to ~10° of the equator in the case of aqua surface.

The monsoon circulation interacts actively with the hydrological cycle. The circulation brings moisture from the trade wind oceanic regime to the monsoon region and feeds the monsoon rain. The latent heat of condensation released from monsoon rain, combined with the associated radiative heating of clouds, strengthens the land-sea thermal contrast and enhances the monsoon circulation which reinforces the large-scale exchange of moisture and energy, forming a positive feedback between monsoon circulation and monsoon rainfall. Further, the highland plateau which acts as an elevated heat source through surface heat flux, and mountains which limit rains to its windward side significantly affect monsoon circulation and geographical distribution of the monsoon rainfall.

1.3. Indian monsoon system:

The Indian monsoon system is the most dominant among regional monsoon systems. This circulation system has two modes i.e., southwest (SW) monsoon in summer and northeast (NE) monsoon in winter. In the summer monsoon from June to September, the lower tropospheric wind blows from the southwest direction over the Indian subcontinent, hence it is known as the SW monsoon or the Indian summer monsoon (ISM) [*Gadgil, 2003*]. The wind reverses its direction from southwest to northeast in the winter season from October to December [*Rajeevan et al., 2012*], hence it is known as the NE monsoon. The rainfall of India is largely governed by the summer monsoon circulation system, called Indian summer

monsoon rainfall (ISMR). India as a whole receives ~80% of annual rainfall during the summer monsoon season [V Kumar et al., 2010], while the amount varies from 60% to 90% over different states of India except Tamil Nadu and Jammu&Kashmir [Indian Meteorological Department (IMD) report]. Different regions of India receive variable amounts of summer monsoon rainfall ranging from the maximum of >2000 mm in the southwestern Indian coast and north-east region, and the minimum of ~300-600 mm in Rajasthan and Tamil Nadu [IMD report, <chrome-extension://efaidnbmnnnibpcajpcglclefindmkaj/https://imetsociety.org/wp-content/pdf/docs/MM2.pdf>]. The annual variability of the ISMR is also higher for regions getting higher rainfall and lower for regions getting lower rainfall. The topography, and spatial distribution of climatological (1961-1990 average) summer monsoon rainfall, its contribution to total annual rainfall in terms of percentage, and its interannual variability in terms of one standard deviation rainfall amount across India, are presented in Fig. 1.1. The winter monsoon contributes marginally (11%) to annual rainfall for India, except the states of Tamil Nadu and Kerala which receive 30-60% of annual rainfall during this season, amounting to a maximum of > 500mm [Rajeevan et al., 2012].

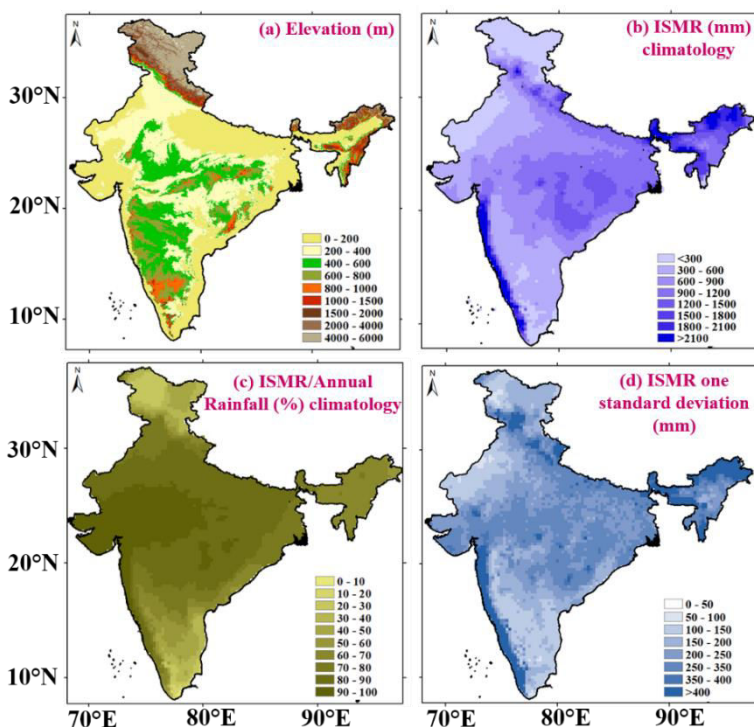


Fig. 1.1 a) Topographic Map of India. Spatial distribution of (b) climatological (1961-1990 average) summer monsoon rainfall, (c) climatological contribution of summer monsoon rainfall to the annual rainfall in terms of percentage, and (d) interannual variability (1961-1990) of summer monsoon rainfall in term of one standard deviation rainfall amount across India.

1.3.1 Drivers of ISMR variability:

Some semi-permanent systems embedded in the Indian summer monsoon circulation responsible for the spatiotemporal variability of the ISMR [*Koteswaram, 1958; Joseph and Raman, 1966; Ramage, 1971; Raghavan, 1973; Krishnamurti and Findlater, 1978*] are mentioned below.

- (i) **Heat low:** During the northward march of the sun in the northern hemisphere, a large input of power comes from the heated arid surface of northwest India, Pakistan, Saudi Arabia, and the Middle Eastern countries to the atmosphere above it, giving rise to a trough of low pressure over these regions. Vertical extension of heat low is limited to 850hPa, with a well-marked ridge above. Intense heat low acts as a suction device that draws moist air along the monsoon trough and is related to good ISMR.
- (ii) **Monsoon trough over central India:** It is an elongated zone of low pressure along the Indo-Gangetic plains (IGP) [*Das, 1968*] accompanied by cyclonic wind shear. The monsoon trough vertically spreads up to the mid-troposphere (500hPa) and has a tilt toward the south, hence causing maximum rainfall over the southward of the trough axis [*Ramage, 1971*]. The eastern side of the trough oscillates in a north-south direction. Southward movement results in active/vigorous monsoon over the major parts of India, while northward movement results in break/dry monsoon across India except heavy rainfall across the Himalayan foothills.
- (iii) **Low-level jet (LLJ) stream/ Somali jet:** It is an interhemispheric cross-equatorial flow of air attaining maximum speed in July between 1-1.5 km (850hPa) above mean sea level (AMSL) at the western side of the Indian monsoon regime along the eastern edge of Africa. The increase cross equatorial flow brings more moisture to the Indian land mass and causes more rainfall over India.

- (iv) **Surface Mascarene high:** It is a zone of high-pressure area, dominated by an anticyclonic circulation, observed around the Mascarene islands during the boreal summer. This modulates the strength of the cross equatorial flow which brings rain to the Indian summer monsoon region.
- (v) **Tibetan Anticyclone:** This is an upper tropospheric (9-12 km AMSL) anticyclonic circulation observed above the Tibetan plateau. It is marked around 300-200hPa level with center 30°N, 90°E and extends 70°E-110°E. The east-west shifting of this anticyclone causes variability in the monsoon activity over India.
- (vi) **Tropical easterly jet (TEJ) stream:** It is the concentrated outflow of the Tibetan anticyclonic circulation, observed over the northern Indian Ocean at 150hPa. It runs from the east coast of Vietnam to the west coast of Africa. The stronger the wind in the TEJ, the more rainfall is observed across the Indian monsoon region.

In addition to these factors, the uneven topography across India (Fig. 1.1a) significantly contributes to the spatial variability of the ISMR, affecting regions from district level to the continental level. The temporal variability of ISMR, which spans from decadal to synoptic time scales (excluding the orbital time scale), along with other influencing factors beyond these semipermanent systems, are summarized in Table 1.1

Table 1. 1 Temporal variability of Indian summer monsoon rainfall and their driving factors.

Scale	Factors	Factors' Description	Relation to ISMR	References
Synoptic (few days)	Low-pressure systems (LPS): Lows Depressions, Deep depressions, Cyclonic storms	LPS form over the head of the Bay of Bengal (BoB) and move northwestward and northward	60% of monsoon precipitation happened on LPS days, contributing significantly to the summer monsoon rainfall	[V Krishnamurthy and Ajayamohan, 2010; Praveen et al., 2015]
	Monsoon onset vortex	A low-pressure region forms over the southeast Arabian Sea	Modulate the length of the rainy season	[Xavier et al., 2007]

	Midtropospheric cyclones	Occurs in the west coast of India near Gujarat	Heavy rain along the west coast near Gujarat	[Miller, 1968; Choudhury et al., 2018]
Intraseasonal Oscillations	<u>30-60 days oscillation</u> Mechanisms: Convection-radiation-surface heat flux feedback, Air-sea interaction, Easterly vertical shear on moist Rossby waves, Moisture mode theory	Northward propagation of cloudiness and rainfall from the equatorial Indian Ocean to the Indian landmass	Active (Break) spell causing enhanced (decreased) rainfall over central and western India and decreased (enhanced) rainfall over southeast peninsula and northeast India	[Goswami et al., 1984; Keshavamurthy and Rao, 1992; B Wang and Xie, 1997; Krishnan et al., 2000; Raymond and Fuchs, 2009]
	<u>10-20 days oscillation</u>	Westward propagation of events from the BoB to the Indian landmass		[Krishnamurti and Ardanuy, 1980]
	<u>10-20 days oscillation</u>	Eastward propagation to east-central India from higher latitudes		[Karmakar et al., 2017]
	Madden-Julian Oscillation (MJO) 30-70 days	A zonally oriented tropical convective disturbance that propagates eastward	Phase and strength of MJO could influence the onset and duration of active and break events of ISMR Eg. Phase 1&2: favor strong convection over the equatorial Indian Ocean and subsidence over the monsoon trough region Phase 3-5: intense rainfall over the IGP	[Madden and Julian, 1972; Pai et al., 2011; Taraphdar et al., 2018; Singh and Bhatla, 2019]
Interannual	El Niño Southern Oscillation (ENSO)	Involves variation in winds and SST over the tropical Pacific Ocean	Reduced rainfall during the El Niño event and enhanced rainfall during the La Niña event	[Rasmusson and Carpenter, 1983; Shukla, 1987; Mishra et al., 2012; Chakravorty et al., 2016; Chowdary et al., 2017; Zhou et al., 2019]
	Atlantic Niño/Southern Tropical Atlantic (STA)	SST in the southeastern tropical Atlantic extending from the Angola coast to the Gulf of Guinea in boreal spring and summer	Cold SSTs in the STA region in spring and summer increase the ISMR	[Huang and Shukla, 2005; Yadav et al., 2018]

	Indian Ocean Dipole (IOD)	SST gradient between the western equatorial Indian Ocean and the southeastern equatorial Indian Ocean	Positive IOD leads to increased ISMR	[Saji et al., 1999; Ashok et al., 2001; Ashok et al., 2004; Krishnan and Swapna, 2009]
	Western North Pacific low-level circulation (Pacific-Japan Pattern)	Anticyclonic and cyclonic low-level circulation anomalies over the tropical western north Pacific and around Japan respectively	Enhances the rainfall over the southern and northern parts of India	[Srinivas et al., 2018; Gnanaseelan and Chowdary, 2019]
	South Asian high	Upper-level anticyclonic circulation of the Indian summer monsoon system	Control onset, active and break spell of ISMR	[Wei et al., 2019]
	Eurasian snow	Snow cover over Eurasia	Excessive snow cover is associated with a weak monsoon	[Vernekar et al., 1995; Pandey et al., 2022]
Multidecadal (20-40 years)	Pacific Decadal Oscillation (PDO)	Ocean-atmosphere climate variability centered over the mid-latitude Pacific basin.	Warm (Cold) phase of PDO associated with deficit (Excess) ISMR	[L Krishnamurthy and Krishnamurthy, 2014]
	Atlantic Multidecadal Oscillation (AMO)	Ocean-atmosphere climate variability over the north Atlantic basin	Warm (Cold) phase of PDO associated with excess(deficit) ISMR	[Goswami et al., 2006; Joshi and Ha, 2019]

India occupies only 2.4% of the land area and receives only 4% of global precipitation. Out of 4000 km³ of total annual precipitation, only 1100 km³ (i.e., ~27%) is utilizable. Rainfed agriculture occupies about 51 percent of the country's net sown area and accounts for nearly 40 percent of the total food production of India [*Department of Agriculture and Farmers Welfare*, <https://agriwelfare.gov.in/>]. Rainfed agriculture and its associated sectors are a substantial source of employment in India. 70% of rural households still depend primarily on agriculture for their livelihood, with 82% of farmers being small and marginal [*Food and Agricultural Organisation, India*]. Agriculture has long been the backbone of India's economy. According to the Economic Survey 2020-2021 (<https://www.indiabudget.gov.in/budget2021->

22/economicsurvey/doc/echapter_vol2.pdf), it is contributing 20% to the national gross domestic product.

Although rainfall during the summer monsoon is such an important natural phenomenon for India, it is highly erratic and spatiotemporally uneven, compelling indiscriminate extraction of ubiquitous groundwater. India is the largest extractor of groundwater in the world, and this 2nd most populous country is also the 13th most water-stressed country in the world [Upadhyaya *et al.*, 2013; Hora *et al.*, 2022]. Thus, rainfall during summer monsoon is the most important factor for the socio-economic well-being of 1.38 billion people (18% of the global population) in India. However, a significant spatial variability [P Guhathakurta *et al.*, 2015, Fig. 1.1b] and temporal variability [Joshi and Pandey, 2011, Fig. 1.1d] in the ISMR amount distribution across India is evident.

A major change in the pattern of spatio-temporal variability of rainfall affects human and other life forms and disturbs the established harmony between human civilization, environment, and ecology [Pal and Al-Tabbaa, 2009; Wassmann *et al.*, 2009; Kavitha and Kumar, 2020]. Occurrence of many natural calamities like floods, droughts, landslides, crop failures, and famines in India have been reported in the past and are known to be associated with extreme precipitation variability [Parthasarathy *et al.*, 1987; V Mishra and Shah, 2018; Dikshit *et al.*, 2020]. However, its frequency has increased in recent decades affecting the livelihood of millions of people due to extreme rainfall variability [Gulati *et al.*, 2009; P Guhathakurta *et al.*, 2011; O Singh and Kumar, 2013; Cho *et al.*, 2016; P Guhathakurta *et al.*, 2017]. Therefore, studying historical rainfall variability is necessary and very important to understand its linkages with meteorology, hydrology, and climatology, and to improve the risk management practices in agricultural and other industries [Joshi and Pandey, 2011; Mondal *et al.*, 2015].

1.4. Motivation:

To understand the historical ISMR variability, rainfall trend analysis has been carried out by several researchers at varied spatial and temporal scales over India [*Pulak Guhathakurta and Rajeevan, 2008; P Singh et al., 2008; Basistha et al., 2009; Krishnakumar et al., 2009; Raj and Azeez, 2010; Joshi and Pandey, 2011; Rana et al., 2012; Patra et al., 2012; Jain et al., 2013; Subash and Sikka, 2014; Nair et al., 2014; Mondal et al., 2015; Sushant et al., 2015; S Kundu et al., 2015; P Guhathakurta et al., 2015; M Kumar et al., 2016; Jana et al., 2017; Kaur et al., 2017; S Kundu et al., 2017; Sanikhani et al., 2018; Biswas et al., 2019; Saini et al., 2020; Praveen et al., 2020; R Singh et al., 2021*].

In most of the above studies, the Mann-Kendal test and linear least square regression statistical tests have been used to detect long-term trends in rainfall. The purpose of the linear least squares regression test in the above studies was to assess the presence or absence of a linear trend in rainfall [*Sharad K Jain and Kumar, 2012*] even though the trend of rainfall time series is very unlikely to be linear one [*World Meteorological Organization technical report, 1966*]. The Mann- Kendall statistical test is used for the assessment of monotonic increasing and decreasing trends in the data set [*Mann, 1945; Kendall, 1975*] and is not best suited for a time series with multiple peaks and valleys.

A significant limitation of monotonic rainfall trend analyses in long-term data is their inability to capture short-term trends spanning multiple decades within the long-term dataset. For example, as demonstrated by Pulak Guhathakurta and Rajeevan [2008], the linear trendline in the all-India summer monsoon rainfall time series for the 1901 to 2003 period does not indicate any trend ($R^2 = 0.0016$). However, Fig. 1.2b, redrawn from the published data series for 1901 to 2003 by Pulak Guhathakurta and Rajeevan [2008], reveals significant increasing and decreasing trends for the multi-decadal periods of 1901-1947 and 1947-1987 (purple lines)

at the 0.1 and 0.05 significance levels, respectively. The year 1947 is identified from the 31-year moving average rainfall pattern (green line) as the point with the highest moving average rainfall amount. It is situated between years with progressively increasing and decreasing moving average rainfall amounts, indicating a trend reversal. Furthermore, applying the 31-year Cramer's t-test to the rainfall time series of 1901-2003, shows that the Cramer's t-values (blue squares) close to 1947 (blue circle) exceed +1.96, suggesting the rainfall amount is significantly higher than the long-term mean (1901-2003 average) at the 0.05 significance level. These rainfall signatures suggest certain processes that cannot be identified through linear and monotonic trend analysis of long-term data, necessitating a finer spatiotemporal analysis of the ISMR pattern considering these insights.

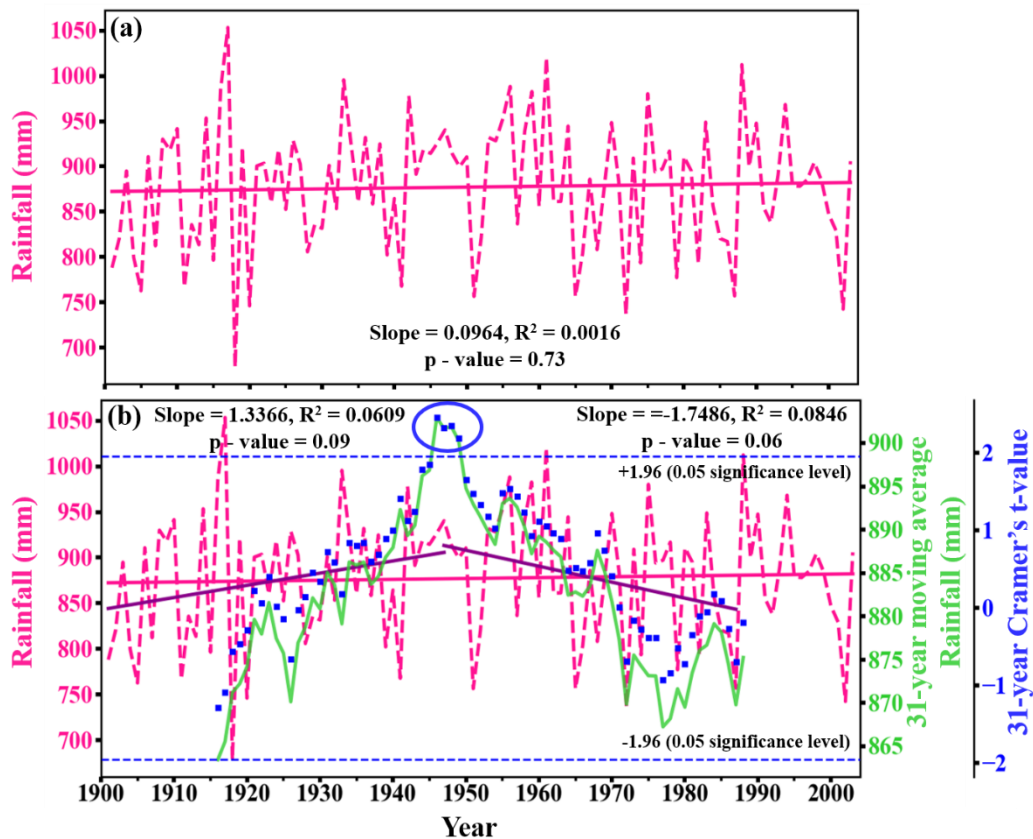


Fig. 1. 2 (a) 1901-2003 summer monsoon rainfall time series (pink dotted line) and the associated trend (pink solid line) of India (b) 31-year moving average rainfall time series (green solid line), 31-year Cramer's t-test values (blue squares), and two multidecadal trends (Purple solid line) are added in (a) (Modified after Guhathakurta and Rajeevan (2008)).

There are studies in which rainfall trend analysis has been done at a finer spatial scale of district level to even station and grid level [*P Singh et al.*, 2008; *Raj and Azeez*, 2010; *Patra et al.*, 2012; *Rana et al.*, 2012; *Sushant et al.*, 2015; *Jana et al.*, 2017; *Kaur et al.*, 2017; *S Kundu et al.*, 2017; *Sanikhani et al.*, 2018; *R Singh et al.*, 2021]. However, these studies are based on linear and monotonic trend analyses and have inferential limitations of this methodology as discussed above.

Another approach to studying smaller time-scale rainfall variability involves dividing a long time series of rainfall into arbitrarily chosen decadal or multidecadal epochs for which linear and monotonic trend analyses are conducted. For example, *P. Guhathakurta et al.* [2015] performed a 30-year epochal rainfall trend analysis (1901-1930, 1931-1960, 1961-1990, 1991-2011) for four homogeneous regions of India. Similarly, *Subash et al.* [2011] analyzed 30-year epochs (1889-1918, 1919-1948, 1949-1978, 1979-2008) for four meteorological sub-divisions of central northeast India. *Sharad Kumar Jain et al.* [2013] split the 1871-2008 rainfall time series of four meteorological subdivisions of northeast India into two parts (1871-1950, 1950-2008) for a smaller time scale study. However, because the periods in these studies are arbitrarily chosen, the rainfall trend that begins in one epoch and ends in the next may not be accurately captured.

In some studies, change point analysis has been conducted using the Standard Normal Homogeneity (SNHT) Test [*Alexandersson*, 1986] and the Pettitt test [*Pettitt*, 1979]. These tests identify a specific time (t_k) within a long-term time series (t_1 to t_n) where the mean rainfall for the period (t_1 to t_k) is significantly different from the mean rainfall for the remaining period (t_k to t_n). This is achieved by averaging the deviation of each year's rainfall (within the chosen time bracket) from the long-term mean of the entire time series, normalized by the standard deviation for the entire series. A particular time in the time series is identified as a change point

when the difference in mean rainfall before and after that point is statistically significant [Alexandersson, 1986]. This approach has been used in various studies [Basistha et al., 2009; Taxak et al., 2014; Jaiswal et al., 2015; Adeyeri et al., 2017; Jana et al., 2017; S. K. Kundu and Mondal, 2019; Praveen et al., 2020]. Despite its widespread use, the major limitation of the change point analysis method is that it fails to capture trends that begin before the identified change point and continue beyond it.

In addition to trend analysis, harmonic analysis techniques such as Fourier and wavelet analysis have been used to capture multi-decadal rainfall variability in long-term rainfall time series. These techniques help identify dominant periodic components in rainfall datasets and their correlation with large-scale oscillations. For instance, Sahoo and Kumar Yadav [2022] identified significant 2-year and 7-year periodicities in north India, 2-year periodicities in central India, and 2-year and 8-year periodicities in south India that greatly influenced summer monsoon rainfall from 1901 to 2020. Das et al., [2020] have analyzed the wavelet coherence between monthly precipitation in each homogeneous region and large-scale oscillations such as the IOD, SST over NINO3.4, PDO, and North Atlantic Oscillation (NAO) from 1951 to 2015. They found that NAO and PDO had impacts at inter-annual scales across all regions. Additionally, in the northeast, NAO exhibited an impact at inter-decadal scales. The IOD influenced all regions at a scale of 8-16 months. Significant inter-annual scale coherence between SST and monthly precipitation was observed in northwest India and west central India. Thomas and Abraham [2022], in a recent study, established a coherent relationship between Kerala's rainfall and sunspot numbers on an 8–12-year scale across all seasons. Despite these efforts, there remains much to be understood about the complex dynamics of rainfall variability in India's diverse regions over time.

In order to go beyond the current level of understanding, it is essential to identify significant rainfall trends as well as the time window over which this trend is observed, within an extended time series, in which it may be challenging otherwise to discern any long-term trend so that research can advance further to ascertain relative contribution of above factors (ENSO, IOD, PDO, AMO, NAO, land-ocean thermal contrasts, etc) in the identified rainfall trend.

1.5. Objectives:

With this background in the knowledge gap in the domain of ISMR, the aim of this thesis work is:

1. To propose a robust method for identifying significant multi-decadal rainfall trends and the specific time windows during which these trends occur, by pinpointing trend reversals in long-term rainfall datasets.
2. To identify prominent regional rainfall trend signatures by analyzing district-level rainfall trends across India using the proposed method.
3. To identify and understand the underlying governing processes and factors.

1.6. Study Area:

District-wise summer monsoon rainfall patterns from 1901 to 2020 have been analyzed across four homogeneous regions of India. These regions are delineated by the India Meteorological Department (IMD) and are currently used for many operational purposes (https://mausam.imd.gov.in/imd_latest/contents/rainfall_over_homogeneous.php). These regions are; (1) northwest India, (2) northeast India, (3) central India, and (4) south peninsular India, and are made up of a group of meteorological subdivisions such that over substantial

portions of each of the meteorological subdivisions that make up the region is positively and significantly correlated with the area-weighted rainfall variation over the region as a whole.

IMD has delineated 36 meteorological subdivisions in India: 34 on the mainland, one is Andaman and Nicobar, and the other is Lakshadweep. These 34 sub-divisions are grouped into the above four homogeneous regions (Fig. 1.3). The subdivision's boundary is demarcated based on the homogeneity and coherence criteria. The measure used for homogeneity is the spatial standard deviation of the climatological mean seasonal rainfall of the districts/stations in the subdivision around the value of the climatological sub-divisional mean rainfall (the average of rainfall at all the stations/districts in the sub-division). The measure used for coherence is the correlation coefficient of the sub-divisional rainfall with the district/station rainfall as well as the pairwise correlation of the district/station rainfall for all the districts/stations in the sub-division.

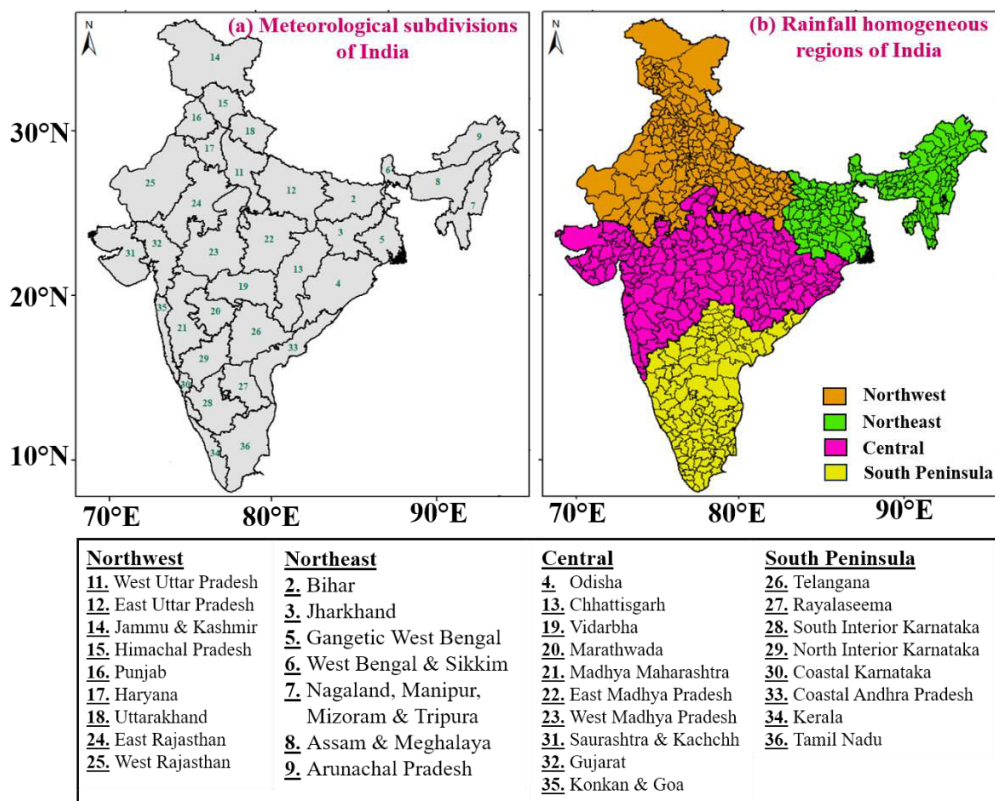


Fig. 1. 3 (a) Meteorological subdivisions, and (b) Rainfall homogeneous regions of India as defined by the IMD. Andaman and Nicobar, and Lakshadweep are not considered.

The rainfall homogeneous region of Northwest India comprises 9 meteorological sub-divisions (West Uttara Pradesh, East Uttar Pradesh, Jammu & Kashmir, Himachal Pradesh, Punjab, Haryana, Uttarakhand, East Rajasthan, and West Rajasthan), covering 205 districts, and ~30.6% of the geographic area of India. The climate in Rajasthan state of this region is arid and semi-arid, while Jammu & Kashmir, Himachal Pradesh, and Uttarakhand experience a highland climate. The rest of the area is prevailed by a humid subtropical climate. The majority of annual rainfall, exceeding 75%, occurs during the summer monsoon season across most of the region (Rajasthan: 91%, Punjab: 79%, Haryana: 82%, Uttar Pradesh: 89% and Uttarakhand: 79%) except Himachal Pradesh (61%) and Jammu & Kashmir (44%) where westerern disturbances contribute significantly to the annual rainfall during the months of January and February.

The rainfall homogeneous region of Northeast India spread across 7 meteorological sub-divisions (Bihar, Jharkhand, Gangetic West Bengal, West Bengal & Sikkim, Nagaland-Manipur-Mizoram-Tripura, Assam & Meghalaya, and Arunachal Pradesh) covering 175 districts, and ~16.7% of the geographical area of India. The prevailing climate in most of the region is a humid subtropical one, except for Sikkim and Arunachal Pradesh, where a highland climate is experienced. More than 60% of annual rainfall occurs during summer monsoon season with above 80% in Bihar and Jharkhand (Arunachal Pradesh: 64%, Tripura: 60%, Mijoram: 67%, Assam: 65%, Nagaland: 67%, Sikkim: 63%, West Bengal:77%, Meghalaya: 71%, Bihar: 85%, and Jharkhand: 84%).

The rainfall homogeneous region of Central India spans across 10 meteorological sub-divisions (Odisha, Chhattisgarh, Vidarbha, Marathwada, Madhya Maharashtra, East Madhya Pradesh, West Madhya Pradesh, Saurashtra & kachchh, Gujarat, and Konkan & Goa), and comprises 178 district, covering ~33.4% of geographical area of India. In the western segment

of this region, Gujarat experiences arid and semi-arid climate, and Maharashtra experiences tropical wet and dry climate, while Goa witnesses tropical wet climate. The climate changes to humid subtropical and tropical wet and dry towards the east in Madhya Pradesh, Chhattisgarh, and Odisha. Central India gets majority (over 80%) of its annual rainfall in the summer monsoon season (Gujarat: 96%, Goa: 90%, Maharashtra: 89%, Madhya Pradesh: 92%, Chhattisgarh: 90% and Odisha: 80%). The monsoonal rainfall in Central India is significantly influenced by synoptic-scale weather systems such as lows and depressions originating over the BoB. These systems contribute around 35–40% of the total summer monsoonal rainfall in the region, as reported by Vishnu et al. [2016].

The rainfall homogeneous region of South Peninsula comprises 8 meteorological subdivisions (Telangana, Rayalaseema, South Interior Karnataka, North Interior Karnataka, Coastal Karnataka, Coastal Andhra Pradesh, Kerala, and Tamil Nadu), 120 districts and covers ~19.3% of the geographical area of India. The western part of this region, i.e. the windward side of the Western Ghats, experiences a tropical wet climate. The climate transitions to arid on the leeward side of the Western Ghats and tropical wet and dry climate in farther east. Western Ghats play a dominant role in capturing moisture-laden winds from the Arabian Sea and causing heavy orographic rainfall in the windward side. South Peninsula gets a majority of rainfall during southwest monsoon season (Kerala: 68%, Karnataka: 74%, Andhra Pradesh: 57% and Telangana: 79% of annual rainfall) except Tamil Nadu, which receives most of its rainfall during northeast monsoon season (49% of annual rainfall).

There are some studies in which India is also divided into six [*Kale and Nagesh Kumar*, 2018; *Maity*, 2020; *Saini et al.*, 2022] regions grouping various states, in a manner slightly different from IMD. In this study, we have used the IMD system of four rainfall homogeneous regions.

To achieve the first thesis objective, a methodology has been proposed, which comprises of a bunch of statistical tools and has been discussed in detail in the next chapter.

Chapter 2

Proposed method

2.1. Data retrieval:

In our study, the daily observed gridded rainfall dataset of the IMD with a high spatial resolution (0.25° latitude \times 0.25° longitude) and a longer period of data availability (1901–2020) has been used [Pai *et al.*, 2014]. This gridded dataset is based on a total of 6955 rain gauge stations across India and was generated using all standard quality control measures viz. removal of coding and typing errors in the station data, missing data and duplicate station check, extreme value check, and homogenization. Shepard's inverse distance weighted interpolation (IDW) scheme [Shepard, 1968] is used for interpolating station rainfall data into $0.25^\circ \times 0.25^\circ$ regular grids, including the barriers and directional effects. A detailed description of the generation of this high-resolution daily gridded dataset for the Indian subcontinent (6.5 – 38.5° N and 66.5 – 100.5° E) is given in Pai *et al.*, [2014]. This daily gridded 120 years (1901–2020) rainfall dataset was downloaded in NetCDF format from the IMD (<http://www.imdpune.gov.in>) with the help of the IMDLIB package (<https://doi.org/10.5281/zenodo.4405233>) using Python software.

2.2. Conversion of gridded rainfall time series to district rainfall time series:

In our study, a district has been considered as the smallest geographical unit for rainfall pattern analysis because the larger regional rainfall pattern is an integration of smaller geographical unit. Further, a district is also the smallest administrative unit in India and it is desirable to analyse district rainfall climatology for better hydrological and water management, agricultural, and other administrative purposes [Guhathakurta and Rajeevan, 2008].

The daily district rainfall time series has been prepared from the daily gridded rainfall time series by an area-weighted average rainfall method [Pai et al., 2014], taking into consideration the grid boxes that lie inside the district boundary wholly or partially. The area weight allocated to each grid box is a multiplicative outcome of the fractional grid box area encircled by the district periphery and cosine of the latitude of its center point. The cosine factor is necessary for area compensation of high latitude grid boxes as the area decreases due to the convergence of the meridians. Accordingly, the area weighted rainfall has been computed as:

$$R_{(district)} = \sum A_i \times \cos(\theta_i) \times R_i$$

where $R_{(district)}$ is the rainfall of the district, A is the fractional area of the grid box covered by the district, θ is the latitude and R is the rainfall at the grid point (center) of the corresponding grid box i .

The daily rainfall time series of the district has been converted to seasonal rainfall time series using Python software. Summer monsoon rainfall time series is calculated by adding the daily rainfall values from June to September and analyzed further.

2.3. Multidecadal patterns in summer monsoon rainfall:

Each district's monsoonal rainfall time series is converted to rainfall anomaly time series, wherein rainfall anomaly is calculated as the percentage departure from climatological standard normal rainfall. The percentage departure of rainfall from climatological normal is used so that climatological rainfall trends of different time frames can be well compared. The average summer monsoon rainfall for 30 years, between 1961–1990, has been used as the climatological standard normal as suggested by the World Meteorological Organization (WMO) as a historical standard for supporting long-term climate change assessment [Organization, 2017]. We have adopted the 31-year moving average method to the rainfall

departure time series, which lucidly unravels the rainfall climatic trend at interdecadal (i.e., decadal to multidecadal) timescales [Mohapatra and Mohanty, 2007; Guhathakurta and Rajeevan, 2008; Mourato et al., 2010; Lupikasza, 2010; Preethi et al., 2011; Lee et al., 2012; Marani and Zanetti, 2015; Ghosh et al., 2016; Portela et al., 2020]. In climate studies, it is a common practice of using 30-year span for moving average analysis. Average of any climatological elements such as precipitation and temperature over this time span is referred to as “climate normal” by the World Meteorological Organization [Organization, 2017], which represents the climatic condition likely to be experienced at a given region. Moreover, the use of a 30-year period is a scientific convention based on the Central Limit Theorem, that at least 25 or 30 data points are required to obtain a reliable estimate of the mean and standard deviation [Hogg et al., 1977]. Therefore, in our study, we have computed 31-year averaged summer monsoon rainfall departure time series for trend analysis to represent a multi-year trajectory of rainfall amount change, which is an aspect of the climate system and unlikely to be caused by short-term (i.e., yearly) variability.

The moving average of rainfall percentage departure time series, in 1901–2020 dataset, for Bijapur district of Karnataka is shown in Fig. 2.1 as an example. The black curve denotes the 31- year moving average time series, which starts from 1916 and ends in 2005 because the averaged value over each successive 31-year window is placed at its centre. Accordingly, the first point (1916) is the midpoint of 1901–1931 time-window, and each successive point in the black curve is the mid-point of the next 31 years’ time window, with the last point (2005) being the midpoint of 1990–2020 time-window. Each bar in Fig. 2.1 represents total summer monsoon rainfall amount (mm) for each year, in which purple bar and pink bar, respectively, indicates year having rainfall higher and lower than the climatological standard rainfall (441.3 mm). The moving average pattern shows two decreasing trends in the initial and the final part with an increasing trend in between. A prominent low (valley) is seen in 1930s,

where the trend has changed from decreasing to increasing. Similarly, a prominent peak is observed in 1960s, where the trend has changed from increasing to decreasing.

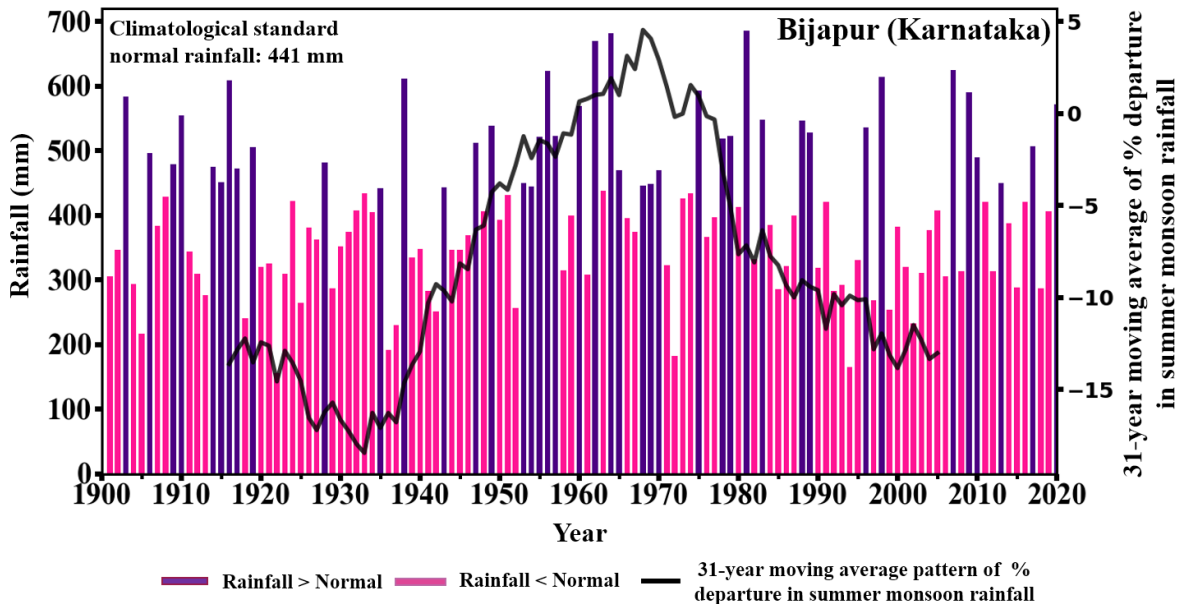


Fig. 2. 1 Time series in summer monsoon rainfall of Bijapur district (Karnataka) from 1901 to 2020 (represented by bars). Purple (pink) bars indicate higher (lower) rainfall than the climatological standard normal of 441 mm. The black curve shows the 31-year moving average pattern of % departure from the climatological standard normal. The overall pattern displays three distinct trends, with two decreasing trends alternating with an increasing trend. Rainfall trend reversals occurred in the 1930s and 1960s, evident from the inflection points (around valley and peak) in the moving average % departure pattern.

2.4. Rainfall pattern recognition:

Following three criteria have been conceived and adopted in this study for rainfall pattern recognition:

- a) Number of inflection points (IP)
- b) Type of inflection points
- c) Year of inflection point

An inflection point in a time series refers to the year around which the rainfall trend reverses, i.e., from decreasing to increasing or vice versa. This is the trend reversal point in the moving average percentage departure pattern. Identification of such points and the

corresponding year(s) in the time series is important as it signifies the prominent change in rainfall regime and the associated causal processes.

We have used 15-year of sliding trend (slope) analysis method [Kothawale *et al.*, 2010] (1916 to 1930; 1917 to 1931;; 1991-2005) in the time series of 31-year moving average % departure, for identification of the inflection points. The 15 years' trend (denoted by green squares in Fig. 2.2) has been placed at the midpoint of each successive 15 years' time window. Accordingly, the first point 1923 is the midpoint of 1916–1930 each successive point is the midpoint of next 15 years' time-window and the last point (1998) is the midpoint of 1991-2005. The inflection point is identified when the value of sliding trend changes the sign, i.e., from positive to negative or vice versa; and the same sign of trend is maintained at least for 10 consecutive years prior or after the year of inflection point. Accordingly, among the identified inflection years, those prior to 1926 and after 1995, have not been considered in order to obtain a pattern of at least a decade span. The rainfall departure pattern that does not have any inflection points is called a monotonic increasing or decreasing trend based on the sign of the sliding trend, where a positive sign signifies an increasing trend and a negative sign signifies a decreasing trend.

The rainfall departure trend of the Bijapur district (Fig. 2.2) reverses at two points and these are 1931 (identified by the upward arrow) and 1967 (identified by the downward arrow). These are the two inflection points in the moving average rainfall departure pattern of Bijapur. Before 1931, the sliding slope values are consistently negative and a decreasing trend is observed. After 1931, the trend is increasing up to 1967, and the sliding slope values are consistently positive. This increasing trend is followed by a decreasing trend after 1967, and the sliding slope values are consistently negative again.

There are two types of inflection points possible in this approach, which are named as Low-type (L-type) and High-type (H-type). L-type inflection point refers to a change in rainfall trend from decreasing to increasing (valley), and the H-type inflection point refers to a change in rainfall trend from increasing to decreasing (peak) (Fig. 2.2).

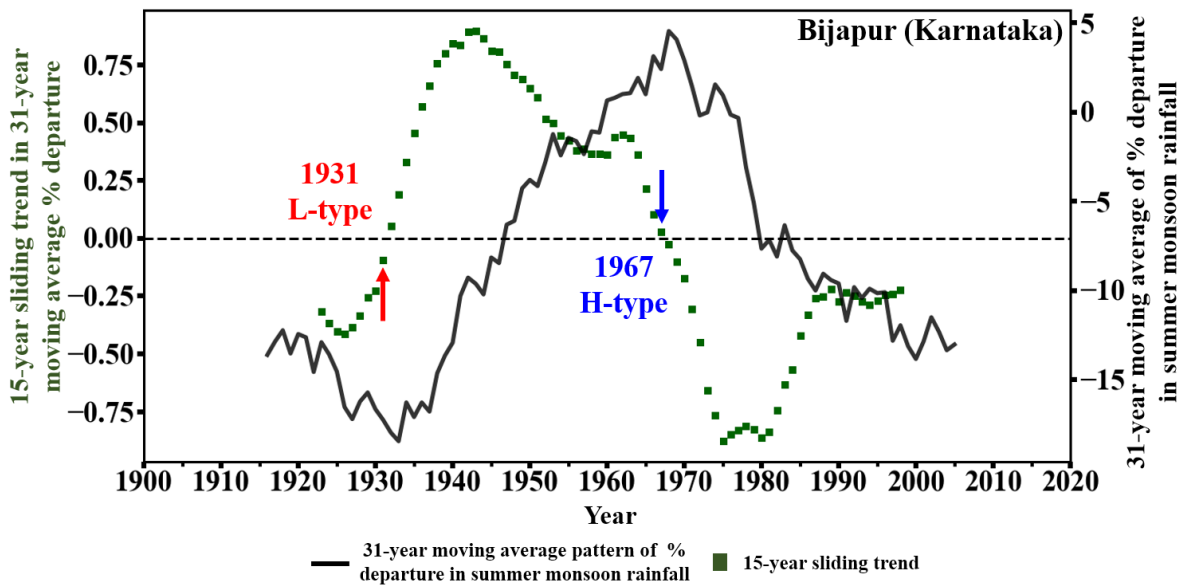


Fig. 2. 2 15-year sliding trend value (green squares) for the 31-year moving average of % departure in summer monsoon rainfall. Consistent positive values indicate increasing trend and negative values indicate decreasing trend. Inflection points, where the trend changes from positive to negative (H-type: 1967) or negative to positive (L-type: 1931), signify rainfall trend reversals.

15-year time window is chosen based on a sensitivity analysis using sliding trend windows of 5, 11, 15, 21, and 31 years in the moving average rainfall departure pattern. The results show that a 5-year sliding trend analysis produces scattered and inconsistent trend values, while a 31-year analysis fails to capture the pattern (the initial decreasing trend in Fig. 2.3f). The others (11,15,21, and 25-year) yield inflection years that are closely aligned. However, the inflection points identified using the 15-year window fall between those identified using the 11-year window on one side and the 21-year and 25-year windows on the other side. Consequently, the 15-year time span is chosen as it strikes a balance between

capturing trends accurately and maintaining consistency. It is noticed that using 11-year, 21-year, or 25-year windows instead of 15-year would not significantly alter the final results (Fig. 2.3).

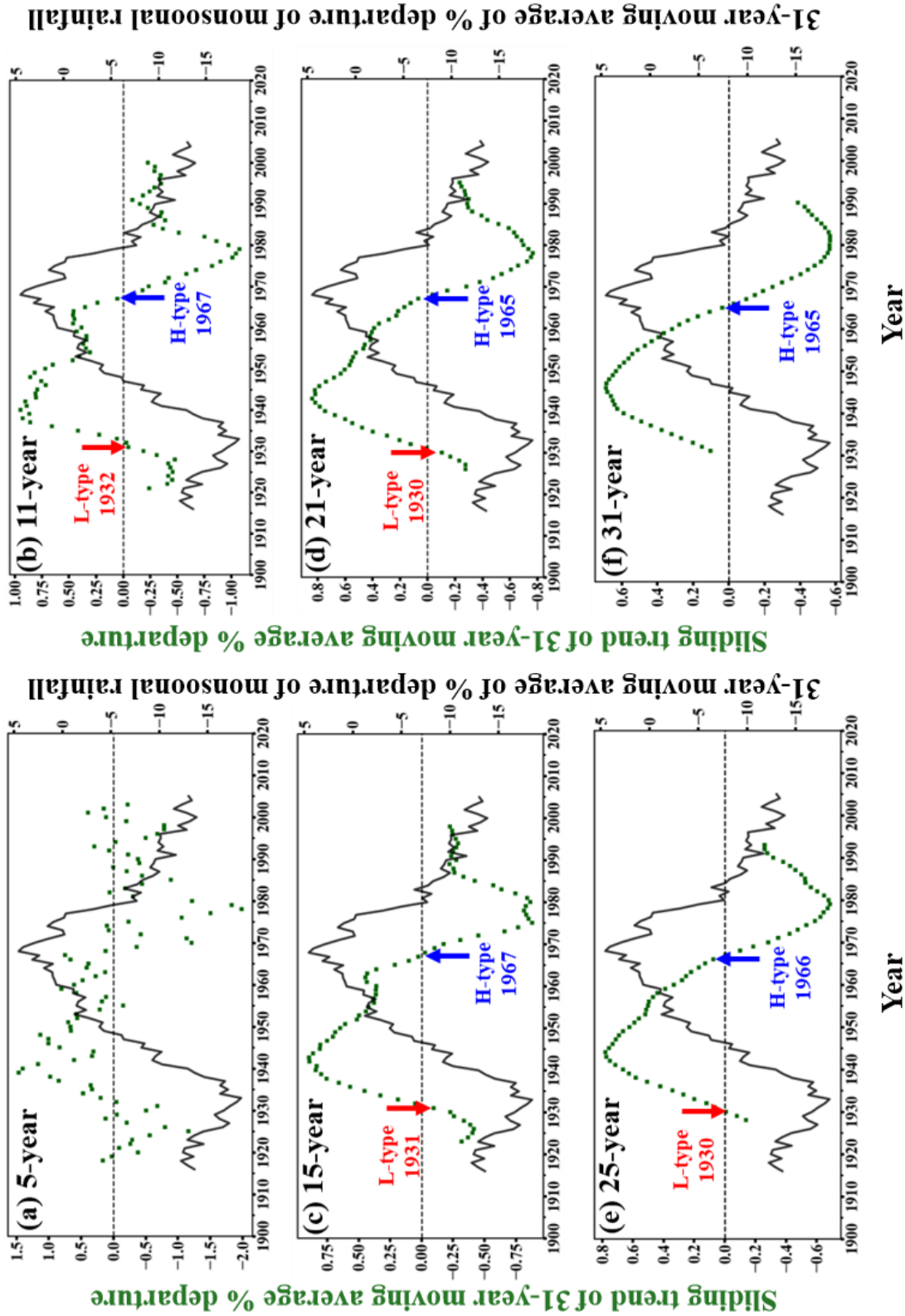


Fig. 2.3 (a) 5-year, (b) 11-year, (c) 15-year, (d) 21-year, (e) 25-year, and (f) 31-year sliding trend analysis in the moving average monsoonal rainfall % departure time series of Bijapur district, Karnataka.

It may be noted that due to spatio-temporal differences in rainfall variability, the identified year of inflection points for all the districts of a region may not necessarily coincide. Therefore, it is necessary to find out common time period of years in which majority of inflection points coincide, and hence that time period can be regarded as the one during which major change in rainfall trend occurred over the region. In order to mathematically identify such time period(s), both the types of inflection points (L-type and H-type) have been separately clustered by K-means clustering technique.

2.5. K-means clustering of inflection points:

K-means clustering is a classification method that divides a set of n observations (x_1, x_2, \dots, x_n) into mutually exclusive clusters (C_1, C_2, \dots, C_k), so that the observations within each cluster are similar to each other as much as possible, and as dissimilar as much as possible to the observations in other clusters. A cluster is defined by its center as the mean of observational data. This clustering technique uses an iterative algorithm to minimize the sum of squares of distances from each observation to its center over all clusters. For this study, observations (x_i to x_n) are years of inflection points for districts' moving average rainfall % departure pattern, and the cluster will be the time bracket in years, with its centre point, in which most of the years of inflection will coincide.

The formula for final cluster identification in the iteration method is:

$$\min \sum_{j=1}^K \sum_{i=1}^n ||x_i^{(j)} - c_j||^2$$

Here, $||x_i^{(j)} - c_j||$ is the distance between observation point $x_i^{(j)}$ and cluster center c_j in cluster j . This algorithm moves observations among the clusters until the sum cannot be decreased any further. Hence, similarities of observations within each cluster are strengthened

while dissimilarities among the observations of other clusters are maximized. This machine learning approach of clustering data points has widely been followed due to its simplicity of implementation [Ramos, 2001; Sönmez and Kömüscü, 2011; Zahmatkesh et al., 2015; Gupta and Jain, 2018].

2.6. Identification of optimal number of clusters:

K-means clustering technique is used for grouping all the identified L-type and H-type inflection points by using the 15-year sliding slope method for each region. The optimum number of clusters is identified from the K-means elbow method [Paul et al., 2022; Guerreiro Miranda et al., 2023].

A cluster centre would be representative when the data points will be normally distributed [Mishra et al., 2019]. Normality check is performed through z-score using skewness and kurtosis [Kim, 2013; Mishra et al., 2019] for each identified cluster to ensure its normal distribution. Skewness and excess kurtosis are both sensitive to outliers and small sample sizes. Additionally, standard error also depends on sample size, and it decreases with increasing sample size. In view of the above limitations, a Z-test for normality is performed using skewness and excess kurtosis, to ensure the normality at 0.05 level of confidence (Mishra et al. 2019). A Z-score could be obtained by dividing the skewness value or excess kurtosis value with their standard errors.

$$Z = \frac{\text{Skew value}}{SE_{\text{skewness}}}$$

$$Z = \frac{\text{Excess kurtosis}}{SE_{\text{excess kurtosis}}}$$

The threshold value at 0.05 alpha level is ± 1.96 for small sample size ($n < 50$) and ± 3.29 for medium sample size ($50 < n < 300$). If the Z-score is beyond the threshold value, then the null hypothesis will be rejected and the distribution is concluded as non-normal [Kim, 2013]. In our study the final cluster number in both L-type and H-type inflection points is

decided based on the normality test performed on the clusters identified using the elbow method.

However, K-means clustering may encounter limitations, including the subjective determination of the ideal number of clusters using the elbow method and convergence towards different cluster centroids based on the initial randomly chosen centroids. These limitations introduce subjectivity into the K-means algorithm, such as sensitivity of centroids and overlapping of cluster members. To address this, a two-sample Student's *t*-test is performed to examine whether the clusters of L-type/H-type inflection points obtained for each region significantly differ from each other.

2.7. Identification of prominent clusters:

To identify the prominent clusters among the optimum number of clusters of L-type and H-Type inflection points for each region, an additional area-based criterion was used, according to which a cluster has been considered prominent if the sum of areas of districts under that cluster represents at least one-third (33%) of the total regional area. The centers (calculated as district weighted mean of the cluster range of years) of these prominent clusters have been considered as the prominent trend reversal event for each region.

Multiple checkpoints are kept in the methodology to ensure mathematical accuracy and statistical significance, and to assure that the rainfall trend reversals have been genuinely identified in this study.

Additionally, we have conducted another exercise, where we have superimposed the normalised frequency of H-type/L-type inflection points. The superimposition is organized in three ways:

- (i) Pairs consisting of only H-type inflection points from the regions (6 pairs: northeast & south peninsula, northeast & central, northeast & central, south peninsula & central, south peninsula & northwest, central & northwest).
- (ii) Pairs consisting of only L-type inflection points from the regions (6 pairs: northeast & south peninsula, northeast & central, northeast & central, south peninsula & central, south peninsula & northwest, central & northwest).
- (iii) Pairs consisting of an L-type inflection point from one region with an H-type inflection point from another region (12 pairs: northeast L-type & south peninsula H-type, northeast L-type & central H-type, northeast L-type & northwest H-type, south peninsula L-type & northeast H-type, south peninsula L-type & central H-type, south peninsula L-type & northwest H-type, central L-type & northeast H-type, central L-type & south peninsula H-type, central L-type & northwest H-type, northwest L-type & northeast H-type, northwest L-type & south peninsula H-type, and northwest L-type & central H-type).

The motive behind this exercise is to examine if the superimposition of frequency of inflection points is heightened which indicates prominence. Heightened superimposed frequency between inflection points of similar nature (H-type with H-type/L-type with L-type) suggests a coherent pattern whereas heightened frequency between inflection points of opposite nature (L-type with H-type) suggests a dipole pattern.

2.7. Cramer's *t*-test:

Cramer's *t*-test is a standard test of significance to analyse the stability of the climate and to prove climate variability [*Mitchell Jr*, 1966]. It is a moving *t* statistic that compares the mean of each successive time window period with the mean of entire period [*Lawson et al.*, 1981]. It helps to isolate significant periods of abnormal averages, if any. The peculiar features

of atmospheric circulation can be explored against the background of these periods of abnormal average [Mooley and Parthasarathy, 1984].

In this study, the mean, \bar{x} and the standard deviation, S , are calculated for each district rainfall series for total number of years, N (120 years), under investigation. This long-term average has been compared with each successive n -year period's (31-years) rainfall average, \bar{x}_k through the t -statistics. The Cramer's t -value (t_k) is computed as,

$$t_k = \left(\frac{n(N-2)}{N-n(1+\tau_k^2)} \right)^{\frac{1}{2}} \tau_k$$

where τ_k is a standardized measure of difference between averages given as,

$$\tau_k = \frac{(\bar{x}_k - \bar{x})}{S}$$

For the significance of Cramer's t -value at 95% confidence level, the required threshold Cramer's t -value is ± 1.96 [Mooley and Parthasarathy, 1984]. One example of this test is shown for the Bijapur district (Fig. 2.4), where maroon dots represent Cramer's t -values and the maroon lines denote the 95% confidence level threshold value (± 1.96).

Local maxima or local minima in the long-term rainfall pattern are identified by the years of H-type or L-type of inflection points in which rainfall is, respectively, higher or lower than the adjacent time periods. The local maxima or minima signifies climate extremes only if rainfall maxima or minima is significantly higher or lower than the long-term average (1901-2020 summer monsoon rainfall average). In order to ascertain that the identified local maxima (minima) in rainfall is significantly higher (lower) than the long-term average rainfall, the Cramer's t -test is used in our study. Thus, the Cramer's t -test ascertains if the year of inflection point actually represents the year of significantly higher (lower) rainfall than the long-term climatological mean rainfall or just the year of rainfall trend reversals. For example, for Bijapur

district (Fig. 2.4), it has been ascertained based on the Cramer's t -test that the L-type (H-type) inflection point in year 1931 (1967) actually represents the climate extreme of anomalously lower (higher) rainfall compared to the long-term average rainfall.

A flow chart of this complete methodology of identifying trend reversal and anomalous years in the long-term pattern of summer monsoon rainfall is presented in Fig. 2.5.

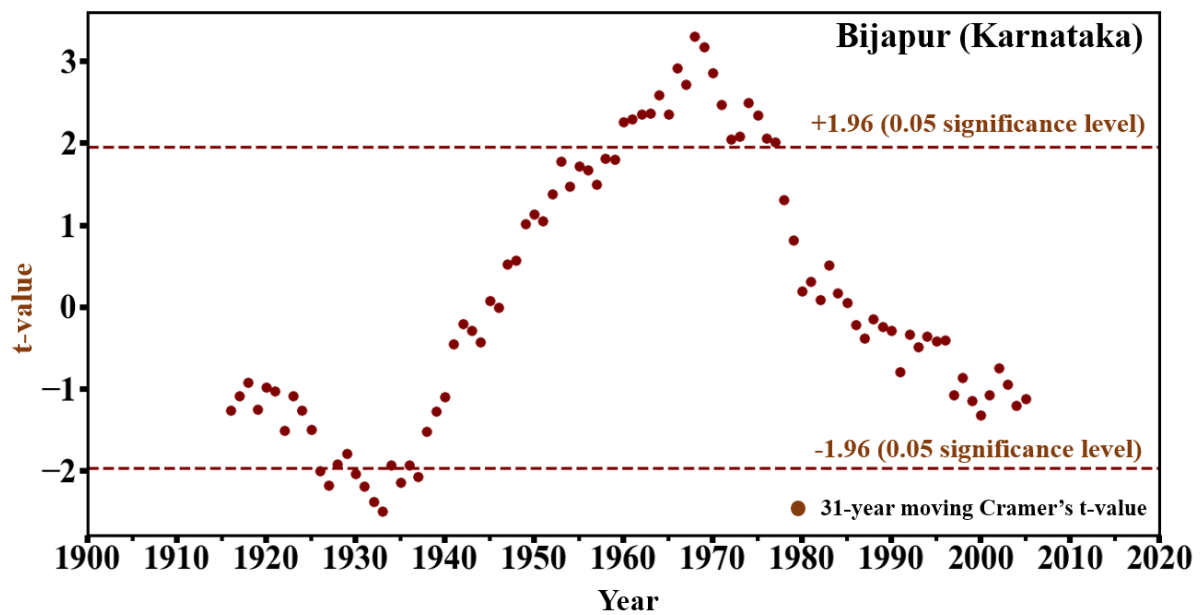


Fig. 2. 4 31-year moving Cramer's t -value (maroon dots). Years with t -values beyond ± 1.96 (significant at 0.05) indicate extreme rainfall significantly higher or lower than the long-term (1901–2020) average. 1931 and 1967 are not only point of rainfall trend reversal but also year of extreme rainfall for Bijapur district, as the climatological rainfall is significantly lower and higher respectively, than the long-term average.

Using the robust methodology as discussed above, prominent summer monsoon rainfall trends and trend reversal events have been identified in the four rainfall homogeneous regions of India, which are discussed in the next chapter.

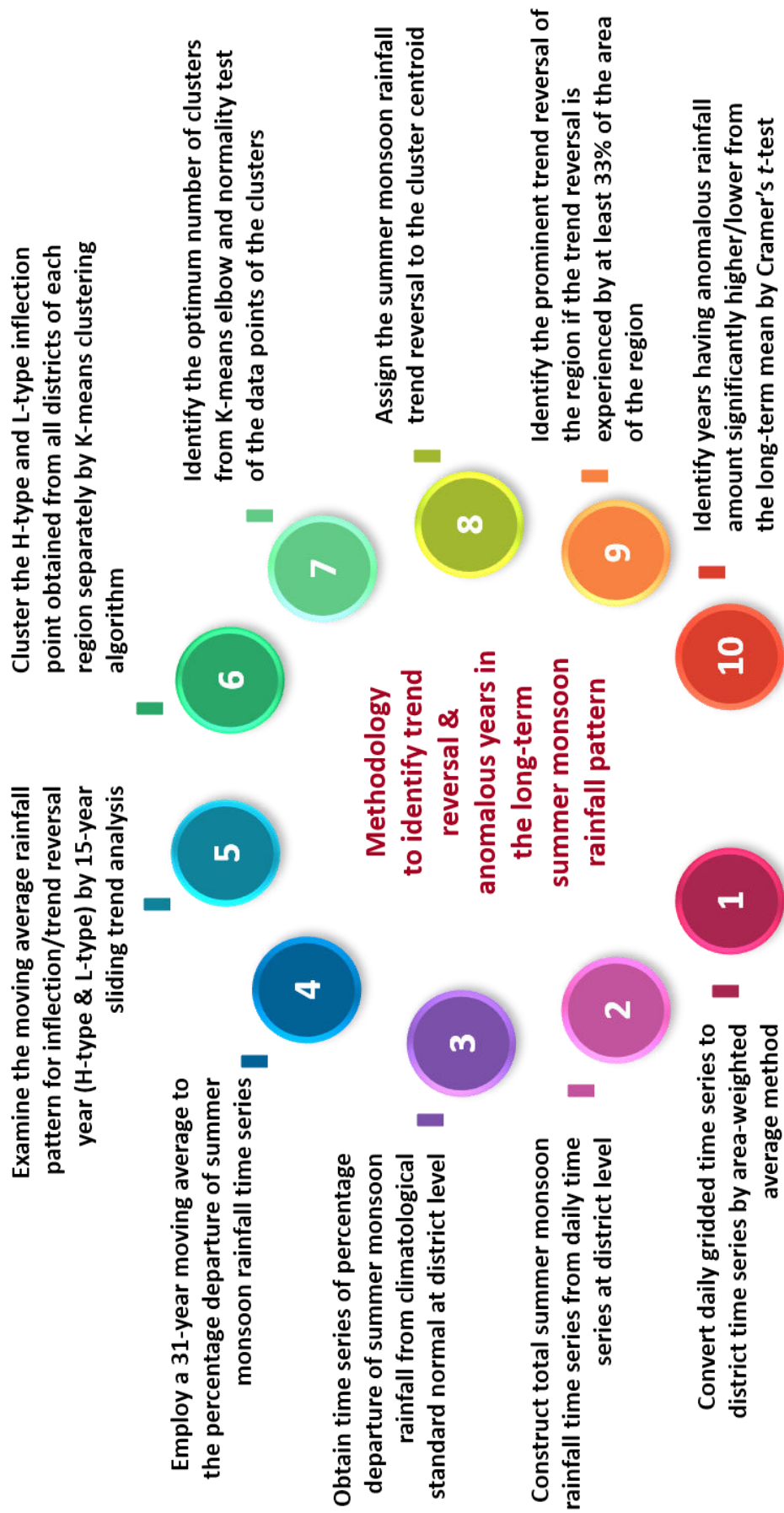


Fig. 2. 5 Methodology flow chart for identification of trend reversal and anomalous years in the long-term summer monsoon rainfall pattern.

Chapter 3

Prominent summer monsoon rainfall trends and trend reversal events observed in four rainfall homogeneous regions of India

The methodology described in the previous chapter has been used to identify and analyze the inflection points within the rainfall patterns across the four rainfall homogeneous regions of India, encompassing a total of 678 districts. Among these districts, 18 displayed a monotonically increasing or decreasing trend in the 31-year moving average rainfall departure. Additionally, 58 districts exhibited a fluctuating pattern in their 31-year moving rainfall departure, characterized by frequent changes in the sliding trend's sign, indicating an erratic rainfall pattern over short period. This inconsistency is termed a non-systematic pattern within this study, posing challenges in pinpointing precise inflection points in the 31-year moving average rainfall departure pattern in these districts. Conversely, the remaining 602 districts demonstrated a systematic rainfall pattern, with consistently positive or negative sliding trend values and a clear change in trend sign at certain points, facilitating the accurate identification of inflection points. The distribution of districts exhibiting the aforementioned rainfall patterns across regions is detailed in Table 3.1.

Table 3. 1 The total number of districts of each region along with the districts having monotonic trends lacking inflection points, exhibiting non-systematic trends, and where inflection points were identified in the moving average rainfall departure patterns and studied further.

Region	Total District	Districts having a monotonic trend	Districts having a non-systematic trend	Districts having systematic trends with inflection points
Northwest	205	5	19	181
Central	178	4	6	168
Northeast	175	3	19	153
South peninsula	120	6	14	100
Total	678	18	58	602

3.1. Distribution of inflection points:

The distribution of L-type and H-type inflection points in 31-year moving average curve of rainfall departure from climatological normal for 601 districts distributed over four rainfall homogeneous regions of India, as identified from sliding trend analysis, is shown in northeast. 3.1(a-d) through histograms for each region. In this histogram plot, each bar represents the total number of districts (y-axis) having H-type or L-type of inflection points for a particular year (x-axis). Histograms in Fig. 3.1(a-d) reveal that the inflection points of H- and L-type are grouped around a narrow temporal range (~ 2 decades) in the northeast and south peninsula (Fig. 3.1c&d) but spread over a much wider temporal range in northwest and central India (Fig. 3.1a&b).

In the northeast region (Fig. 3.1c), two distinct groups of H-type inflection points are separated by one distinct group of L-type inflection points. These three groups of inflection points indicate at least three rainfall trend reversals from 1901 to 2020 in a sequence of “increase-decrease-increase-decrease” in rainfall trend, along with its approximate time window. In the south peninsula (Fig. 3.1d), the opposite pattern is seen, i.e., two distinct groups of L-type inflection points are separated by one distinct group of H-type inflection points. This also indicates at least three rainfall trend reversals along with their approximate time windows but in an opposite sequence of trend reversal (decrease-increase-decrease-increase).

In south India (Fig. 3.1b) one large group of H-type inflection points and one large group of L-type inflection points are spread over a long period of several decades indicating at least two rainfall trend reversals. However, since the years of inflection points are spread over a very long period, it is not possible to identify a specific time window when rainfall trends are reversed. In the northwest region (Fig. 3.1a), the distinct groups of H-type and L-type inflection points are not identifiable since they are spread over the entire time series. Additionally, both

the H- and L-type inflection points are observed during the same years in different districts. This suggests geographical inhomogeneity in rainfall with different rainfall patterns observed in different districts during the same years.

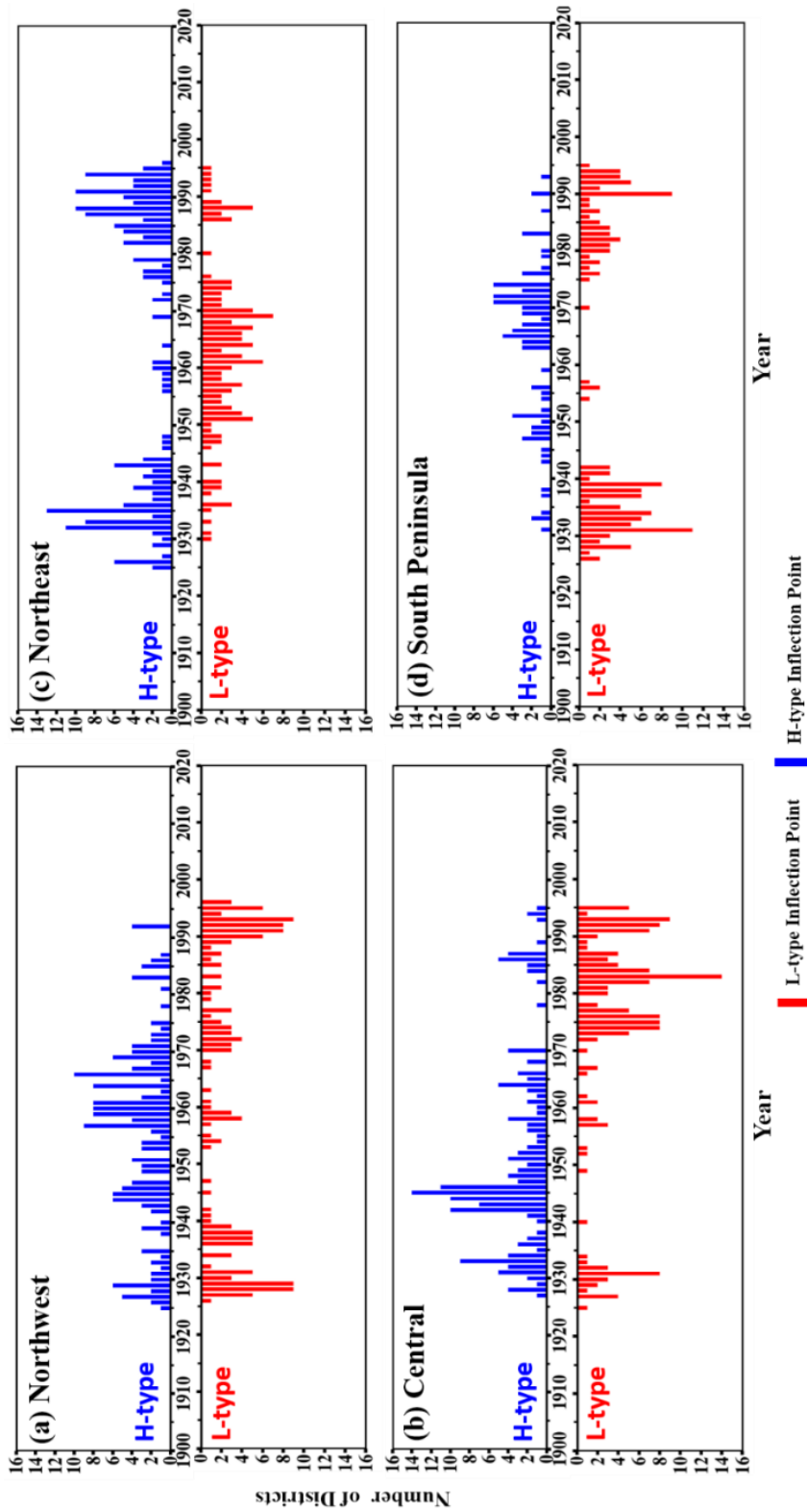


Fig. 3. 1 Histogram plot of H-type (peak between an increasing and a decreasing trend; blue bar) and L-type (valley between a decreasing and an increasing trend; red bar) inflection points identified from the districts' moving average % departure patterns of summer monsoonal rainfall coming under (a) northwest, (b) central, (c) northeast, (d) south peninsular India. Each bar corresponding to a specific year indicates the number of districts experiencing an inflection point in that particular year.

3.2. Identification of optimal number of clusters:

To mathematically identify the statistically significant and distinct time windows of rainfall trend reversals from the year wise distribution of L-type and H-type inflection points (Fig. 3.1a-d), K-means clustering using elbow method, and normality check of clusters through skewness and excess kurtosis was performed, following detailed methodology discussed in Chapter-2. This revealed that the optimum number of clusters for both L- and H-type inflection points for each region works out to be three. This indicates that each of the four regions has experienced three rainfall trend reversals, although it cannot be discerned visually for the northwest (Fig. 3.1a) and central India (Fig. 3.1b). It is necessary to reiterate that three rainfall trends are even visually identifiable for the northeast (Fig. 3.1c) and south peninsula (Fig. 3.1d). The final number of optimal clusters, their ranges, centers, skewness, kurtosis, standard errors, and Z-scores are shown in Table 3.2.

These three optimal clusters of both L- and H-type (i.e. total 6 clusters in each region) identified for each of the four regions, represent rainfall trend reversal events. However, these trend reversal events are obviously of different magnitudes affecting variable percentages of geographical areas of the respective region. Therefore, it is also necessary to ascertain which among these six identified optimal rainfall trend reversals in each region, are prominent ones, affecting a substantial area (at least 33%) of a given region.

Table 3. 2 Cluster range, cluster center, skewness, excess kurtosis, their standard errors, and Z-scores of all H-type and L-type clusters for four rainfall homogeneous regions of India.

Northwest											
H-type											
Cluster No.	Size	Cluster Range	Cluster Center	Skewness	Standard Error	Z-Score	Excess Kurtosis	Standard Error	Z-Score		
1.	61	1925-1949	1938	-0.20	0.31	0.64	-1.56	0.60	2.60		
2.	98	1950-1972	1962	-0.12	0.24	0.50	-0.81	0.48	1.68		
3.	21	1973-1992	1983	-0.17	0.50	0.34	-1.00	0.97	1.03		
L-type											
Cluster No.	Size	Cluster Range	Cluster Center	Skewness	Standard Error	Z-Score	Excess Kurtosis	Standard Error	Z-Score		
1.	59	1926-1947	1933	0.65	0.31	2.09	-0.50	0.61	-0.81		
2.	39	1953-1977	1967	-0.40	0.38	-1.05	-1.38	0.74	1.86		
3.	55	1981-1996	1991	-1.04	0.32	-3.25	0.72	0.63	1.14		

Table 3. 2 Continuing

Central										
H-type										
Cluster No.	Size	Cluster Range	Cluster Center	Skewness	Standard Error	Z-Score	Excess Kurtosis	Standard Error	Z-Score	
1.	104	1927-1950	1940	-0.55	0.24	2.29	-1.09	0.47	2.31	
2.	42	1951-1970	1960	0.00	0.37	0.00	-1.20	0.72	1.67	
3.	20	1978-1995	1987	0.32	0.51	0.62	0.05	0.99	0.05	
L-type										
Cluster No.	Size	Cluster Range	Cluster Center	Skewness	Standard Error	Z-Score	Excess Kurtosis	Standard Error	Z-Score	
1.	24	1925-1934	1930	-0.50	0.47	1.06	-0.40	0.92	0.44	
2.	14	1949-1967	1959	-0.04	0.60	-0.07	-0.79	1.15	-0.69	
3.	118	1970-1995	1983	0.09	0.22	0.41	-1.22	0.44	-2.77	

Table 3. 2 *Continuing*

H-type										
Cluster No.	Size	Cluster Range	Cluster Center	Skewness	Standard Error	Z-Score	Excess Kurtosis	Standard Error	Z-Score	
1.	81	1925-1948	1935	0.18	0.27	0.67	-0.46	0.53	0.87	
2.	22	1956-1978	1968	-0.24	0.49	0.49	-1.59	0.95	1.67	
3.	85	1979-1996	1988	-0.29	0.26	1.11	-0.65	0.52	1.25	
L-type										
Cluster No.	Size	Cluster Range	Cluster Center	Skewness	Standard Error	Z-Score	Excess Kurtosis	Standard Error	Z-Score	
1.	37	1930-1955	1946	-0.60	0.39	1.50	-1.00	0.76	1.31	
2.	72	1956-1976	1966	0.00	0.28	0.00	-0.94	0.56	1.67	
3.	18	1980-1995	1989	-0.21	0.54	0.39	0.61	1.04	0.59	

Northeast

Table 3. 2 Continuing

South peninsula										
H-type										
Cluster No.	Size	Cluster Range	Cluster Center	Skewness	Standard Error	Z-Score	Excess Kurtosis	Standard Error	Z-Score	
1.	26	1931-1956	1946	-0.72	0.46	1.57	-0.60	0.89	0.67	
2.	51	1959-1977	1969	-0.25	0.33	0.76	-0.79	0.66	1.19	
3.	9	1979-1993	1985	0.25	0.72	0.35	-1.28	1.40	0.12	
L-type										
Cluster No.	Size	Cluster Range	Cluster Center	Skewness	Standard Error	Z-Score	Excess Kurtosis	Standard Error	Z-Score	
1.	74	1926-1942	1934	0.06	0.28	0.21	-0.96	0.55	1.74	
2.	5	1954-1970	1959	1.39	0.91	1.52	0.12	2.00	0.06	
3.	55	1975-1995	1986	-0.29	0.32	0.90	1.18	0.63	1.87	

3.3. Identification of prominent clusters:

To identify the prominent clusters of L-type and H-Type inflection points, from the six optimal clusters available for each of the regions, an additional area-based criterion was used, according to which a cluster has been considered prominent if the sum of areas of districts under that cluster represents at least one-third (33%) of the total regional area. The Fig. 3.2 shows the range of years for each cluster (cluster range); year of trend reversal (cluster centre: calculated as district weighted mean of the cluster range of years); % of total number of affected districts in the region; and the % of total geographical area of affected districts in the region.

As per the area-based criteria, two H-type clusters [(range: 1925–1948; center: 1935; area: 49%) and (range: 1979–1996; center: 1988; Area: 43%)] and one L-type cluster (range: 1956–1976; center: 1966, area: 38%) have been identified as prominent clusters in the northeast India (Fig. 3.2c). In contrast, in south peninsula, one H-type cluster (range: 1959–1977; center: 1969; area: 45%) and two L-type clusters [(range: 1926–1942; center: 1934; area: 67%) and (range: 1975–1995, center: 1986; area: 45%)] are identified as prominent clusters (Fig. 3.2d).

In northwest India, one H-type cluster (range: 1950–1972, center: 1962; area: 37%) and one L-type cluster (range: 1981–1996; center: 1991; area: 32%) are prominent (Fig. 3.2a). It is to be noted that in northwest India area covered for the L-type cluster is only fractionally less than the benchmark of 33%, but since it also coincides in time with prominent L-type clusters in central and south peninsula, it was considered as prominent. Similarly, in central India, one H-type cluster (range: 1927–1950, center: 1940; area: 62%) and one L-type cluster (range: 1970–1995; center: 1983; area: 74%) are identified as prominent clusters (Fig. 3.2b).

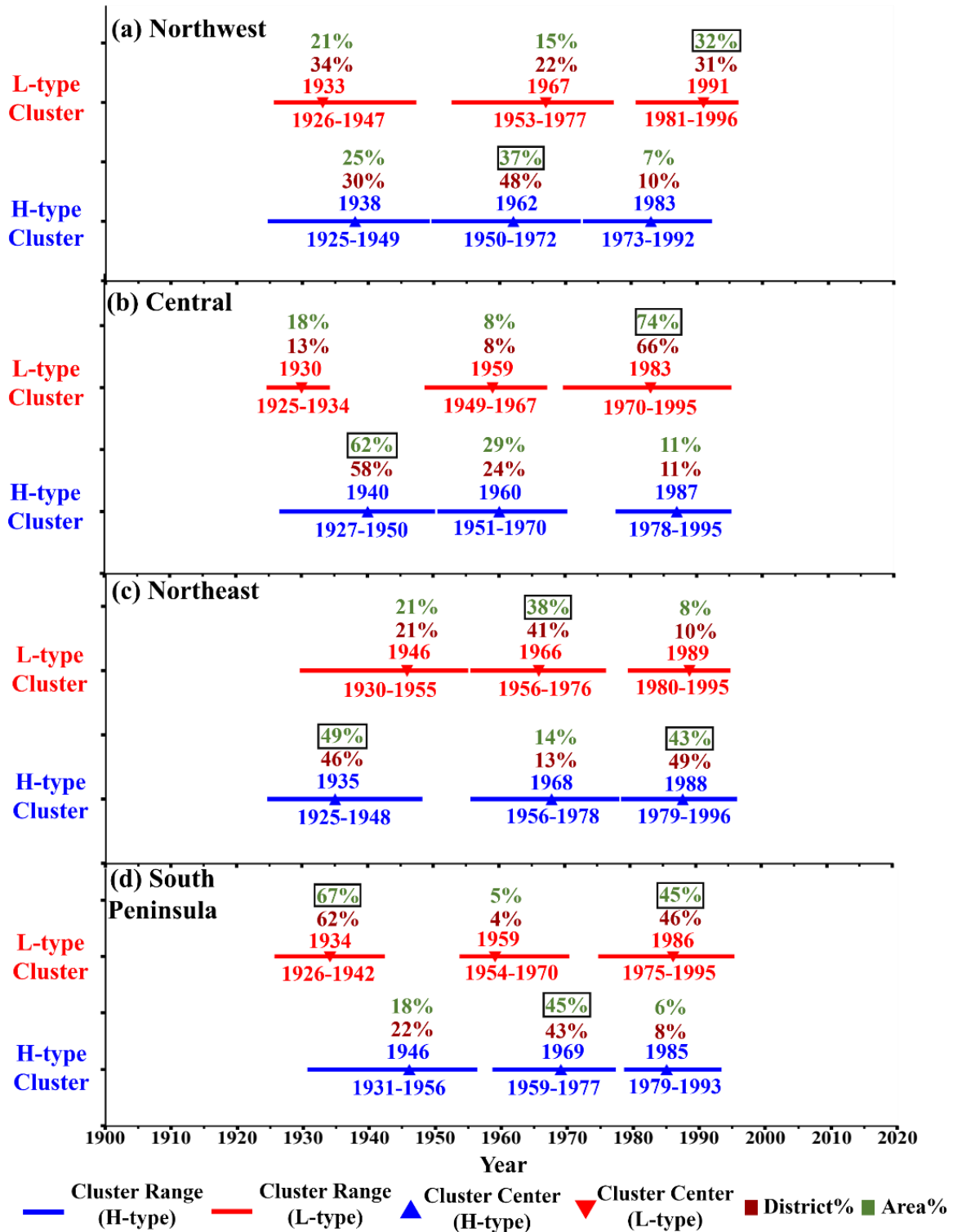


Fig. 3. 2 Cluster range, cluster center, district and area covered by each cluster in terms of percentage of six L-type and H-type clusters identified from K-means clustering technique for (a) northwest, (b) central, (c) northeast, (d) south peninsular India. The green-colored numbers denote the percentage of area covered, while maroon-colored numbers represent the percentage of districts of the region. Clusters highlighted with a rectangle, indicating prominent clusters.

In Fig. 3.3a-d the centers of all prominent clusters for each region are shown. These cluster centres represent major trend reversal points in the rainfall history of India during 1901-2020. Thus, in northeast India (Fig. 3.3c), the multidecadal summer monsoon rainfall since 1901 has undergone three major trend reversals as follows: (1) from increasing to decreasing rainfall trend around 1935; (2) from decreasing to increasing rainfall trend around 1966; (3) from increasing to decreasing rainfall trend around 1988.

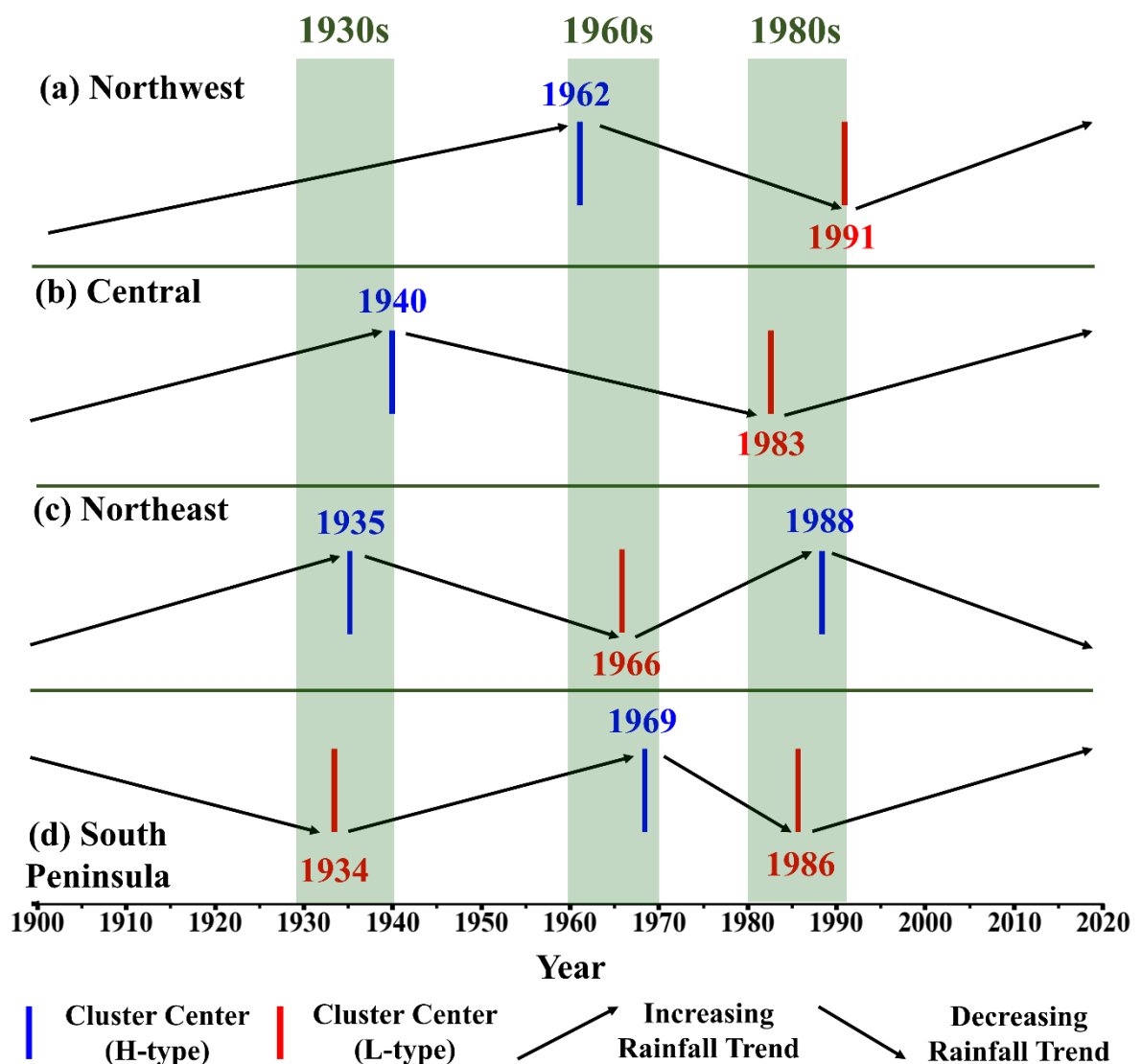


Fig. 3. 3 The prominent summer monsoon rainfall trend reversals and rainfall trends observed in (a) northwest, (b) central, (c) northeast, and (d) south peninsular India. The identified trend reversals are categorized into three periods: the 1930s, 1960s, and 1980s.

The rainfall in northwest India has undergone two major trend reversals (Fig. 3.3a), namely, (1) from increasing to decreasing trend around 1962; and (2) from decreasing to increasing trend around 1991.

The rainfall in central India (Fig. 3.3b), has also undergone two trend reversals, namely, (1) from increasing to decreasing trend around 1940; and (2) from decreasing to increasing trend around 1983.

The rainfall in the south peninsula has undergone three major trend reversals (Fig. 3.3d) in the rainfall history, namely, (1) from a decreasing to an increasing trend around 1934; (2) from an increasing to a decreasing trend around 1969; and (3) from decreasing to increasing trend around 1986.

One of the most important outcomes of this study (Fig. 3.3) is that there are three distinguishable decades, during which a large geographical area of India experienced reversals in the rainfall trend in the 120 years of records in India. During the decades of the 1930s, and 1960s three out of four rainfall homogenous regions of India experienced rainfall trend reversals. It is also evident that the decade of the 1980s was the most widespread in terms of rainfall variability in India because the rainfall in all the four rainfall-homogeneous regions of India has undergone major trend reversals during this decade. Three regions (northwest, central, and south peninsula) witnessed the rainfall trend reversal from decreasing to increasing but the rainfall in the other region (northeast) underwent the opposite trend reversal i.e. from increasing to decreasing trend. In other words, rainfall in the northwest, central, and south peninsula tended to increase from the 1980s onwards, the northeast India had an opposing tendency of decreasing from the 1980s onwards.

Apart from the identification of prominent rainfall trend reversals in the long-term data, it is also important to examine the severity of change in the rainfall amount associated with the identified prominent trend reversal, using Cramer's *t*-test. The motive of performing Cramer's *t*-test is to additionally examine if the rainfall in the trend reversal years is significantly different (higher or lower) from long-term average rainfall.

It is observed that, for a given cluster of H-type (L-type) inflection years, rainfall in the inflection years of some districts is higher (lower) compared to the long-term average at a 95% confidence level. It is important to reiterate that regardless of whether the rainfall during the inflection year is significantly different from the long-term average or not, the fact remains that the inflection year demarcates the systematic change in the rainfall trend. In Table 3.3, the number and area proportion of such districts having rainfall in the inflection year significantly different from the long-term average for region-wise prominent clusters is presented.

In the 1930s trend reversal, during which the rainfall trend changed from increasing to decreasing in northeast and central India, and decreasing to increasing in south peninsular India, 30-40% of districts of the region have rainfall significantly different (wetter in northeast and central India, and dryer in south peninsular India) from the long-term average, affecting 30-50% of the geographical area of the region.

In the 1960s trend reversal, during which the rainfall trend changed from increasing to decreasing trend in northwest and south peninsular India, and decreasing to increasing trend in northeast India, 10-30% of districts of the region have rainfall significantly different (wetter in northwest and south peninsular India, and dryer in northeast India) from the long-term average, affecting 10-20% of the geographical area of the region.

Similarly in the 1980s trend reversal, during which the rainfall trend changed from decreasing to increasing in northwest, central, and south peninsular India, and increasing to decreasing trend in northeast India, 5-25% of districts of the region had rainfall significantly different (drier in northwest, central, and south peninsular India, and wetter in northeast India) from the long-term average affecting up to 25% of the geographical area of the region.

From the above-mentioned insights and observations from Cramer's *t*-test, it is inferred that the three identified trend reversals in the 1930s, 1960s, and 1980s are crucial for highlighting systematic changes in long-term rainfall in India. Further, Cramer's *t*-test proves that the rainfall trend reversals during the decade of 1930s are far more severe compared to that in the 1960s and 1980s as the number of districts and the areas experiencing significant variation in rainfall amount (compared to the long-term average) is higher in 1930s than the other two decades. In other words, the rainfall trend reversal during the period around the 1930s was the most severe in the last 120 years of Indian summer monsoon rainfall history.

Table 3. 3 Number of districts and its percentage to the total number of districts of the region, area of districts and its percentage to the total area of the region, having inflection points and rainfall at the inflection years significantly different from the long-term average, within the prominent clusters.

Region	Range of prominent clusters of inflection points Cluster center (H) = H-type cluster (L) = L-type cluster	Number of districts having inflection point within the cluster (% of total district in region)	Number of districts having rainfall in the inflection years significantly different from long-term average (% of total districts in region)	Area (km ²) of districts having inflection point within the cluster (% of total area in region)	Area of districts having rainfall in the inflection years significantly different from long-term average (% of total area in region)
(a)	(b)	(c)	(d)	(e)	(f)
Northwest Total districts: 205 Total area: 1.01 × 10 ⁶ km ²	1950-1972 1962 (H)	98 (48%)	46 (22%)	3.73 × 10 ⁵ (37%)	1.18 × 10 ⁵ (12%)
	1981-1996 1991 (L)	55 (27%)	15 (7%)	3.21 × 10 ⁵ (32%)	5.46 × 10 ⁴ (5%)
Central Total districts: 178 Total area: 1.10 × 10 ⁶ km ²	1927-1950 1940 (H)	104 (58%)	70 (39%)	6.87 × 10 ⁵ (62%)	4.69 × 10 ⁵ (43%)
	1970-1995 1983 (L)	118 (66%)	38 (21%)	8.16 × 10 ⁵ (74%)	2.31 × 10 ⁵ (21%)

Table 3. 3 continuing

Region	Range of prominent clusters of inflection points Cluster center (H) = H-type cluster (L) = L-type cluster	Number of districts having inflection point within the cluster (% of total district in region)	Number of districts having rainfall in the inflection years significantly different from long-term average (% of total districts in region)	Area (km ²) of districts having inflection point within the cluster (% of total area in region)	Area of districts having rainfall in the inflection years significantly different from long-term average (% of total area in region)
(a)	(b)	(c)	(d)	(e)	(f)
Northeast Total districts: 175 Total area: $5.51 \times 10^5 \text{ km}^2$	1925-1948 1935 (H)	81 (46%)	52 (30%)	2.68×10^5 (49%)	1.72×10^5 (31%)
	1956-1976 1966 (L)	72 (41%)	25 (14%)	2.08×10^5 (38%)	7.63×10^4 (14%)
	1979-1996 1988 (H)	85 (49%)	18 (10%)	2.36×10^5 (43%)	5.51×10^4 (10%)
South Peninsula Total districts: 119 Total area: $6.38 \times 10^5 \text{ km}^2$	1926-1942 1934 (L)	74 (62%)	36 (30%)	4.28×10^5 (67%)	2.43×10^5 (38%)
	1959-1977 1969 (H)	51 (43%)	12 (10%)	2.85×10^5 (45%)	6.76×10^4 (11%)
	1975-1995 1986 (L)	55 (46%)	7 (6%)	2.87×10^5 (45%)	10^4 (4%)

3.4. Superimposed normalized frequency of inflection points:

We have superimposed the normalized frequency of H-type/L-type inflection points between the regions pairwise to examine if the superimposition of the frequency of inflection points is heightened which indicates prominence.

We observed amplified superimposed frequency during the time window where prominent trend reversal events were identified, marked by ticks in Fig. 3.4. In pairs of H-type inflection points (Fig. 3.4a), peaks were observed in the 1930s for northeast & central, and central & northwest pairs, and in the 1960s for the south peninsula & northwest pair. For L-type inflection point pairs (Fig. 3.4b), peaks were observed in the 1930s for south peninsula & central, and south peninsula & northwest pairs, and in the 1980s for south peninsula & central, south peninsula & northwest, and central & northwest pairs. These peaks signify coherence in rainfall trend reversals among regions.

An asymmetric rainfall pattern is discerned from the peaks of superimposed frequency between northeast L-type & south peninsula H-type, northeast L-type & northwest H-type in the 1960s (Fig. 3.4ci), south peninsula L-type & northeast H-type in the 1930s and 1980s, and south peninsula L-type & central H-type in the 1930s (Fig. 3.4cii), central L-type & northeast H-type in the 1980s (Fig. 3.4ciii), northwest L-type & northeast H-type in the 1980s (Fig. 3.4civ). This analysis corroborates the conclusions drawn regarding the prominent cluster and trend reversals obtained from the methodology utilized in the study. Thus, this exercise proves the robustness of the prominent clusters identified by the current study.

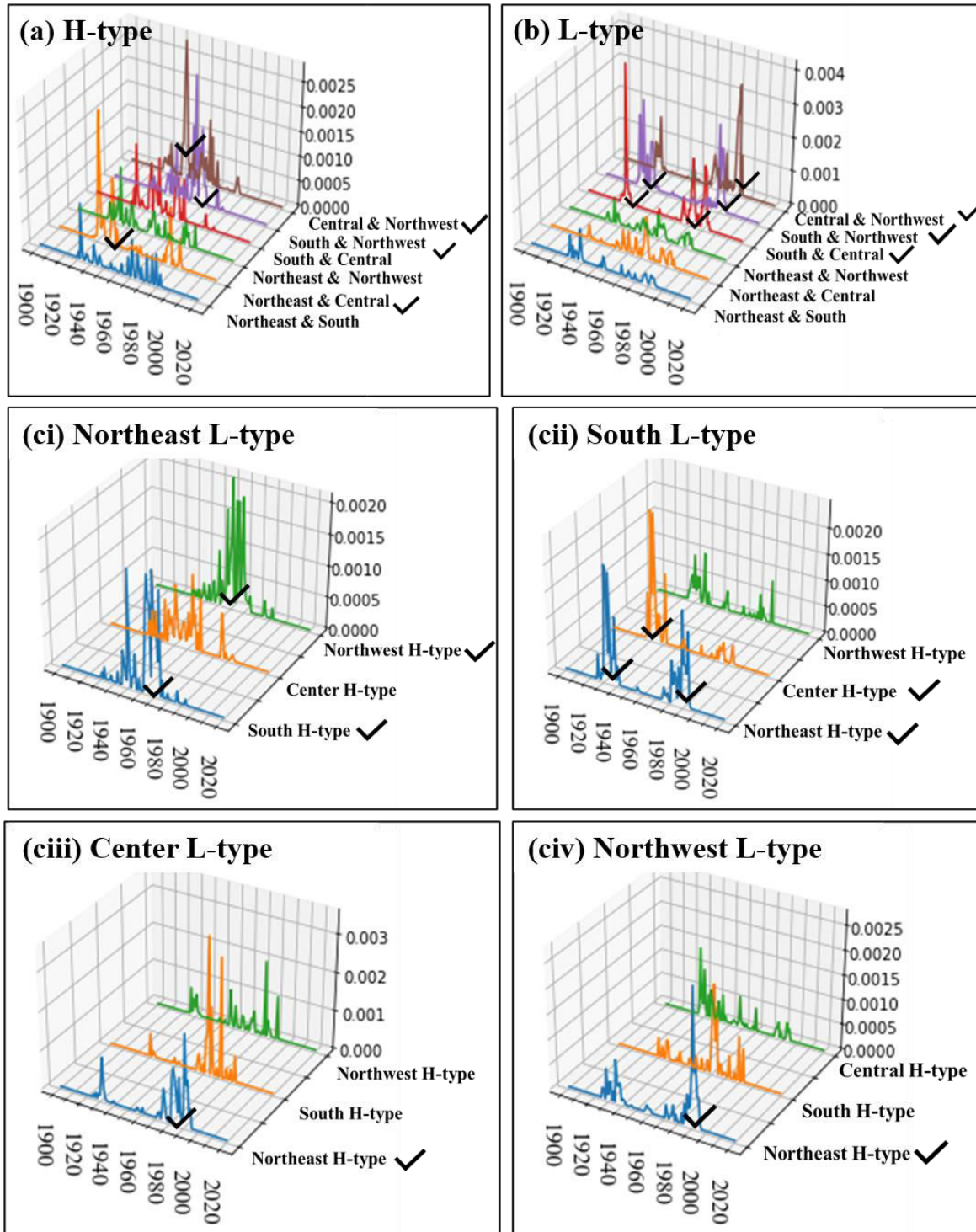


Fig. 3. 4 Amplified superimposed frequency of inflection points of similar types (a) H-type and (b) L-type of all regions, pairwise, signifying coherence in rainfall trend reversals among regions. Amplified superimposed frequency of opposite types of inflection points (c) L-type of one region with H-type of other regions signifying asymmetry in rainfall trend reversal.

3.5. Spatiotemporal distribution of prominent rainfall trend reversals:

The geographical distribution of the districts in those regions, which experienced the prominent rainfall trend reversals (i.e. affecting at least 33% area) during the identified time period centered around 1930s, 1960s and 1980s (Fig. 3.2 and Fig. 3.3) are given in Fig. 3.4a-c.

The 1930s trend reversal is experienced by more than one-third geographical area of central, northeast, and south peninsular India as shown in Fig. 3.4a. However, this rainfall trend reversal in 1930s is experienced only by a small geographical area (< 25%) in northwest India and hence not shown in Fig. 3.4a. The 1960s rainfall trend reversal is experienced by a significant geographical area (~ 33%) of northeast, northwest, and south peninsular India as shown in Fig. 3.4b. However, this rainfall trend reversal centered around 1960s was experienced by smaller (29%) than threshold geographical area in central India.

Unlike 1930s, and 1960s, the rainfall trend reversal centered around 1980s is prominently experienced by all the four rainfall homogeneous regions of India Fig. 3.4c. The most striking feature is that the L-type rainfall trend reversal (decreasing to increasing) is experienced by three (northwest, central and south peninsula) of the four regions of India. Thus, almost entire India experienced this L-type rainfall trend reversal and can be regarded as the most prominent episode of shift in rainfall pattern, in terms of its geographical extent. It is noteworthy that the fourth region (northeast) also experienced the rainfall trend reversal around 1980s, but of contrasting type (H-type: i.e. from increasing to decreasing rainfall) compared to other three regions.

3.6. Meridional and zonal asymmetry in rainfall:

It is important to note that based on the spatial distribution of districts experiencing these three prominent rainfall trend reversals (in 1930s, 1960s and 1980s), as discussed above and shown in Fig. 3.4a-c, it is possible to identify distinct zonal (east-west) and meridional (north-south) asymmetry of rainfall trend reversal patterns across India. As an important outcome of this study, one meridional asymmetry, and the two zonal asymmetries in rainfall trend reversals have been identified, as described in the following.

A distinct meridional (north-south) asymmetry in rainfall trend reversal has been identified (Fig. 3.4a) for 1930s with two regions (central & northeast vs. south peninsula) of coherent rainfall trend reversals of contrasting nature. Another important finding from the spatiotemporal distribution of rainfall trend reversals is a zonal (east-west) asymmetry (Fig. 3.4b) in 1960s, with two coherent rainfall trend reversal regions, namely, northwest and south peninsula having contrasting pattern compared to that in northeast India. The second zonal asymmetry in rainfall trend reversal is observed (Fig. 3.4c) in 1980s, in which coherent rainfall regions of northwest, central and south peninsula experience rainfall trend reversal which is in contrast with that in the northeast region.

It is necessary to realize that the three constrained periods (1930s, 1960s, and 1980s) and the three zonal and meridional asymmetries are being identified so unambiguously for the first time in this study. Therefore, this finding has improved the current level of understanding about summer monsoon rainfall trend reversals in India. It also highlights an important phenomenon about the history of ISM rainfall which needs to be examined further in more detail to decipher the underlying causal mechanism.

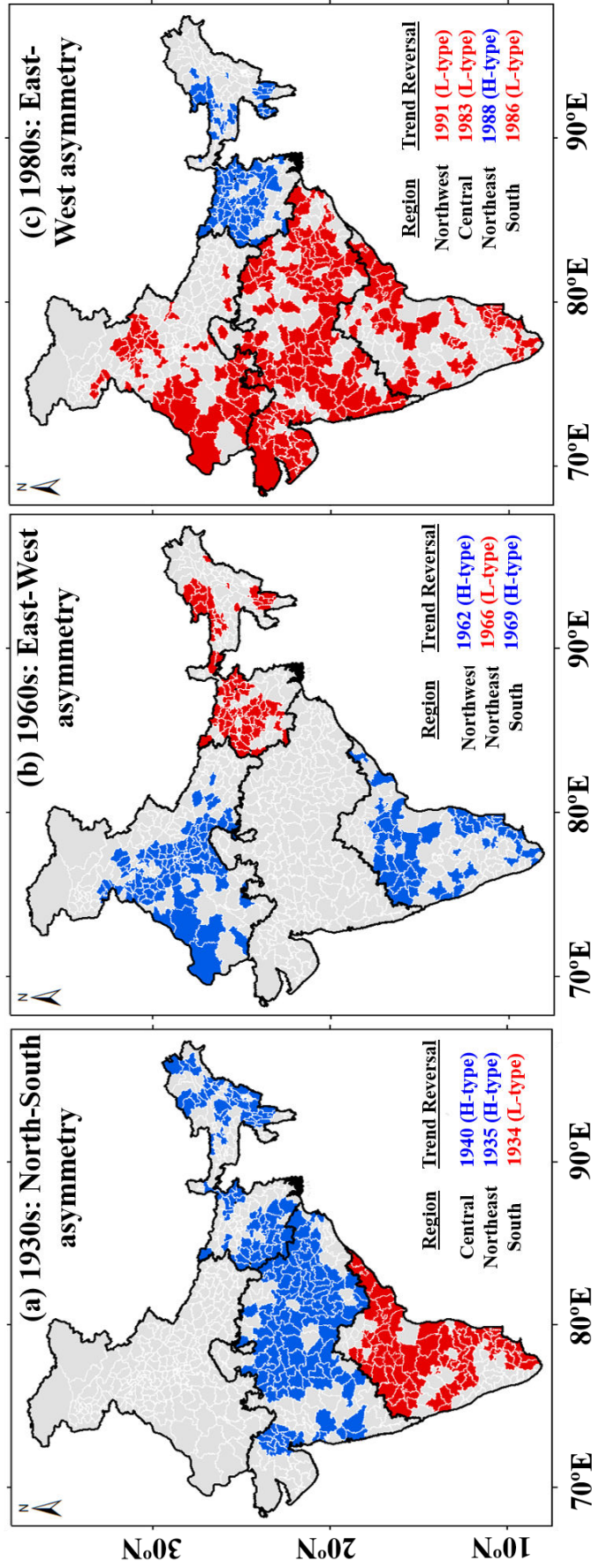


Fig. 3. 5 Districts within the homogeneous rainfall regions underwent the three prominent summer monsoon rainfall trend reversal events around (a) the 1930s, (b) the 1960s, and (c) the 1980s.

Another important point emerging from this study is that it may be possible that rainfall coherent regions as seen today, may not necessarily be the same throughout the rainfall history. Since the geographical extent of the rainfall trend coherent regions seems to vary in different time segments as described above, considering the fixed rainfall homogeneous regions and meteorological subdivisions for studying long-term rainfall trend and rainfall governing processes might have obscured the scale/dimension and timeframes of the possible causal processes. This study highlights the necessity to carry out further analysis in the identified time windows and corresponding coherent regions to understand region-wise rain governing systems in more detail.

3.7. Summary:

In this study, we have observed prominent multidecadal summer monsoon rainfall trends and trend reversal points in the long-term rainfall time series from 1901-2020, across four rainfall homogeneous regions of India at district level. Minute details of spatial and temporal variations in rainfall trends have been discerned as follows:

1. Using the robust methodology of rainfall pattern identification [*Chakra et al.*, 2023], three prominent rainfall trend reversal events have been identified as: (1) 1930s; (2) 1960s; and (3) 1980s.
2. During rainfall trend reversal in 1930s, the trend changed from increasing to decreasing in central and northeast India, while in the south peninsula, the trend changed from decreasing to increasing giving rise to a north-south asymmetry of rainfall patterns over India. In northwest India, no prominent reversal is observed during 1930s.
3. During rainfall trend reversal in 1960s, the trend changed from increasing to decreasing in south peninsula and northwest India, while in northeast India, the trend changed from

decreasing to increasing giving rise to an east-west asymmetry of rainfall pattern. In central India, no prominent reversal is observed during this period.

4. Unlike 1930s and 1960s, the rainfall trend reversal in 1980s is experienced in all the four homogeneous regions. In three out of four regions, (i.e. south peninsula, central, and northwest India), the trend changed from decreasing to increasing, while in the fourth region (northeast), the opposite trend of increasing to decreasing rainfall is observed, resulting in an east-west asymmetry of rainfall pattern over India.
5. In terms of the geographical extent of the observed trend reversal, 1980s is the most prominent among the three identified events, ~50% of geographical area of India.
6. In terms of magnitude of rainfall amount variation (i.e. wetter period or drier period compared to long-term) during these three trend reversal events, investigated through Cramer's *t*-test, the 1930s turns out to be the most prominent event as more than 30% of the region had rainfall significantly different (higher in central and northeast India; and lower in south peninsular India) during this period.
7. The observed temporal changes in the identified spatial asymmetry of rainfall pattern signify that the so-called rainfall homogeneous regions must have changed over time.

Therefore, this study also opens up a new front of research for hydrologists, meteorologists, and modelers to understand region-wise rain governing systems in more detail by focusing on distinct trends within specific time frames. A graphical summary of the region-wise ISMR rainfall pattern is presented below in Fig. 3.6.

It is very important and challenging to identify the underlying processes and controlling factors for each of the identified rainfall trend reversals. This, however, would require concerted research efforts by the meteorology community. Nonetheless, efforts made in this direction, as part of this study, have provided new insights into ISMR in the context of early twentieth century warming vs. mid-twentieth century cooling.

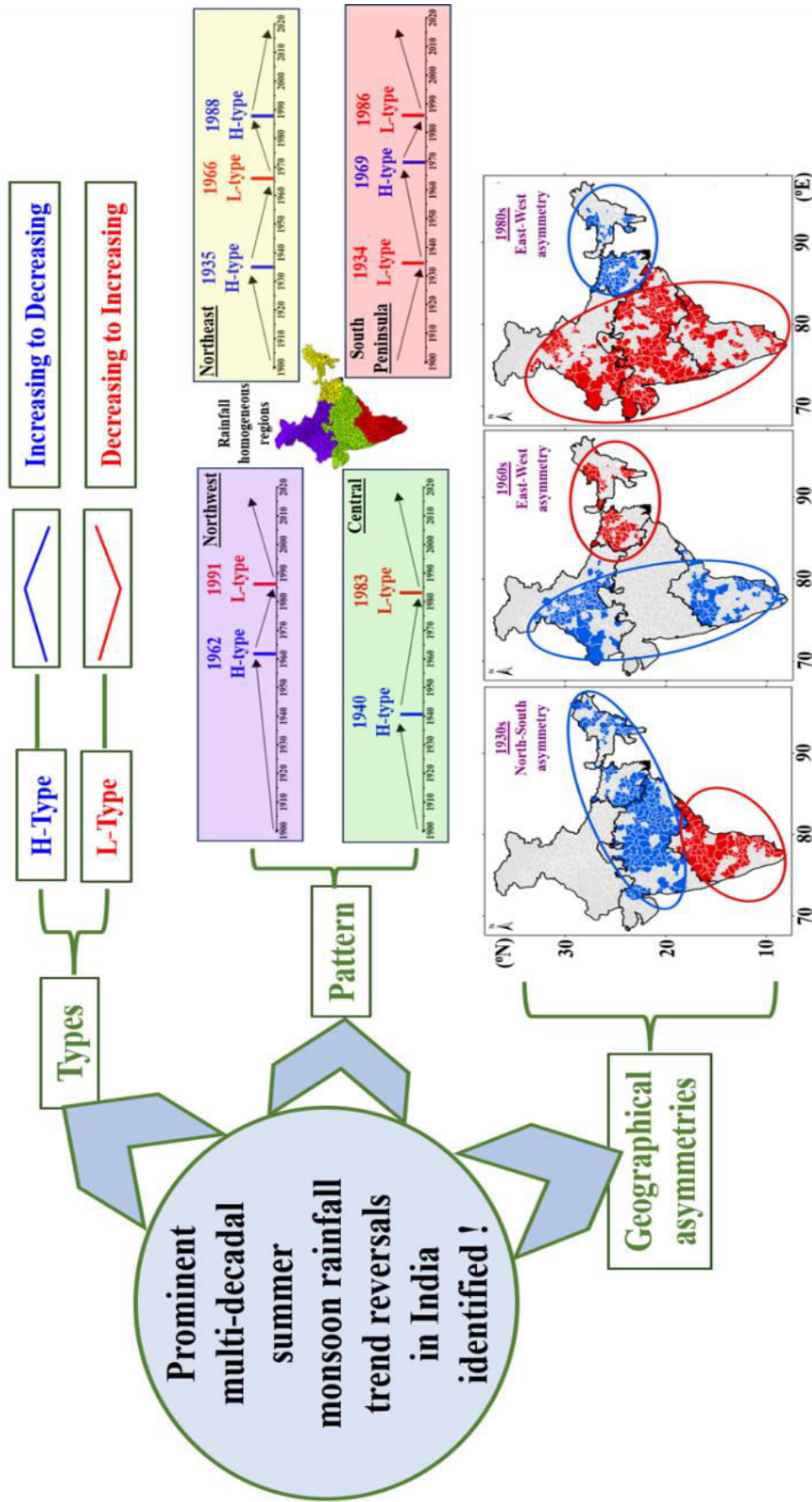


Fig. 3. 6 Graphical summary of region-wise summer monsoon rainfall pattern.

Chapter 4

Insights into Indian summer monsoon rainfall variability: Early twentieth century warming vs. Mid-twentieth century cooling

4.1. Introduction:

The fluctuation of summer monsoon rainfall has a substantial impact on agricultural systems in India and thus affects the livelihood of more than a billion people [Xavier *et al.*, 2007; Falga and Wang, 2022]. This underscores the importance for researchers to extensively investigate factors contributing to various temporal patterns such as synoptic, intraseasonal, interannual, and interdecadal variability [Chowdary *et al.*, 2021] in ISMR.

The notable decline observed in the ISMR during the latter half of the twentieth century has been thoroughly investigated, with various factors and processes being attributed to it. These include the anthropogenic aerosol induced slowing down of tropical meridional overturning circulation [Bollasina *et al.*, 2011], east-west shifting of monsoon circulation due to increased sea surface temperature (SST) in the Indo-Pacific warm pool which is anchored by increased greenhouse gas [Annamalai *et al.*, 2013], south-eastward shifting of boundary between ascent and descent due to increasing SST difference between equatorial east Pacific and central north pacific [Salzmann and Cherian, 2015], decreasing recycled component of precipitation as a consequence of deforestation [Paul *et al.*, 2016], and irrigation induced circulation change [Chou *et al.*, 2018] etc.

Therefore, the reasons behind the decreasing trend in ISMR are diverse and multifaceted, offering an opportunity to reanalyze the factors behind distinct rainfall patterns

during the late twentieth century. For a comprehensive understanding of the rainfall governing processes, it is necessary to investigate the rainfall patterns and factors over a longer period.

However, the ISMR patterns and governing factors in the early twentieth century remain unexplored. An important finding, but at the All-India level, has been shown by Annamalai et al. (2013) in the All-India Rainfall (AIR) index time series, where an increasing trend in the 31-year running mean AIR anomalies during the first half of the twentieth century was observed, peaking in the 1940s, followed by a subsequent decline.

In this work, by analyzing region-wise ISMR at the district level, a prominent ISMR trend reversal was identified in the 1930s across India. This trend reversal shows meridional asymmetry: an increasing to decreasing trend in central and northeast India and a decreasing to increasing trend in south peninsular India. Additionally, the 1930s experienced anomalous rainfall significantly higher than the long-term mean in central and northeast India and lower in south peninsular India. The causal processes behind this ISMR peak and valley in the early twentieth century and the meridional asymmetry in the ISMR trend need to be investigated in detail.

This period of anomalous rainfall falls within a historical timeframe known as the early twentieth-century warming (ETCW), which spans from the late 19th century to the mid-20th century, peaking around the 1940s (Hegerl et al., 2018). This is the most pronounced warming period in the historical global climate record before the recent warming. Many regional anomalies during the ETCW period, such as Arctic warming, dust bowl drought and heat waves in North America, drought in Australia, and hot summers combined with cold winters in Europe, have been reported [Hegerl et al., 2018]. Following the ETCW, there was a period of cooling during the mid-twentieth century, commonly known as the mid-century

cooling (mid-20C cooling), which occurred primarily from the 1940s to the 1970s and was most pronounced in the northern hemisphere [Hegerl *et al.*, 2018]. However, whether the anomalous rainfall signature in the 1930s and the north-south asymmetrical rainfall pattern have any connection to the multidecadal phases of temperature change during the ETCW and mid-20C cooling periods has not been investigated.

This chapter investigates the probable controlling factors of the ISMR to understand the overall dynamics of ISMR patterns during this timeframe and their connection to the multidecadal ETCW and mid-20C cooling events, which are discussed in detail in the subsequent sections.

4.2. Data & Methods:

The methodology and the data used for the identification of the summer monsoon rainfall pattern have been discussed in Chapter 2. For the understanding of the 1930s rainfall signature, the annual frequency data of monsoon depressions and storms of BoB origin are obtained from IMD e-Atlas (<http://14.139.191.203/AboutEAtlas.aspx>). Monthly product of European Centre for Medium-Range Weather Forecasts reanalysis of the 20th Century (ECMWF ERA-20C) [Poli and Staff, 2017] data is used in this study which includes (i) zonal (u , ms^{-1}), meridional (v , ms^{-1}), and vertical wind (ω , Pa s^{-1}) speed, (ii) relative humidity (RH, %), and (iii) specific humidity (q , kg/kg). Land surface and SST datasets are obtained from Climatic Research Unit gridded Time Series (CRU TS v. 4.05) [Harris *et al.*, 2020] and Hadley Centre Global Sea Ice and Sea Surface Temperature (HadISST) [Rayner *et al.*, 2003] respectively.

Inorder to understand the relative contributions of changes in individual environmental conditions in the changes in the frequency of depressions and storms, the

following expression of Genesis Potential Index (GPI) is used [Emanuel and Nolan, 2004; Li et al., 2013].

$$\delta GPI = \alpha 1 \times \delta \left(\frac{H}{50} \right)^3 + \alpha 2 \times \delta |10^5 \eta|^{\frac{3}{2}} + \alpha 3 \times \delta (1 + 0.1 V_{shear})^{-2} + \alpha 4 \times \delta \left(\frac{V_{pot}}{70} \right)^3$$

Where,

$$\alpha 1 = \overline{|10^5 \eta|^{\frac{3}{2}}} \times \overline{(1 + 0.1 V_{shear})^{-2}} \times \overline{\left(\frac{V_{pot}}{70} \right)^3},$$

$$\alpha 2 = \overline{\left(\frac{H}{50} \right)^3} \times \overline{(1 + 0.1 V_{shear})^{-2}} \times \overline{\left(\frac{V_{pot}}{70} \right)^3},$$

$$\alpha 3 = \overline{\left(\frac{H}{50} \right)^3} \times \overline{|10^5 \eta|^{\frac{3}{2}}} \times \overline{\left(\frac{V_{pot}}{70} \right)^3},$$

$$\alpha 4 = \overline{\left(\frac{H}{50} \right)^3} \times \overline{|10^5 \eta|^{\frac{3}{2}}} \times \overline{(1 + 0.1 V_{shear})^{-2}}$$

H = Relative humidity (%) at 600hPa,

η = Absolute vorticity (s^{-1}) at 850hpa,

V_{shear} = Vertical wind shear (ms^{-1}) between 200hPa and 850hPa,

V_{pot} = Maximum tropical cyclone potential intensity (ms^{-1})

The bar ($\bar{\quad}$) represents the summer monsoon seasonal climatology, and δ represents the difference value of individual parameter between two time frames.

Further, zonal, meridional wind component and specific humidity are used to calculate vertically integrated moisture transport (VIMT, kg/ms) from 1000hPa to 300 hPa over Arabian Sea and the BoB [Konwar et al., 2012]. VIMT is defined as,

$$VIMT = \frac{1}{g} \sum_{j=1}^j q_j(u_j, v_j) \Delta p_j$$

where, g is the acceleration due to gravity, q_j is the specific humidity, u_j is the zonal wind, v_j is the meridional wind, and Δp_j is the thickness of j th pressure level.

4.3 Results & Discussion:

4.3.1 Observed prominent summer monsoon rainfall trend reversals in the ETCW period:

The prominent ISMR trend reversals for the central, northeast, and south peninsular India were identified in 1940, 1935, and 1934, respectively, referred as the 1930s trend reversal. Northwest India has not experienced this reversal significantly. Fig. 4.1 displays the spatial distribution of districts in all three homogeneous regions, excluding northwest India, that experienced the 1930s trend reversal event. A pronounced north-south asymmetry in trend reversal is evident.

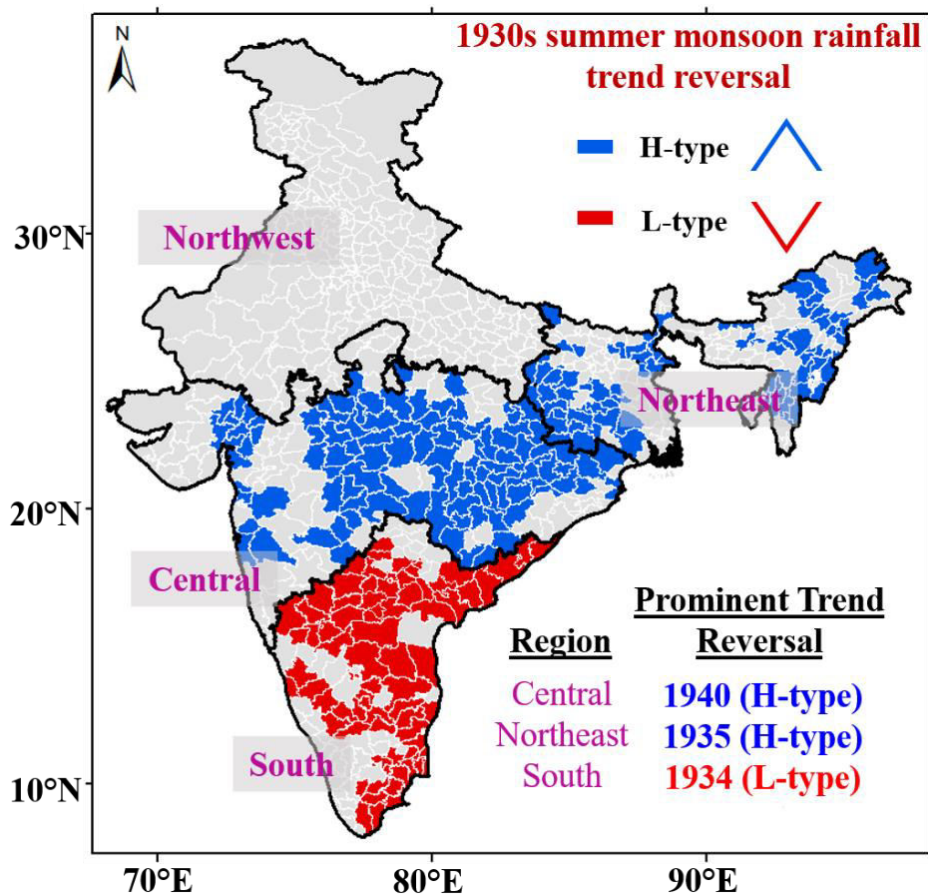


Fig. 4. 1 Spatial distribution of districts experiencing 1930s summer monsoon rainfall trend reversal.

From Cramer's t-test, it is evident that, 30% geographical area of south peninsula experienced significantly lower rainfall compared to the long-term average, while 30-40% of the northeast and central India experienced significantly higher rainfall during the 1930s trend reversal event (Table 3.3, Chapter 3).

4.3.2 Occurrences of monsoon depressions originated from BoB:

The dynamics over the Arabian Sea play a dominant role in governing rainfall over the south peninsula [Joseph and Simon, 2005; Konwar et al., 2012], whereas both the Arabian Sea and the BoB are crucial for central and northeast India [Mohapatra and Mohanty, 2004; Konwar et al., 2012; S Vishnu et al., 2016]. It is well known that summer monsoon over India is maintained by the northward progression of ITCZ [Sikka and Gadgil, 1980] and westward or north-westward propagation of synoptic-scale disturbances (monsoon depressions and cyclonic storms) to the Indian mainland generally formed from BoB (Fig. 4.2a) or cross over to BoB from the south-China sea [Wang et al., 2006]. While cyclonic storms can occur during the summer monsoon period, they are relatively uncommon. Therefore, we categorize monsoon depressions and storms of higher intensities as monsoon depressions. These synoptic systems are very important, especially for central India as they act as a significant source of moisture (>35%) [S Vishnu et al., 2016; Hunt and Fletcher, 2019].

To analyze the north-south asymmetry in rainfall trends, various meteorological parameters were studied, including the frequency of monsoon depressions over the BoB. The annual time series of monsoon depressions originating over BoB from 1901 to 2020 Fig. 4.2b shows an increasing trend in the first half of the century, followed by a decrease. A similar pattern is noted in the rainfall trends in central and northeast India, with reversals around 1940 and 1935, respectively. The period 31-year window around 1940 (1925–1955) stands out as having the highest number of these monsoon depressions compared to adjacent time frames,

aligning perfectly with the trend reversals in central India and closer to the trend reversal of northeast India.

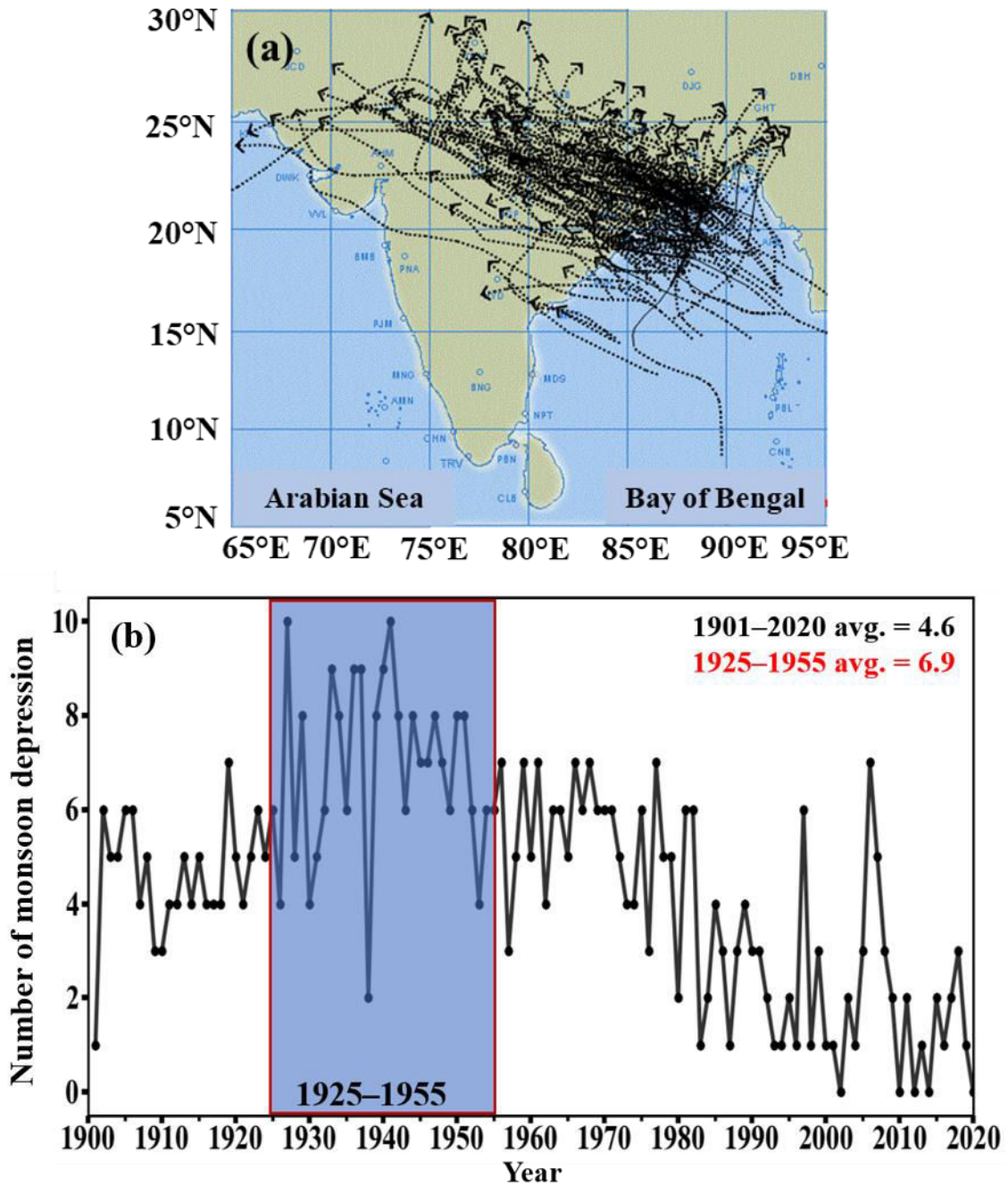


Fig. 4. 2 (a) Track of depressions and storms forming over the Bay of Bengal, (b) Annual time series of low-pressure systems forming over the Bay of Bengal during the summer monsoon season.

To further assess whether the average number of these monsoon depressions during the 1925–1955 window significantly exceeds the long-term average (1901–2020), a two-sample t-test was conducted at a 0.05 significance level. The average number of monsoon depressions during the 1925–1955 window is 6.87, which is significantly higher (50% more) than the long-term average of 4.56 ± 0.44 at a 0.05 significance level.

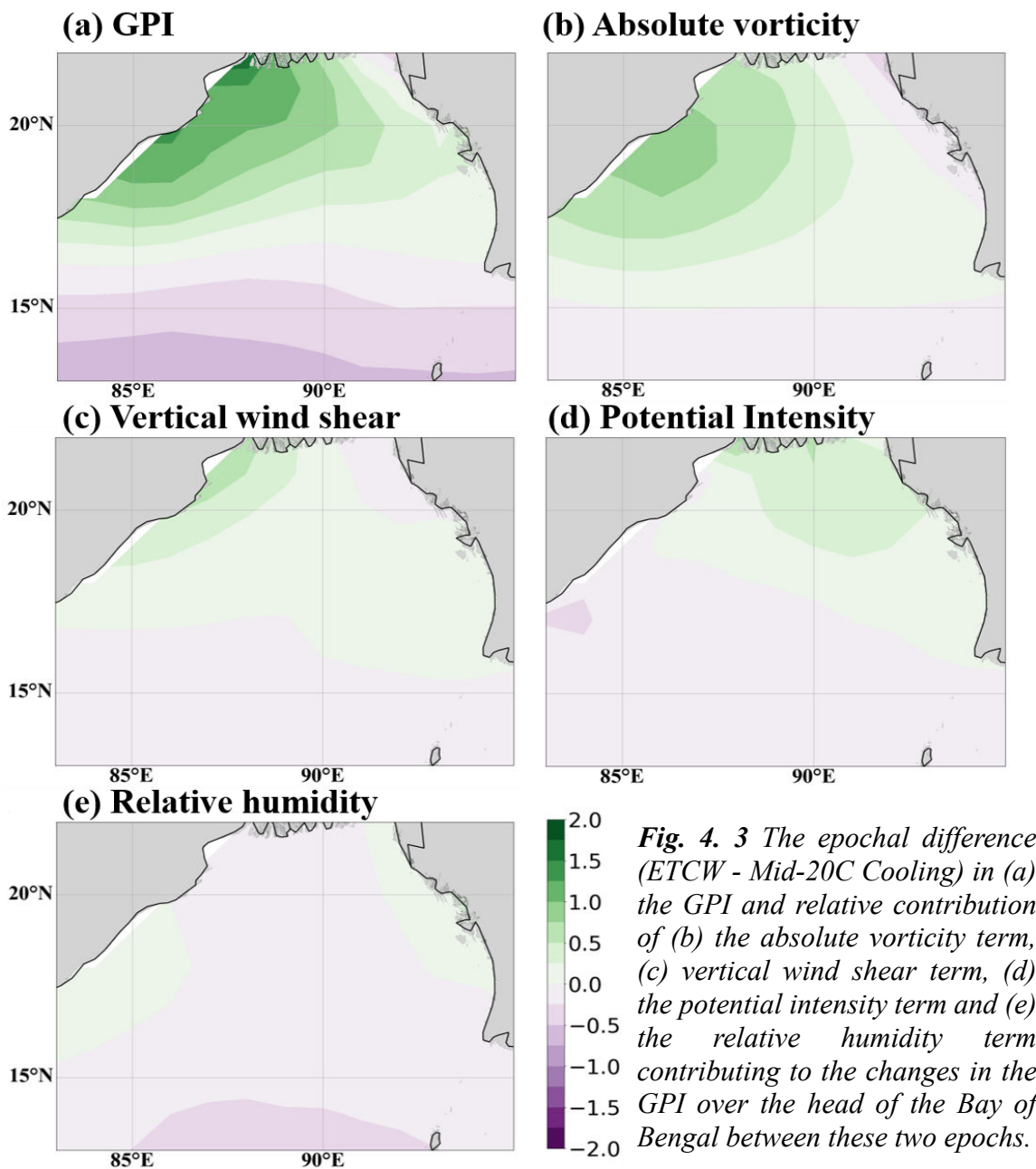
From 1891, the earliest year for which data is accessible, until the present day, the highest occurrences of these monsoon depressions happened during the ETCW period within the time window of 1925–1955. This timeframe aligns with the peak in rainfall observed in central and northeast India. This increased number of monsoon depressions might have caused the anomalous higher rainfall over central and northeast India. This observation prompts the question of what alterations in the environmental parameters may be accountable for the development and intensification of these monsoon depressions during 1925–1955 in comparison to other periods.

Studies by Vishnu et al., [2016] and Prajeesh et al., [2013] indicate that a reduction in mid-tropospheric relative humidity over the BoB is linked to the decreased monsoon depression frequency. In this study, to identify the environmental factors exerting a dominant effect on the increased frequency of monsoon depressions during 1925–1955, a similar GPI-based approach as Vishnu et al. [2016] has been employed. Two-time frames are considered: (1) 1925–1955 during the ETCW period (referred to ETCW subsequent descriptions) and (2) 1956–1986 during mid-20C cooling period (referred to as mid-20C cooling in subsequent descriptions). Changes in GPI and associated environmental parameters between these two-time frames were observed using the ERA20C reanalysis datasets, and HadISST dataset.

It's worth noting that the preceding thirty-year period before the 1925–1955 window, specifically, 1894–2024, was not taken into consideration due to limitations in data availability.

4.3.3 Fluctuations in environmental parameters affecting monsoon depression genesis over the BoB:

Fig. 4.3 illustrates the GPI difference between ETCW and mid-20C cooling period, highlighting the contribution of various environmental parameters to the GPI difference over the BoB region (12.5-22.5°N, 82.5-95°E). The GPI difference is positive over the head of the BoB, indicating a higher GPI in ETCW compared to mid-20C cooling (Fig. 4.3a). The maximum value of the difference is 1.73, approximately 34% of the climatological GPI (i.e., 5), signifying a 34% increase in GPI during ETCW.



The relative contributions of environmental parameters to the higher GPI or increased occurrence of monsoon depressions in ETCW are depicted in Fig. 4.3b–e. Positive values are observed for absolute vorticity, vertical wind shear, and potential intensity, while negative values are noted for relative humidity over the BoB. This implies that higher absolute vorticity and potential intensity, along with lower vertical wind shear in ETCW, contribute to an increased formation of monsoon depressions compared to the mid-20C cooling. The contribution of absolute vorticity to GPI change is more pronounced (71%), followed by vertical wind shear (20%).

To comprehend the factor contributing to the increased 850hPa absolute vorticity and decreased vertical wind shear in ETCW and their connection to the large-scale monsoon system, we further studied the epochal difference (ETCW – mid-20C cooling) of lower and upper-level circulation at 850hPa and 200hPa, vertical wind shear between 200hPa and 850hPa. In conjunction with above analysis, we also examined the VIMT, as well as the gradients of SST and land surface temperature for these two epochs over the Indian monsoon region, as detailed in the following sections.

4.3.4 Epochal difference in meteorological parameters:

Fig. 4.4 depicts the summer monsoon climatology (averaging data from 1925 to 1986) and the epochal differences in 850hPa wind speed and wind direction (Fig. 4.4a & b), as well as VIMT magnitude and direction between 1000hPa to 300hPa (Fig. 4.4c & d). The climatology map (Fig. 4.4a & c) reveals the presence of the low-level jet stream (LLJ), responsible for transporting moisture from the Arabian Sea to the Indian landmass during the summer monsoon season. With a core wind speed ranging between 18 to 20 m/s, the LLJ facilitates the transport of 1400-1600 kg/m/s of moisture from the Arabian Sea to the Indian landmass. Multiple studies, including those by Chakraborty et al. [2009], Sandeep and Ajayamohan [2015], and

P. V. Joseph and Anu Simon [2005], have proposed a direct linkage between the magnitude of the LLJ over the Arabian Sea and the strength of the ISMR.

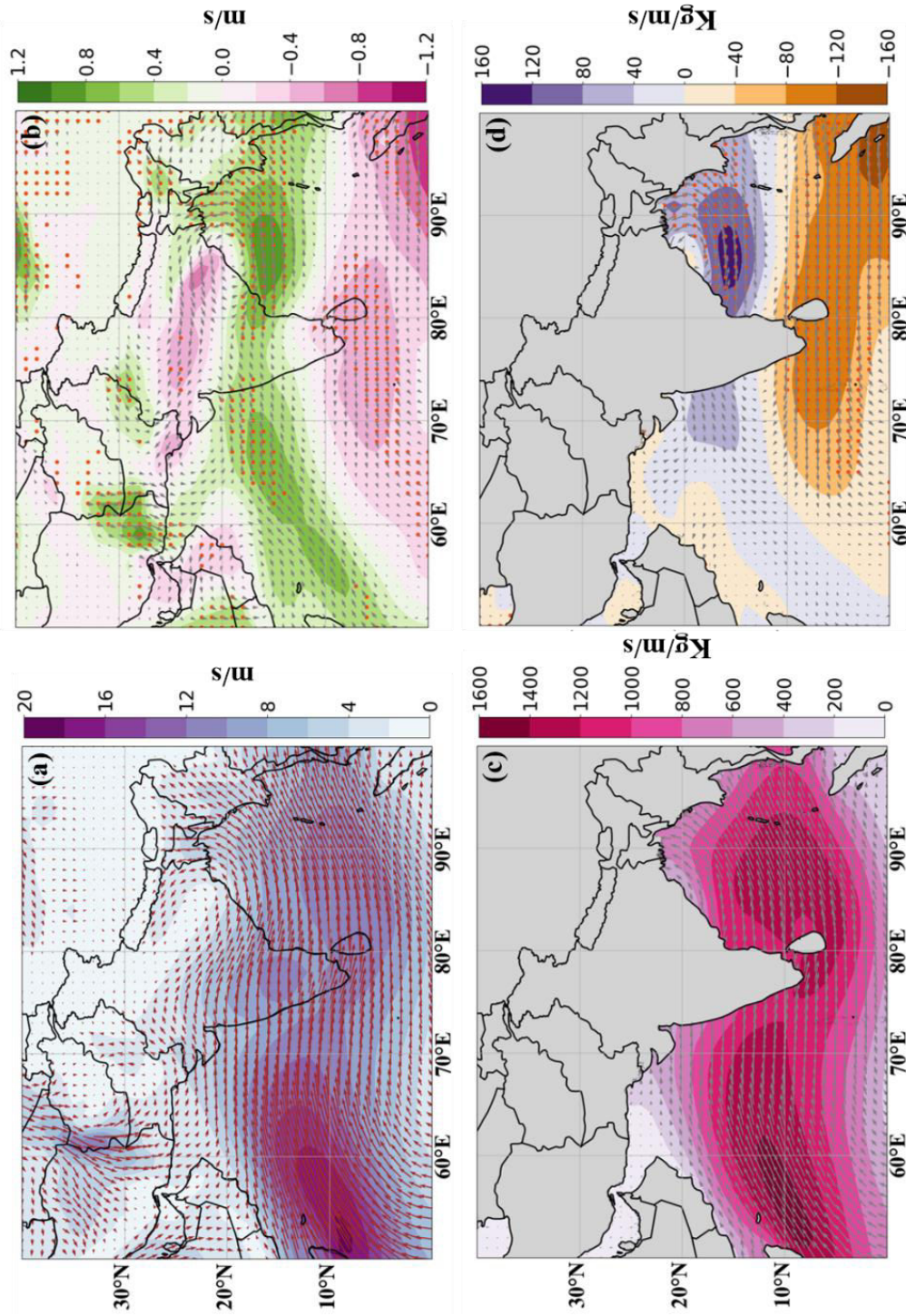


Fig. 4 (a) 1925-1986 climatology of 850hPa wind speed (shaded) and wind direction (vector), (b) epochal difference (ETCW avg.) of 850hPa wind speed (shaded) and direction (vector) over Indian Summer monsoon region, (c) 1925-1986 climatology of vertical integrated moisture transport VMIT (shaded) and direction (vector), (d) epochal difference of VMIT (shaded) and direction (vector). Red dots represent statistically significant difference in the wind speed and VMIT between ETCW and mid-20C cooling period at 0.05 level of significance.

Positive values over 10-20°N in the difference maps between the ETCW and mid-20C cooling periods in 850hPa wind indicate a strengthening of the LLJ over the Arabian Sea, signifying an intensification of summer monsoon circulation during the ETCW. Conversely, the negative values over the southern Arabian Sea (0-10°N) suggest increased wind strength in the mid-20C cooling period. Moreover, positive values are also evident which indicates intensified wind speed over the BoB in ETCW. The epochal difference pattern in the VIMT aligns with the 850hPa wind pattern, supporting these observations Fig. 4.4d.

The strengthening of the LLJ and wind over the BoB during the ETCW, along with their weakening during the mid-20C cooling period, resulted in higher rainfall during the ETCW and lower rainfall during the mid-20C cooling period, creating a decreasing trend over central and northeast India. Conversely, the weakening of wind over the southern Arabian Sea during the ETCW and its strengthening during the mid-20C cooling period caused lower rainfall during the ETCW and higher rainfall during the mid-20C cooling period, leading to an increasing trend over southern peninsular India. This dynamic contributed to the north-south disparity in the ISMR trend, marked by decreasing rainfall in central and northeast India and increasing rainfall in the southern peninsula observed after the 1930s, as the transition from the ETCW to the mid-20C cooling periods occurred.

Thus, Fig. 4.4 illustrates the shift in the background summer monsoon circulation over the Indian region from stronger during the ETCW to weaker during the mid-20C cooling period. Additionally, an anomalous cyclonic circulation is evident over the head of the BoB in the epochal difference plots of 850hPa wind and VIMT (Fig. 4.4b&d). The increased wind speed and anomalous cyclonic circulation likely caused the increased vorticity, which was conducive to the intensification of monsoon depressions over the head of the BoB during the ETCW.

To further comprehend the drivers of intensifying monsoon circulation and the notably increased vorticity over the head BoB, we examined the temperature (SST over Ocean and 2m air temperature over land; Fig. 4.5) pattern between these two epochs. The crucial role of land-sea thermal contrast, characterized by higher temperatures over the northern Indian landmass and lower temperatures in the western Indian Ocean, in driving the Indian summer monsoon, is clearly illustrated in the temperature climatology map (Fig. 4.5a). Anomalous heating over the northern Indian landmass and cooling over the western Indian Ocean during the ETCW, as observed in the epochal difference map (Fig. 4.5b), resulted in an increased land-sea thermal contrast. This enhanced thermal gradient during ETCW facilitated a stronger LLJ, stronger wind and an anomalous cyclonic circulation over BoB, thereby contributing to higher rainfall over central and northeast India through intensified monsoon circulation and escalated monsoon depression.

Conversely, during the mid-20th century cooling period, an opposite pattern emerged with anomalous heating in the western Indian Ocean and cooling over the northern landmass. This reversal weakened the land-sea thermal contrast, leading to a weakened LLJ and monsoon circulation, and resulting in less rainfall over central and northeast India. The anomalous heating over the Indian Ocean likely caused increased rainfall in southern peninsular India during the mid-20th century cooling period. This highlights the role of temperature patterns during these two multidecadal periods in the north-south rainfall trend disparity and rainfall extremes.

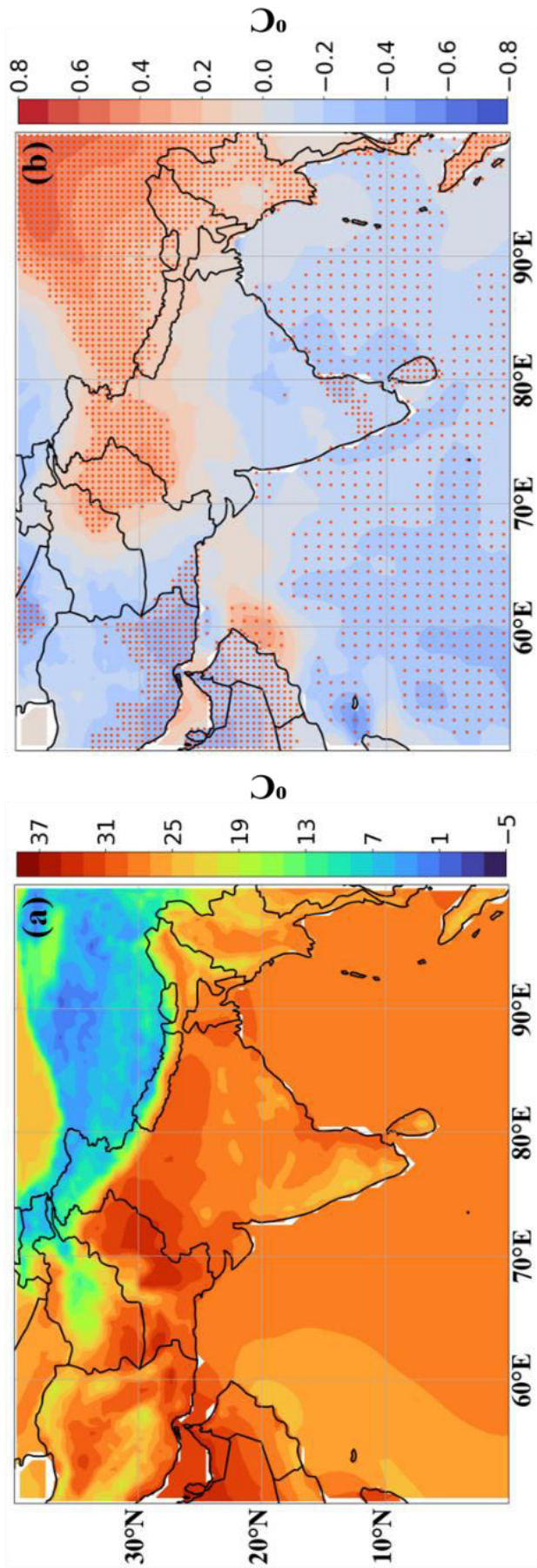


Fig. 4. 5 (a) 1925-1986 climatology (b) Epochal difference (ETCW avg.- Mid-20C cooling avg.) of sea surface temperature and 2m air temperature over the land mass. Red dots represent statistically significant difference in the temperature between ETCW and mid-20C cooling period at 0.05 level of significance.

In addition to absolute vorticity, vertical wind shear also contributes significantly to the escalation of monsoon depressions in ETCW. To delve deeper into the dynamics of decreased vertical wind shear and the role of temperature behind it, the epochal differences of 200hPa wind speed and direction, vertical wind shear and direction, and upper tropospheric circulation and temperature are studied and presented in Fig. 4.6.

Positive value over the 0-10°N belt, the core zone of TEJ, in the epochal difference plot of 200hPa wind (Fig. 4.6a) indicates the strengthening of TEJ during the ETCW, which further supports the strengthening of monsoon circulation. However, negative values observed over the head BoB suggests weakening of TEJ in that region during ETCW. Thus, a significant increase in lower-level (850hPa) wind speed along with a decrease in upper-level (200hPa) wind speed is observed over the head of the BoB during the ETCW, as depicted in Fig. 4.4b and Fig. 4.6a. This could potentially lead to a reduction in vertical wind shear (Fig. 4.6b), creating conditions favourable for the development of depressions and storms.

The heightened intensity of the LLJ and TEJ corresponds well with the intense summer monsoon circulation. Enhanced LLJ and moisture transport lead to increased convection and upper tropospheric warming over the Indian subcontinent, supporting a stronger TEJ [Krishnamurti and Bhalme, 1976; Pattanaik and Satyan, 2000; Joseph and Simon, 2005; Abish *et al.*, 2013]. However, our findings reveal a surprising weakening of the TEJ over the head of the BoB during the ETCW, likely due to the advection of upper tropospheric cold air from other regions, which outweighs the convective heating associated with the enhanced monsoon locally over the BoB.

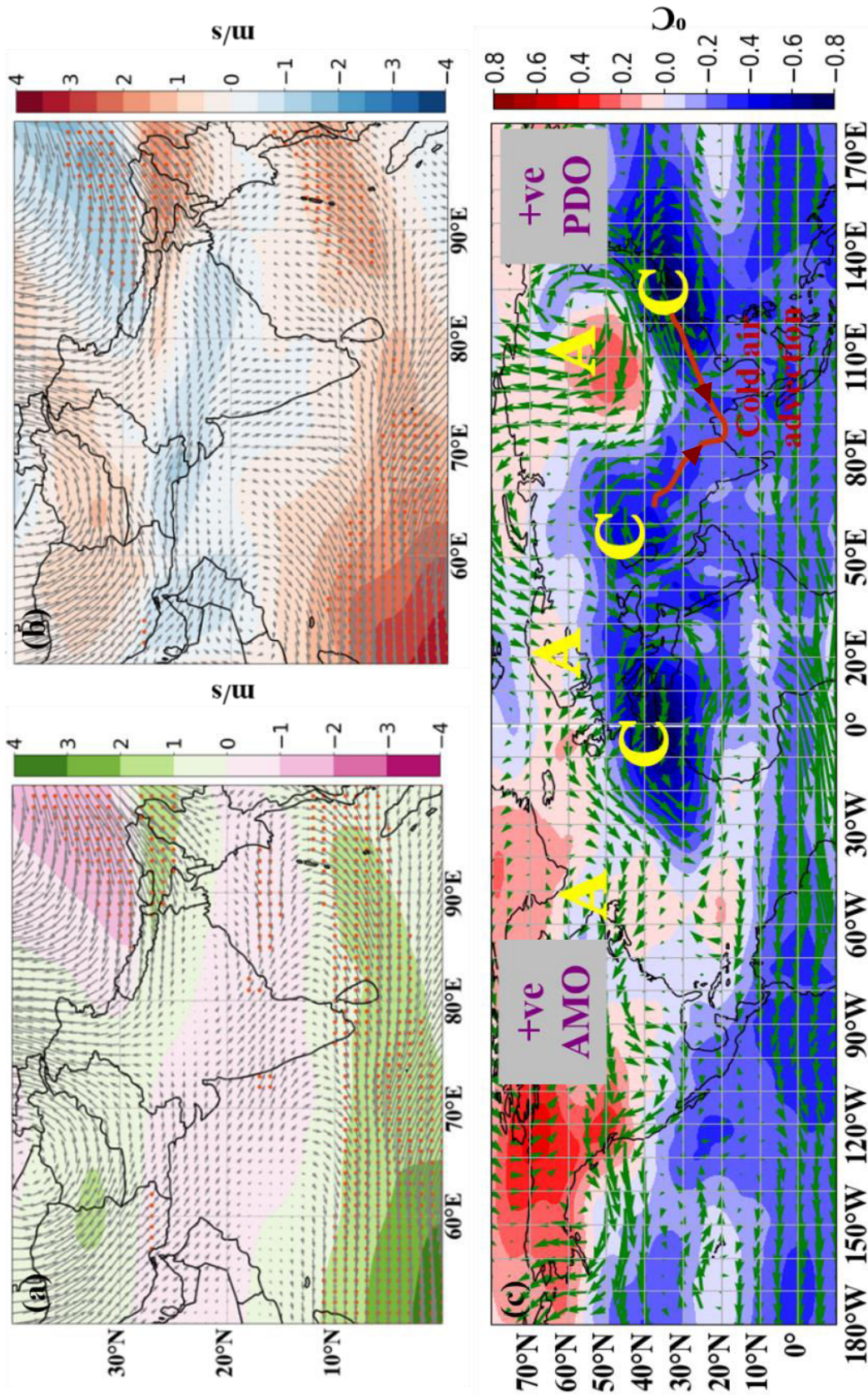


Fig. 4. 6 Epochal difference (ETCW avg.- Mid-20C cooling avg.) (a) 200hPa wind speed and direction, (b) vertical wind shear and direction, and (c) average upper tropospheric temperature (shaded) and wind direction (vector) between 200hPa and 500hPa. Red dots in a and b represent statistically significant differences in the 200hPa wind speed and vertical wind shear between the ETCW and mid-20C cooling period at 0.05 level of significance.

To further investigate the decrease in TEJ wind speed over the northern BoB, we examined the epochal average tropospheric temperature and wind circulation between 200hPa and 500hPa, as shown in Fig. 4.6c. We observed anomalous cold air advection to northern India and the head BoB from an adjacent anomalously colder and cyclonic regime (Fig. 4.6c). One of these intense cooling regimes is over the western Pacific Ocean, likely influenced by the positive phase of the PDO. This phase, characterized by cooler SST over the western Pacific Ocean and warmer SST over the Eastern Pacific Ocean, is noted by Mantua and Hare [2002], and Vishnu et al. [2018], and is evident during the ETCW. Another cooling regime, likely influenced by the positive phase of the AMO, is also evident during the ETCW. The alternating cyclonic and anticyclonic anomalies from the Atlantic to the Asian region shown in Fig. 4.6c indicate the atmospheric teleconnection mechanism by which the AMO affects the ISMR [Zhang et al., 2020]. Positive AMO induces anomalous upper tropospheric warming over the South Asian High, enhancing the tropospheric temperature gradient between the Indian Ocean and the South Asian subcontinent, resulting in a stronger TEJ, stronger monsoon circulation, and increased ISMR [Luo et al., 2018; Nath and Luo, 2019]. This study confirms the strengthening of the Indian summer monsoon circulation during the ETCW, as evident from both the lower (stronger LLJ) and upper-level (stronger TEJ) circulation patterns described earlier. However, the cold surge of wind originating from the anomalously colder and cyclonic circulation regime associated with the positive phases of the AMO and PDO, which can decrease TEJ wind speed over the northern BoB, is an important observation of this study. Upper tropospheric temperature changes are known to significantly impact TEJ intensity, as suggested by Abish et al. [2013].

4.3.5 Factors responsible for the temperature variation in ETCW and mid-20C cooling:

The ETCW period, characterized by accelerated warming, and the mid-20C cooling period, marked by a slowdown [Yao et al., 2017] showed a latitudinal temperature asymmetry globally and within the Indian summer monsoon region [Cai et al., 2006; Yao et al., 2017; Diao and Xu, 2022]. During the mid-20C cooling period, the northern hemisphere mid-latitudes experience a pronounced cooling trend, the southern hemisphere mid-latitudes undergo moderate warming. This phenomenon is attributed to internal multi-decadal variability stemming from Pacific and Atlantic ocean-atmosphere interactions, as well as post-World War II anthropogenic aerosol emissions due to rapid industrial expansion [Diao and Xu, 2022]. This interhemispheric temperature asymmetry prompts oceanic heat redistribution, particularly through intensified northward cross-equatorial heat transport in the Atlantic and Indo-Pacific Oceans. In the Indo-Pacific region, a cross-equatorial overturning cell generates northward flow in the upper 250 meters of the basin, resulting in heat divergence from the equator to 20 degrees south latitude. This leads to cooling of water temperatures in that region and warming in the northern tropical part of the basin [Cai et al., 2006]. Consequently, warming occurs over the northern Indian Ocean while cooling is observed over the Indian landmass, contributing to the weakened land-sea thermal contrast resulted into weakened monsoon circulation and decreased ISMR over the central and northeast India. However, anomalous warming over the northern Indian Ocean caused increased rainfall over the south peninsula during this period.

Conversely, during ETCW, the greater rate of warming over land compared to sea increases the land-sea thermal contrast, thereby enhancing monsoon circulation. This results in a strengthened LLJ and winds over the northern Bay of Bengal, leading to increased rainfall over central and northeast India.

4.4 Summary:

An examination of the 31-year moving average of summer monsoon rainfall across India over a span of 120 years (1901-2020) reveals abnormal rainfall patterns during the 1930s in two adjacent regions. Central and northeast India exhibit significantly higher rainfall compared to the long-term average (1901-2020), while south peninsular India experiences notably lower rainfall. Apart from the anomalous rainfall in the 1930s, there is a discernible decreasing trend in rainfall in central and northeast India and an increasing trend in the south peninsula.

The increased monsoon rainfall in central and northeast India during the 1930s coincides with the highest occurrences of monsoon depression from the BoB. The significant contribution of these depressions to the total summer monsoon rainfall in these regions supports that this increase was driven by a higher number of monsoon depressions

Elevated 850 hPa absolute vorticity and reduced vertical wind shear contribute to the higher number of formations of depressions over the BoB during this period. This period coincides with the ETCW phase, during which the heated landmass generated a significant thermal gradient, driving winds from the BoB towards the landmass. This results in increased low-level wind speeds and anomalous cyclonic circulation, therefore, increasing low-level vorticity, which is conducive to the formation of more monsoon depressions. Additionally, the upper-level winds weakened due to a cold wind surge from two adjacent anomalous cyclonic and colder regions influenced by positive AMO and PDO phases. This combination of decreased vertical wind shear and increased vorticity contributes to the heightened occurrences of these monsoon depressions during ETCW, resulting in anomalous rainfall in central and northeast India.

During the subsequent mid-20C cooling period, colder temperatures in the northern Indian landmass, including Tibet, reduced the thermal gradient, leading to decreased low-level wind speeds and fewer monsoon depressions.

The transition from the ETCW to the mid-20C cooling period saw a decrease in the land-sea thermal contrast. The decreased LLJ strength during the cooling period led to reduced rainfall in central and northeast India, while anomalous warming over the northern Indian Ocean increased the rainfall over the southern peninsula. Thus, a decreasing trend in rainfall is observed in central and northeast India, and an increasing trend in rainfall is observed in south peninsular India from ETCW to mid-20C cooling. A graphical summary is presented in the Fig. 4.7.

This study identified factors and mechanisms influencing ISMR during the ETCW and mid-20C cooling periods. Anomalous occurrences of depressions and storms in the 1930s led to higher rainfall in central and northeast India, a regional anomaly during ETCW. Temperature changes from ETCW to the mid-20C cooling period contributed to the north-south ISMR trend asymmetry.

Valuable insights into probable causal factors for early twentieth century (1930s) rainfall variability are presented in this chapter. Similarly, exciting causal factors and processes must be there for other two rainfall trend reversals identified in 1960s and 1980s, which are not explored as part of this study. However, it opens up an avenue for research leading up to causal factors for rainfall trend reversals in 1960s and 1980s. The summary of the current research and the scope for future research it has generated is discussed in the next chapter.

Chapter 5

Summary and scope for future works

5.1. Summary:

This doctoral study aims to identify patterns of the ISMR variability over a 120 years period (1901-2020), with a finer spatiotemporal resolution, examine its coherence within and across homogeneous rainfall regions, and understand the underlying processes and factors. The research analyzes district-wise summer monsoon rainfall data from 1901 to 2020 across India. Additionally, various meteorological parameters such as SST, 2m air temperature, winds, humidity, vorticity, and geopotential height have been examined over the Indian summer monsoon domain to understand the processes governing rainfall.

Previous studies on ISMR have limitations in terms of usage of long-term trend analysis methods, which can obscure smaller-scale trends and anomalies. To enhance the current level of understanding of ISMR, it is crucial to identify significant rainfall trends and anomalies, determine the specific time windows in which these trends occur, compare these trends across different spatial domains in India, and further investigate the factors and processes influencing rainfall over specific temporal and spatial domains. This thesis aims to achieve these objectives. The detailed explanations of all inferences drawn from this study are provided in individual chapters, with major outcome summarized as follows:

5.1.1. Proposed methodology:

The Chapter-2 presents a methodology for identifying rainfall trends over shorter time scales within a long-term time series by detecting trend reversals. The process of identifying these trend reversals in a long-term dataset involves several statistical tools, which are discussed step-by-step in the following sections:

1. Computing daily rainfall time series for each district from daily gridded rainfall time series by area-weighted average method.
2. Constructing district-wise summer monsoon rainfall (total rainfall from June to September) time series.
3. Creating % departure time series, expressing deviations from the climatological standard normal (1961–1990 summer monsoon rainfall average).
4. Applying a 31-year moving average to % departure time series to reveal multidecadal summer monsoon rainfall patterns.
5. Identifying summer monsoon rainfall trend reversals or inflection points with a 15-year sliding analysis. We categorized them as H-type (formed at the convergence of an increasing and subsequent decreasing trend) and L-type (formed at the convergence of a decreasing and an increasing trend).
6. Clustering inflection points through the K-means clustering technique.
7. Determining optimal clusters via the Elbow method and Normality test (a z-test which uses skewness, excess kurtosis, and their standard error for calculation of the z score).
8. Associating trend reversals with cluster centers (weighted average of inflection years of cluster).
9. Identifying prominent trend reversal events impacting at least one-third of a region's area.

5.1.2. Prominent summer monsoon rainfall trends and trend reversal events observed in four rainfall homogeneous regions of India:

The Chapter-3 highlights significant multidecadal summer monsoon rainfall trends and trend reversal points observed in the long-term summer monsoon rainfall time series from 1901 to 2020. Using the proposed methodology, these trends and reversal points are identified at a district level across the four homogeneous rainfall regions of India and are summarized in the following sections:

1. Three prominent rainfall trend reversal events have been identified as: (1) 1930s; (2) 1960s; and (3) 1980s.
2. During rainfall trend reversal in 1930s, the trend changed from increasing to decreasing in central and northeast India, while in south peninsula, the trend changed from decreasing to increasing giving rise to a north-south asymmetry of rainfall patterns over India. In northwest India, no prominent reversal is observed during 1930s.
3. During rainfall trend reversal in 1960s, the trend changed from increasing to decreasing in south peninsula and northwest India, while in northeast India, the trend changed from decreasing to increasing giving rise to an east-west asymmetry of rainfall pattern. In central India, no prominent reversal is observed during this period.
4. Unlike 1930s and 1960s, the rainfall trend reversal in 1980s is experienced in all the four homogeneous regions. In three out of four regions, (i.e. south peninsula, central, and northwest India), the trend changed from decreasing to increasing, while in the fourth region (northeast), the opposite trend of increasing to decreasing rainfall is observed, resulting in an east-west asymmetry of rainfall pattern over India.
5. In terms of the geographical extent of the observed trend reversal, 1980s is the most prominent among the three identified events, ~50% of geographical area of India.
6. In terms of magnitude of rainfall amount variation (i.e. wetter period or drier period compared to long-term) during these three trend reversal events, investigated through Cramer's t-test, the 1930s turns out to be the most prominent event as more than 30% of the region had rainfall significantly different (higher in central and northeast India; and lower in south peninsular India) during this period.
7. The observed temporal changes in the identified spatial asymmetry of rainfall pattern signify that the so-called rainfall homogeneous regions must have changed over time.

5.1.3. Insights into Indian summer monsoon rainfall variability: Early twentieth-century warming vs. Mid-twentieth century cooling:

Chapter 4 examines the causal processes responsible for the significantly higher rainfall in the 1930s (ETCW) compared to the long-term average (1901-2020) in central and northeast India, while noting that south peninsular India experienced notably lower rainfall during this period. It also discusses the factors behind the discernible decreasing trend in rainfall in central and northeast India, contrasted with an increasing trend in the south peninsula from the ETCW to the mid-20th Century cooling period. These processes are summarized as follows:

1. The period of increased rainfall in central and northeast India coincides with the highest occurrences of monsoon depressions and storms from the BoB.
2. Elevated 850 hPa absolute vorticity and reduced vertical wind shear between 200 hPa and 850 hPa contributed to more depressions and storms over the BoB during the 1930s (ETCW) compared to the mid-20th Century cooling period.
3. The ETCW phase created a significant thermal gradient, increasing low-level wind speeds and cyclonic circulation. Positive AMO and PDO phases induced cold wind surges, weakening upper-level winds, which decreased vertical wind shear and increased vorticity, leading to more monsoon depressions and more rainfall over the central and northeast India. ETCW is also marked by increased LLJ, which further caused more rainfall over the central and northeast India.
4. During the mid-20th Century Cooling period, the northern Indian landmass, including Tibet, experienced colder temperatures, reducing the thermal gradient and decreasing low-level wind speeds creating less favorable conditions for forming depressions and storms

and led to decreased rainfall in central and northeast India. Decreased strength in LLJ during this period is also responsible for decreased rainfall over the central and northeast India.

5. Anomalous warming over the northern Indian Ocean during this period caused increased rainfall in the southern peninsula compared to the ETCW period.
6. Thus, the anomalous rainfall in central and northeast India in the 1930s was driven by a higher number of monsoon depressions. Temperature changes from ETCW to mid-20th Century Cooling contributed to the observed north-south asymmetry in ISMR trends.

5.2. Limitations:

This study has certain limitations regarding the data and methods used, which are as follows:

1. **Uncertainty in Rainfall Data:** There is some uncertainty in rainfall data due to the instruments used and the spatial coverage of rainfall stations in the older timeframe. However, the observed rainfall patterns align well with reanalysis products. The IMD gridded rainfall dataset provides an opportunity to study the ISMR over a finer spatial resolution and a longer period. Currently, this is the best dataset available for this type of study.
2. **K-Means Clustering Technique:** The K-means clustering technique used to cluster inflection points has its limitations. These include the subjective determination of the ideal number of clusters using the elbow method and the tendency to converge towards different cluster centroids based on the initial randomly chosen centroids. These limitations introduce subjectivity into the K-means algorithm, such as sensitivity to centroids and the potential overlap of cluster members. To mitigate this, a two-sample Student's t-test is performed to examine whether the clusters of L-type/H-type inflection points obtained for each region significantly differ from each other.

5.3. Scope for the future works:

The significance of this thesis lies in its identification of critical time windows exhibiting significant reversals in summer monsoon rainfall trends, prompting further investigation into the underlying causal factors. Efforts have been made to understand the dynamics behind the observed rainfall patterns, particularly the trend reversal in the 1930s during the ETCW and mid-20th Century Cooling periods. A proposed hypothesis effectively explains the rainfall patterns in the south peninsula, central, and northeast India but only partially accounts for the patterns in northwest India. This suggests that local processes in northwest India may dominate over global influences, warranting further study.

There is ample scope to explore the causal factors and processes responsible for the observed rainfall trend reversals and regional variability, particularly during the 1960s and 1980s. A notable pattern identified in this work is the increasing rainfall trend from the 1960s to 1980s in northeast regions, while the rest of India experienced a decreasing trend. This incoherence in regional ISMR trends requires detailed study to better understand the underlying processes.

These trend reversals are not uniformly experienced across all geographical regions, presenting an intriguing scientific challenge regarding their causal mechanisms. Consequently, this work opens up new research avenues for hydrologists, meteorologists, and modelers to investigate region-specific rainfall governing systems in greater detail by focusing on distinct trends within specific time frames.

References

- Abish, B., P. Joseph, and O. M. Johannessen (2013), Weakening trend of the tropical easterly jet stream of the boreal summer monsoon season 1950–2009, *Journal of Climate*, 26(23), 9408-9414.
- Adeyeri, O., B. Lamptey, A. Lawin, and I. Sanda (2017), Spatio-temporal precipitation trend and homogeneity analysis in Komadugu-Yobe basin, Lake Chad region, *Journal of Climatology and Weather Forecasting*, 5(3), 1000214.
- Anil, N., M. Ramesh Kumar, R. Sajeev, and P. Saji (2016), Role of distinct flavours of IOD events on Indian summer monsoon, *Natural Hazards*, 82, 1317-1326.
- Annamalai, H., J. Hafner, K. Sooraj, and P. Pillai (2013), Global warming shifts the monsoon circulation, drying South Asia, *Journal of Climate*, 26(9), 2701-2718.
- Ashok, K., W. L. Chan, T. Motoi, and T. Yamagata (2004), Decadal variability of the Indian Ocean dipole, *Geophysical Research Letters*, 31(24).
- Ashok, K., Z. Guan, and T. Yamagata (2001), Impact of the Indian Ocean dipole on the relationship between the Indian monsoon rainfall and ENSO, *Geophysical research letters*, 28(23), 4499-4502.
- Basistha, A., D. S. Arya, and N. K. Goel (2009), Analysis of historical changes in rainfall in the Indian Himalayas, *International Journal of Climatology: A Journal of the Royal Meteorological Society*, 29(4), 555-572.
- Bhatla, R., S. Sharma, S. Verma, and B. Gyawali (2020), Impact of Pacific Decadal Oscillation in relation to QBO on Indian summer monsoon rainfall, *Arabian Journal of Geosciences*, 13, 1-9.
- Biswas, B., R. S. Jadhav, and N. Tikone (2019), Rainfall distribution and trend analysis for upper Godavari basin, India, from 100 years record (1911–2010), *Journal of the Indian Society of Remote Sensing*, 47, 1781-1792.
- Bollasina, M. A., Y. Ming, and V. Ramaswamy (2011), Anthropogenic aerosols and the weakening of the South Asian summer monsoon, *science*, 334(6055), 502-505.

- Cai, W., D. Bi, J. Church, T. Cowan, M. Dix, and L. Rotstayn (2006), Pan-oceanic response to increasing anthropogenic aerosols: Impacts on the Southern Hemisphere oceanic circulation, *Geophysical research letters*, 33(21).
- Chakra, S., A. Ganguly, H. Oza, V. Padhya, A. Pandey, and R. Deshpande (2023), Multidecadal summer monsoon rainfall trend reversals in South Peninsular India: a new approach to examining long-term rainfall dataset, *Journal of Hydrology*, 129975.
- Chakraborty, A., R. S. Nanjundiah, and J. Srinivasan (2009), Impact of African orography and the Indian summer monsoon on the low-level Somali jet, *International Journal of Climatology*, 29(7), 983.
- Chakravorty, S., C. Gnanaseelan, and P. Pillai (2016), Combined influence of remote and local SST forcing on Indian Summer Monsoon Rainfall variability, *Climate Dynamics*, 47, 2817-2831.
- Chao, W. C., and B. Chen (2001), The origin of monsoons, *Journal of the Atmospheric Sciences*, 58(22), 3497-3507.
- Cherchi, A., P. Terray, S. B. Ratna, S. Sankar, K. Sooraj, and S. Behera (2021), Indian Ocean Dipole influence on Indian summer monsoon and ENSO: A review, *Indian summer monsoon variability*, 157-182.
- Chou, C., D. Ryu, M.-H. Lo, H.-W. Wey, and H. M. Malano (2018), Irrigation-induced land-atmosphere feedbacks and their impacts on Indian summer monsoon, *Journal of Climate*, 31(21), 8785-8801.
- Choudhury, A. D., R. Krishnan, M. Ramarao, R. Vellore, M. Singh, and B. Mapes (2018), A phenomenological paradigm for midtropospheric cyclogenesis in the Indian summer monsoon, *Journal of the atmospheric sciences*, 75(9), 2931-2954.
- Choudhury, B. A., S. K. Saha, M. Konwar, K. Sujith, and A. Deshamukhya (2019), Rapid drying of Northeast India in the last three decades: climate change or natural variability?, *Journal of Geophysical Research: Atmospheres*, 124(1), 227-237.
- Chowdary, J. S., H. Harsha, C. Gnanaseelan, G. Srinivas, A. Parekh, P. Pillai, and C. Naidu (2017), Indian summer monsoon rainfall variability in response to differences in the decay phase of El Niño, *Climate Dynamics*, 48, 2707-2727.

- Chowdary, J. S., S.-P. Xie, and R. S. Nanjundiah (2021), Drivers of the Indian summer monsoon climate variability, in Indian summer monsoon variability, edited, pp. 1-28, Elsevier.
- Das, J., S. Jha, and M. K. Goyal (2020), On the relationship of climatic and monsoon teleconnections with monthly precipitation over meteorologically homogenous regions in India: Wavelet & global coherence approaches, Atmospheric Research, 238, 104889.
- Diao, C., and Y. Xu (2022), Reassessing the relative role of anthropogenic aerosols and natural decadal variability in driving the mid-twentieth century global “cooling”: a focus on the latitudinal gradient of tropospheric temperature, Climate Dynamics, 59(9-10), 2655-2681.
- Emanuel, K. A., and D. S. Nolan (2004), Tropical cyclone activity and the global climate system, paper presented at Preprints, 26th conf. on hurricanes and tropical meteorology, Miami, FL, Amer. Meteor. Soc. A.
- Falga, R., and C. Wang (2022), The rise of Indian summer monsoon precipitation extremes and its correlation with long-term changes of climate and anthropogenic factors, Scientific reports, 12(1), 11985.
- Gadgil, S. (2003), The Indian monsoon and its variability, Annual Review of Earth and Planetary Sciences, 31(1), 429-467.
- Ghosh, S., H. Vittal, T. Sharma, S. Karmakar, K. S. Kasiviswanathan, Y. Dhanesh, K. Sudheer, and S. Gunthe (2016), Indian summer monsoon rainfall: implications of contrasting trends in the spatial variability of means and extremes, PloS one, 11(7), e0158670.
- Gnanaseelan, C., and J. S. Chowdary (2019), The Indo-Western Pacific climate variability and the impacts on Indian summer monsoon: Two decades of advancement in India, Mausam, 70(4), 731-752.
- Goswami, B. B., R. Murtugudde, and S.-I. An (2021), Role of the Bay of Bengal warming in the Indian summer monsoon rainfall trend, Climate Dynamics, 1-19.
- Goswami, B. N., J. Shukla, E. Schneider, and Y. Sud (1984), Study of the dynamics of the intertropical convergence zone with a symmetric version of the GLAS climate model, Journal of the atmospheric sciences, 41(1), 5-19.

- Goswami, B. N., M. Madhusoodanan, C. Neema, and D. Sengupta (2006), A physical mechanism for North Atlantic SST influence on the Indian summer monsoon, *Geophysical Research Letters*, 33(2).
- Guerreiro Miranda, B., R. Galante Negri, and L. Albertani Pampuch (2023), Using clustering algorithms and GPM data to identify spatial precipitation patterns over southeastern Brazil, *Atmósfera*, 37.
- Guhathakurta, P., and M. Rajeevan (2008), Trends in the rainfall pattern over India, *International Journal of Climatology: A Journal of the Royal Meteorological Society*, 28(11), 1453-1469.
- Guhathakurta, P., M. Rajeevan, D. Sikka, and A. Tyagi (2015), Observed changes in southwest monsoon rainfall over India during 1901–2011, *International Journal of Climatology*, 35(8), 1881-1898.
- Guo, L., A. G. Turner, and E. J. Highwood (2015), Impacts of 20th century aerosol emissions on the South Asian monsoon in the CMIP5 models, *Atmospheric Chemistry and Physics*, 15(11), 6367-6378.
- Gupta, V., and M. K. Jain (2018), Investigation of multi-model spatiotemporal mesoscale drought projections over India under climate change scenario, *Journal of Hydrology*, 567, 489-509.
- Halley, E. (1753), An historical account of the trade winds, and monsoons, observable in the seas between and near the Tropicks, with an attempt to assign the physical cause of the said winds, *Philosophical Transactions of the Royal Society of London*, 16(183), 153-168.
- Harris, I., T. J. Osborn, P. Jones, and D. Lister (2020), Version 4 of the CRU TS monthly high-resolution gridded multivariate climate dataset, *Scientific data*, 7(1), 109.
- Hegerl, G. C., S. Brönnimann, A. Schurer, and T. Cowan (2018), The early 20th century warming: Anomalies, causes, and consequences, *Wiley Interdisciplinary Reviews: Climate Change*, 9(4), e522.
- Hogg, R. V., E. A. Tanis, and D. L. Zimmerman (1977), *Probability and statistical inference*, Macmillan New York.

- Hrudya, P. P. V. H., H. Varikoden, and R. N. Vishnu (2021), Changes in the relationship between Indian Ocean dipole and Indian summer monsoon rainfall in early and recent multidecadal epochs during different phases of monsoon, *International Journal of Climatology*, 41, E305-E318.
- Hrudya, P., H. Varikoden, and R. Vishnu (2021), A review on the Indian summer monsoon rainfall, variability and its association with ENSO and IOD, *Meteorology and Atmospheric Physics*, 133, 1-14.
- Huang, B., and J. Shukla (2005), Ocean–atmosphere interactions in the tropical and subtropical Atlantic Ocean, *Journal of Climate*, 18(11), 1652-1672.
- Hunt, K. M., and J. K. Fletcher (2019), The relationship between Indian monsoon rainfall and low-pressure systems, *Climate Dynamics*, 53(3), 1859-1871.
- Jain, S. K., V. Kumar, and M. Saharia (2013), Analysis of rainfall and temperature trends in northeast India, *International Journal of Climatology*, 33(4), 968-978.
- Jaiswal, R., A. Lohani, and H. Tiwari (2015), Statistical analysis for change detection and trend assessment in climatological parameters, *Environmental Processes*, 2, 729-749.
- Jana, C., N. Alam, D. Mandal, M. Shamim, and R. Kaushal (2017), Spatio-temporal rainfall trends in the twentieth century for Bundelkhand region, India, *Journal of Water and Climate Change*, 8(3), 441-455.
- Joseph, P., and A. Simon (2005), Weakening trend of the southwest monsoon current through peninsular India from 1950 to the present, *Current Science*, 687-694.
- Joseph, P., and P. Raman (1966), Existence of low level westerly jet stream over peninsular India during July, *Mausam*, 17(3), 407-410.
- Joshi, M. K., and A. Pandey (2011), Trend and spectral analysis of rainfall over India during 1901–2000, *Journal of Geophysical Research: Atmospheres*, 116(D6).
- Joshi, M. K., and K.-J. Ha (2019), Fidelity of CMIP5-simulated teleconnection between Atlantic multidecadal oscillation and Indian summer monsoon rainfall, *Climate Dynamics*, 52(7), 4157-4176.

- Kale, G. D., and D. Nagesh Kumar (2018), Trend detection analysis of seasonal rainfall of homogeneous regions and all India, prepared by using individual month rainfall values, *Water Conservation Science and Engineering*, 3, 129-138.
- Karmakar, N., A. Chakraborty, and R. S. Nanjundiah (2017), Space–time evolution of the low- and high-frequency intraseasonal modes of the Indian summer monsoon, *Monthly Weather Review*, 145(2), 413-435.
- Kaur, S., S. K. Diwakar, and A. K. Das (2017), Long term rainfall trend over meteorological sub divisions and districts of India, *Mausam*, 68(3), 439-450.
- Keshavamurthy, R., and M. S. Rao (1992), *The physics of monsoons*, Allied Publishers.
- Kim, H.-Y. (2013), Statistical notes for clinical researchers: assessing normal distribution (2) using skewness and kurtosis, *Restorative dentistry & endodontics*, 38(1), 52-54.
- Konwar, M., A. Parekh, and B. Goswami (2012), Dynamics of east-west asymmetry of Indian summer monsoon rainfall trends in recent decades, *Geophysical research letters*, 39(10).
- Koteswaram, P. (1958), The easterly jet stream in the tropics, *Tellus*, 10(1), 43-57.
- Kothawale, D., A. Munot, and K. K. Kumar (2010), Surface air temperature variability over India during 1901–2007, and its association with ENSO, *Climate Research*, 42(2), 89-104.
- Krishnakumar, K., G. P. Rao, and C. Gopakumar (2009), Rainfall trends in twentieth century over Kerala, India, *Atmospheric environment*, 43(11), 1940-1944.
- Krishnamurthy, L., and V. Krishnamurthy (2014), Influence of PDO on South Asian summer monsoon and monsoon–ENSO relation, *Climate dynamics*, 42, 2397-2410.
- Krishnamurthy, L., and V. Krishnamurthy (2016), Teleconnections of Indian monsoon rainfall with AMO and Atlantic tripole, *Climate dynamics*, 46, 2269-2285.
- Krishnamurthy, V., and R. Ajayamohan (2010), Composite structure of monsoon low pressure systems and its relation to Indian rainfall, *Journal of Climate*, 23(16), 4285-4305.
- Krishnamurti, T. N., and H. Bhalme (1976), Oscillations of a monsoon system. Part I. Observational aspects, *Journal of Atmospheric Sciences*, 33(10), 1937-1954.

- Krishnamurti, T., and J. Findlater (1978), Observational aspects of the low-level cross-equatorial jet stream of the western Indian Ocean, *Monsoon dynamics*, 1251-1262.
- Krishnamurti, T., and P. Ardanuy (1980), The 10 to 20-day westward propagating mode and “Breaks in the Monsoons”, *Tellus*, 32(1), 15-26.
- Krishnan, R., and M. Sugi (2003), Pacific decadal oscillation and variability of the Indian summer monsoon rainfall, *Climate Dynamics*, 21, 233-242.
- Krishnan, R., and P. Swapna (2009), Significant influence of the boreal summer monsoon flow on the Indian Ocean response during dipole events, *Journal of Climate*, 22(21), 5611-5634.
- Krishnan, R., C. Zhang, and M. Sugi (2000), Dynamics of breaks in the Indian summer monsoon, *Journal of the atmospheric sciences*, 57(9), 1354-1372.
- Kumar, K. K., B. Rajagopalan, and M. A. Cane (1999), On the weakening relationship between the Indian monsoon and ENSO, *Science*, 284(5423), 2156-2159.
- Kundu, S. K., and T. K. Mondal (2019), Analysis of long-term rainfall trends and change point in West Bengal, India, *Theoretical and Applied Climatology*, 138, 1647-1666.
- Kundu, S., D. Khare, A. Mondal, and P. Mishra (2015), Analysis of spatial and temporal variation in rainfall trend of Madhya Pradesh, India (1901–2011), *Environmental Earth Sciences*, 73, 8197-8216.
- Lawson, M. P., R. C. Balling Jr, A. J. Peters, and D. C. Rundquist (1981), Spatial analysis of secular temperature fluctuations, *Journal of Climatology*, 1(4), 325-332.
- Lee, J.-J., H.-H. Kwon, and T.-W. Kim (2012), Spatio-temporal analysis of extreme precipitation regimes across South Korea and its application to regionalization, *Journal of hydro-environment research*, 6(2), 101-110.
- Li, J., and Q. Zeng (2000), Significance of the normalized seasonality of wind field and its rationality for characterizing the monsoon, *Science in China Series D: Earth Sciences*, 43, 646-653.
- Li, X., M. Ting, C. Li, and N. Henderson (2015), Mechanisms of Asian summer monsoon changes in response to anthropogenic forcing in CMIP5 models, *Journal of Climate*, 28(10), 4107-4125.

- Li, Z., W. Yu, T. Li, V. Murty, and F. Tangang (2013), Bimodal character of cyclone climatology in the Bay of Bengal modulated by monsoon seasonal cycle, *Journal of Climate*, 26(3), 1033-1046.
- Luo, F., S. Li, Y. Gao, L. Svendsen, T. Furevik, and N. Keenlyside (2018), The connection between the Atlantic Multidecadal Oscillation and the Indian Summer Monsoon since the Industrial Revolution is intrinsic to the climate system, *Environmental Research Letters*, 13(9), 094020.
- Luo, F.-F., S. Li, and T. Furevik (2018), Weaker connection between the Atlantic multidecadal oscillation and Indian summer rainfall since the mid-1990s, *Atmospheric and Oceanic Science Letters*, 11(1), 37-43.
- Lupikasza, E. (2010), Spatial and temporal variability of extreme precipitation in Poland in the period 1951–2006, *International Journal of Climatology: A Journal of the Royal Meteorological Society*, 30(7), 991-1007.
- Madden, R. A., and P. R. Julian (1972), Description of global-scale circulation cells in the tropics with a 40–50 day period, *Journal of Atmospheric Sciences*, 29(6), 1109-1123.
- Maity, S. (2020), Comparative assessment of two RegCM versions in simulating Indian Summer Monsoon, *Journal of Earth System Science*, 129(1), 75.
- Mantua, N. J., and S. R. Hare (2002), The Pacific decadal oscillation, *Journal of oceanography*, 58, 35-44.
- Marani, M., and S. Zanetti (2015), Long-term oscillations in rainfall extremes in a 268 year daily time series, *Water Resources Research*, 51(1), 639-647.
- Miller, F. R. (1968), *Structure of an Arabian Sea summer monsoon system*, University of Hawaii Press.
- Mishra, P., C. M. Pandey, U. Singh, A. Gupta, C. Sahu, and A. Keshri (2019), Descriptive statistics and normality tests for statistical data, *Annals of cardiac anaesthesia*, 22(1), 67.
- Mishra, V., B. V. Smoliak, D. P. Lettenmaier, and J. M. Wallace (2012), A prominent pattern of year-to-year variability in Indian Summer Monsoon Rainfall, *Proceedings of the National Academy of Sciences*, 109(19), 7213-7217.

- Mitchell Jr, J. M. (1966), Climatic change: report of a working group of the Commission for Climatology, (No Title).
- Mohapatra, M., and U. Mohanty (2004), Some characteristics of low pressure systems and summer monsoon rainfall over Orissa, *Current science*, 1245-1255.
- Mohapatra, M., and U. Mohanty (2007), Inter-annual variability of summer monsoon rainfall over Orissa (India) in relation to cyclonic disturbances, *Natural Hazards*, 42, 301-315.
- Mondal, A., D. Khare, and S. Kundu (2015), Spatial and temporal analysis of rainfall and temperature trend of India, *Theoretical and applied climatology*, 122, 143-158.
- Mooley, D., and B. Parthasarathy (1984), Fluctuations in all-India summer monsoon rainfall during 1871–1978, *Climatic change*, 6(3), 287-301.
- Mourato, S., M. Moreira, and J. Corte-Real (2010), Interannual variability of precipitation distribution patterns in Southern Portugal, *International Journal of Climatology*, 30(12), 1784-1794.
- Nath, R., and Y. Luo (2019), Disentangling the influencing factors driving the cooling trend in boreal summer over Indo-Gangetic river basin, India: role of Atlantic multidecadal oscillation (AMO), *Theoretical and Applied Climatology*, 138, 1-12.
- O'hare, G. (1997), The Indian monsoon part 1: The wind system, *Geography*, 218-230.
- Organization, W. M. (2017), WMO guidelines on the calculation of climate normals, edited, World Meteorological Organization Geneva, Switzerland.
- Pai, D., J. Bhate, O. Sreejith, and H. Hatwar (2011), Impact of MJO on the intraseasonal variation of summer monsoon rainfall over India, *Climate Dynamics*, 36, 41-55.
- Pai, D., M. Rajeevan, O. Sreejith, B. Mukhopadhyay, and N. Satbha (2014), Development of a new high spatial resolution (0.25× 0.25) long period (1901-2010) daily gridded rainfall data set over India and its comparison with existing data sets over the region, *Mausam*, 65(1), 1-18.
- Pandey, P., S. Dwivedi, and B. N. Goswami (2022), Trend and variability in the long-term relationship between Eurasian snow cover and Indian summer monsoon rainfall, *International Journal of Climatology*, 42(15), 7751-7765.

- Parthasarathy, B., A. Munot, and D. Kothawale (1994), All-India monthly and seasonal rainfall series: 1871–1993, *Theoretical and Applied Climatology*, 49, 217-224.
- Patra, J. P., A. Mishra, R. Singh, and N. Raghuwanshi (2012), Detecting rainfall trends in twentieth century (1871–2006) over Orissa State, India, *Climatic Change*, 111, 801-817.
- Pattanaik, D., and V. Satyan (2000), Fluctuations of tropical easterly jet during contrasting monsoons over India: A GCM study, *Meteorology and Atmospheric Physics*, 75, 51-60.
- Paul, S., S. Ghosh, R. Oglesby, A. Pathak, A. Chandrasekharan, and R. Ramsankaran (2016), Weakening of Indian summer monsoon rainfall due to changes in land use land cover, *Scientific reports*, 6(1), 32177.
- Paul, Z., A. Keerthana, and A. Nair (2022), Identification of Homogeneous Zones in Kerala Through K-Means Clustering, *Mathematical Statistician and Engineering Applications*, 71(3s), 413-433.
- Poli, P., and N. Staff (2017), *The climate data guide: ERA-20C: ECMWF's atmospheric reanalysis of the 20th century (and comparisons with NOAA's 20CR)*, edited.
- Portela, M. M., L. A. Espinosa, and M. Zelenakova (2020), Long-term rainfall trends and their variability in mainland Portugal in the last 106 years, *Climate*, 8(12), 146.
- Prajeesh, A., K. Ashok, and D. B. Rao (2013), Falling monsoon depression frequency: A Gray-Sikka conditions perspective, *Scientific reports*, 3(1), 2989.
- Prasanna, V. (2014), Impact of monsoon rainfall on the total foodgrain yield over India, *Journal of earth system science*, 123(5), 1129-1145.
- Praveen, B., S. Talukdar, S. Mahato, J. Mondal, P. Sharma, A. R. M. Islam, and A. Rahman (2020a), Analyzing trend and forecasting of rainfall changes in India using non-parametrical and machine learning approaches, *Scientific reports*, 10(1), 1-21.
- Praveen, B., S. Talukdar, Shahfahad, S. Mahato, J. Mondal, P. Sharma, A. R. M. T. Islam, and A. Rahman (2020b), Analyzing trend and forecasting of rainfall changes in India using non-parametrical and machine learning approaches, *Scientific reports*, 10(1), 10342.

- Praveen, V., S. Sandeep, and R. Ajayamohan (2015), On the relationship between mean monsoon precipitation and low pressure systems in climate model simulations, *Journal of Climate*, 28(13), 5305-5324.
- Preethi, B., J. Revadekar, and A. Munot (2011), Extremes in summer monsoon precipitation over India during 2001–2009 using CPC high-resolution data, *International journal of remote sensing*, 32(3), 717-735.
- Raghavan, K. (1973), Break-monsoon over India, *Monthly Weather Review*, 101(1), 33-43.
- Rajeevan, M., C. Unnikrishnan, J. Bhate, K. Niranjana Kumar, and P. Sreekala (2012), Northeast monsoon over India: variability and prediction, *Meteorological Applications*, 19(2), 226-236.
- Ramage, C. S. (1971), *Monsoon meteorology*, (No Title).
- Ramos, M. (2001), Divisive and hierarchical clustering techniques to analyse variability of rainfall distribution patterns in a Mediterranean region, *Atmospheric Research*, 57(2), 123-138.
- Rasmusson, E. M., and T. H. Carpenter (1983), The relationship between eastern equatorial Pacific sea surface temperatures and rainfall over India and Sri Lanka, *Monthly Weather Review*, 111(3), 517-528.
- Raymond, D. J., and Ž. Fuchs (2009), Moisture modes and the Madden–Julian oscillation, *Journal of Climate*, 22(11), 3031-3046.
- Rayner, N., D. E. Parker, E. Horton, C. K. Folland, L. V. Alexander, D. Rowell, E. C. Kent, and A. Kaplan (2003), Global analyses of sea surface temperature, sea ice, and night marine air temperature since the late nineteenth century, *Journal of Geophysical Research: Atmospheres*, 108(D14).
- Saha, M., P. Mitra, and R. S. Nanjundiah (2017), Deep learning for predicting the monsoon over the homogeneous regions of India, *Journal of Earth System Science*, 126, 1-18.
- Sahai, A., A. Grimm, V. Satyan, and G. Pant (2003), Long-lead prediction of Indian summer monsoon rainfall from global SST evolution, *Climate Dynamics*, 20, 855-863.

- Sahoo, M., and R. Kumar Yadav (2022), The Interannual variability of rainfall over homogeneous regions of Indian summer monsoon, *Theoretical and Applied Climatology*, 148(3), 1303-1316.
- Saini, A., N. Sahu, W. Duan, M. Kumar, R. Avtar, M. Mishra, P. Kumar, R. Pandey, and S. Behera (2022), Unraveling intricacies of monsoon attributes in homogenous Monsoon regions of India, *Frontiers in Earth Science*, 10, 794634.
- Saji, N., B. N. Goswami, P. Vinayachandran, and T. Yamagata (1999), A dipole mode in the tropical Indian Ocean, *Nature*, 401(6751), 360-363.
- Salzmann, M., and R. Cherian (2015), On the enhancement of the Indian summer monsoon drying by Pacific multidecadal variability during the latter half of the twentieth century, *Journal of Geophysical Research: Atmospheres*, 120(18), 9103-9118.
- Salzmann, M., H. Weser, and R. Cherian (2014), Robust response of Asian summer monsoon to anthropogenic aerosols in CMIP5 models, *Journal of Geophysical Research: Atmospheres*, 119(19), 11,321-311,337.
- Sandeep, S., and R. Ajayamohan (2015), Poleward shift in Indian summer monsoon low level jetstream under global warming, *Climate Dynamics*, 45(1), 337-351.
- Shepard, D. (1968), A two-dimensional interpolation function for irregularly-spaced data, paper presented at Proceedings of the 1968 23rd ACM national conference.
- Shukla, J. (1987), Interannual variability of monsoons, *Monsoons*, 14, 399-464.
- Sikka, D., and S. Gadgil (1980), On the maximum cloud zone and the ITCZ over Indian longitudes during the southwest monsoon, *Monthly Weather Review*, 108(11), 1840-1853.
- Singh, M., and R. Bhatla (2019), Modulation of active-break spell of Indian summer monsoon by Madden Julian Oscillation, *Journal of Earth System Science*, 128, 1-15.
- Singh, R., S. Sah, B. Das, S. Potekar, A. Chaudhary, and H. Pathak (2021), Innovative trend analysis of spatio-temporal variations of rainfall in India during 1901–2019, *Theoretical and Applied Climatology*, 145(1-2), 821-838.

- Sönmez, İ., and A. Ü. Kömüştü (2011), Reclassification of rainfall regions of Turkey by K-means methodology and their temporal variability in relation to North Atlantic Oscillation (NAO), *Theoretical and applied climatology*, 106(3-4), 499-510.
- Srinivas, G., J. S. Chowdary, Y. Kosaka, C. Gnanaseelan, A. Parekh, and K. Prasad (2018), Influence of the Pacific–Japan pattern on Indian summer monsoon rainfall, *Journal of Climate*, 31(10), 3943-3958.
- Subash, N., A. Sikka, and H. Ram Mohan (2011), An investigation into observational characteristics of rainfall and temperature in Central Northeast India—a historical perspective 1889–2008, *Theoretical and applied climatology*, 103, 305-319.
- Subash, N., and A. Sikka (2014), Trend analysis of rainfall and temperature and its relationship over India, *Theoretical and applied climatology*, 117, 449-462.
- Sushant, S., K. Balasubramani, and K. Kumaraswamy (2015), Spatio-temporal analysis of rainfall distribution and variability in the twentieth century, over the Cauvery Basin, South India, *Environmental management of river basin ecosystems*, 21-41.
- Taraphdar, S., F. Zhang, L. R. Leung, X. Chen, and O. M. Pauluis (2018), MJO affects the monsoon onset timing over the Indian region, *Geophysical Research Letters*, 45(18), 10011-10018.
- Taxak, A. K., A. Murumkar, and D. S. Arya (2014), Long term spatial and temporal rainfall trends and homogeneity analysis in Wainganga basin, Central India, *Weather and climate extremes*, 4, 50-61.
- Thomas, E., and N. P. Abraham (2022), Relationship between sunspot number and seasonal rainfall over Kerala using wavelet analysis, *Journal of Atmospheric and Solar-Terrestrial Physics*, 240, 105943.
- Vernekar, A., J. Zhou, and J. Shukla (1995), The effect of Eurasian snow cover on the Indian monsoon, *Journal of Climate*, 8(2), 248-266.
- Vishnu, S., P. A. Francis, S. C. Shenoi, and S. S. V. S. Ramakrishna (2018), On the relationship between the Pacific Decadal Oscillation and monsoon depressions over the Bay of Bengal, *Atmospheric Science Letters*, 19(7), e825.

- Vishnu, S., P. Francis, S. Shenoi, and S. Ramakrishna (2016), On the decreasing trend of the number of monsoon depressions in the Bay of Bengal, *Environmental Research Letters*, 11(1), 014011.
- Wang, B., and X. Xie (1997), A model for the boreal summer intraseasonal oscillation, *Journal of the Atmospheric Sciences*, 54(1), 72-86.
- Wang, B., J. Liu, H.-J. Kim, P. J. Webster, S.-Y. Yim, and B. Xiang (2013), Northern Hemisphere summer monsoon intensified by mega-El Niño/southern oscillation and Atlantic multidecadal oscillation, *Proceedings of the National Academy of Sciences*, 110(14), 5347-5352.
- Wang, B., Y. Ding, and D. Sikka (2006), Synoptic systems and weather, *The asian monsoon*, 131-201.
- Wang, P., B. Wang, and T. Kiefer (2012), *Global Monsoon across timescales*, edited, pp. 1043-1044, Springer.
- Watanabe, T., and K. Yamazaki (2014), Decadal-scale variation of South Asian summer monsoon onset and its relationship with the Pacific decadal oscillation, *Journal of Climate*, 27(13), 5163-5173.
- Webster, P. J. (1987), *The variable and interactive monsoon*, Monsoons.
- Wei, W., R. Zhang, S. Yang, W. Li, and M. Wen (2019), Quasi-biweekly oscillation of the South Asian high and its role in connecting the Indian and East Asian summer rainfalls, *Geophysical Research Letters*, 46(24), 14742-14750.
- WMO (2017), *WMO guidelines on the calculation of climate normals*, WMO Technical Report.
- Xavier, P. K., C. Marzin, and B. N. Goswami (2007), An objective definition of the Indian summer monsoon season and a new perspective on the ENSO–monsoon relationship, *Quarterly Journal of the Royal Meteorological Society: A journal of the atmospheric sciences, applied meteorology and physical oceanography*, 133(624), 749-764.
- Xavier, P. K., C. Marzin, and B. N. Goswami (2007), An objective definition of the Indian summer monsoon season and a new perspective on the ENSO–monsoon relationship, *Quarterly Journal of the Royal Meteorological Society: A journal of*

the atmospheric sciences, applied meteorology and physical oceanography, 133(624), 749-764.

- Yadav, R. K., and M. K. Roxy (2019), On the relationship between north India summer monsoon rainfall and east equatorial Indian Ocean warming, *Global and Planetary Change*, 179, 23-32.
- Yadav, R. K., G. Srinivas, and J. S. Chowdary (2018), Atlantic Niño modulation of the Indian summer monsoon through Asian jet, *Npj Climate and Atmospheric Science*, 1(1), 23.
- Yao, S.-L., J.-J. Luo, G. Huang, and P. Wang (2017), Distinct global warming rates tied to multiple ocean surface temperature changes, *Nature Climate Change*, 7(7), 486-491.
- Yim, S.-Y., B. Wang, J. Liu, and Z. Wu (2014), A comparison of regional monsoon variability using monsoon indices, *Climate dynamics*, 43, 1423-1437.
- Zahmatkesh, Z., M. Karamouz, and S. Nazif (2015), Uncertainty based modeling of rainfall-runoff: combined differential evolution adaptive metropolis (DREAM) and K-means clustering, *Advances in water resources*, 83, 405-420.
- Zhang, G., G. Zeng, C. Li, and X. Yang (2020), Impact of PDO and AMO on interdecadal variability in extreme high temperatures in North China over the most recent 40-year period, *Climate Dynamics*, 54(5), 3003-3020.
- Zheng, Y., M. Bourassa, M. Ali, and T. Krishnamurti (2016), Distinctive features of rainfall over the Indian homogeneous rainfall regions between strong and weak Indian summer monsoons, *Journal of Geophysical Research: Atmospheres*, 121(10), 5631-5647.
- Zhou, Z. Q., S. P. Xie, and R. Zhang (2019), Variability and predictability of Indian rainfall during the monsoon onset month of June, *Geophysical Research Letters*, 46(24), 14782-14788.

Lists of Publications

Thesis work

Published

1. **Chakra, S.**, Ganguly, A., Oza, H., Padhya, V., Pandey, A., & Deshpande, R. D. (2023). Multidecadal summer monsoon rainfall trend reversals in South Peninsular India: A new approach to examining long-term rainfall dataset. *Journal of Hydrology*, 624, 129975., <https://www.sciencedirect.com/science/article/abs/pii/S0022169423009174>
2. **Chakra, S.**, Oza, H., Ganguly, A., Pandey, A., Padhya, V., & Deshpande, R. D. (2024). Finer aspects of spatio-temporal variations in Indian summer monsoon rainfall trend reversals over the last 120 years. *Climatic Change*, 177(8), 1-22., <https://doi.org/10.1007/s10584-024-03780-9>

Under Preparation

1. **Chakra, S.**, Vishnu, S., Oza, H., Ganguly, A., & Deshpande, R. D. Insights into Indian summer monsoon rainfall variability: Early twentieth century warming vs. Mid-twentieth century cooling.

Contributing author

1. Ganguly, A., Oza, H., Padhya, V., Pandey, A., **Chakra, S.**, & Deshpande, R. D. (2023). Extreme local recycling of moisture via wetlands and forests in North-East Indian subcontinent: a Mini-Amazon. *Scientific Reports*, 13(1), 521., <https://doi.org/10.1038/s41598-023-27577-5>
2. Pandey, A., Padhya, V., Ganguly, A., **Chakra, S.**, & Deshpande, R. D. (2023). Surface water groundwater interaction in water-stressed semi-arid western India: Insights from environmental isotopes. *Journal of Arid Environments*, 208, 104879., <https://doi.org/10.1016/j.jaridenv.2022.104879>

3. Pandey, A., Padhya, V., **Chakra, S.**, Ganguly, A., & Deshpande, R. D. (2022). Groundwater recharge in Central India and its spatio-temporal variation: Insights and implications from oxygen and hydrogen isotopes. *Journal of Hydrology*, 129040., <https://doi.org/10.1016/j.jhydrol.2022.129040>

4. Pandey, A., Padhya, V., **Chakra, S.**, & Deshpande, R. D. (2023). Seasonality in groundwater recharge in Coastal Southwestern India and its hydrological implications based on stable isotopes ($\delta^{18}\text{O}$, δD). *Physics and Chemistry of the Earth, Parts A/B/C*, 130, 103396., <https://doi.org/10.1016/j.pce.2023.103396>